

ISSN 1408-7073

RMZ – MATERIALS AND GEOENVIRONMENT

PERIODICAL FOR MINING, METALLURGY AND GEOLOGY

RMZ – MATERIALI IN GEOKOLJE

REVIJA ZA RUDARSTVO, METALURGIJO IN GEOLOGIJO

Historical Review

More than 80 years have passed since in 1919 the University Ljubljana in Slovenia was founded. Technical fields were joint in the School of Engineering that included the Geologic and Mining Division while the Metallurgy Division was established in 1939 only. Today the Departments of Geology, Mining and Geotechnology, Materials and Metallurgy are part of the Faculty of Natural Sciences and Engineering, University of Ljubljana.

Before War II the members of the Mining Section together with the Association of Yugoslav Mining and Metallurgy Engineers began to publish the summaries of their research and studies in their technical periodical *Rudarski zbornik* (Mining Proceedings). Three volumes of *Rudarski zbornik* (1937, 1938 and 1939) were published. The War interrupted the publication and not until 1952 the first number of the new journal *Rudarsko-metalurški zbornik - RMZ* (Mining and Metallurgy Quarterly) has been published by the Division of Mining and Metallurgy, University of Ljubljana. Later the journal has been regularly published quarterly by the Departments of Geology, Mining and Geotechnology, Materials and Metallurgy, and the Institute for Mining, Geotechnology and Environment.

On the meeting of the Advisory and the Editorial Board on May 22nd 1998 *Rudarsko-metalurški zbornik* has been renamed into "*RMZ - Materials and Geoenvironment (RMZ -Materiali in Geokolje)*" or shortly *RMZ - M&G*.

RMZ - M&G is managed by an international advisory and editorial board and is exchanged with other world-known periodicals. All the papers are reviewed by the corresponding professionals and experts.

RMZ - M&G is the only scientific and professional periodical in Slovenia, which is published in the same form nearly 50 years. It incorporates the scientific and professional topics in geology, mining, and geotechnology, in materials and in metallurgy.

The wide range of topics inside the geosciences are wellcome to be published in the *RMZ -Materials and Geoenvironment*. Research results in geology, hydrogeology, mining, geotechnology, materials, metallurgy, natural and antropogenic pollution of environment, biogeochemistry are proposed fields of work which the journal will handle. *RMZ - M&G* is co-issued and co-financed by the Faculty of Natural Sciences and Engineering Ljubljana, and the Institute for Mining, Geotechnology and Environment Ljubljana. In addition it is financially supported also by the Ministry of Higher Education, Science and Technology of Republic of Slovenia.

Editor in chief

Table of Contents – Kazalo

Hot forming of AISI D2 tool steel

Vročje preoblikovanje AISI D2 orodnega jekla

VEČKO PIRTOVŠEK, T., KUGLER, G., FAJFAR, P., FAZARINC, M., PERUŠ, I., TERČELJ, M. 1

Flow stresses of the AISI A2 tool steel

Krivulje tečenja za AISI A2 orodno jeklo

VEČKO PIRTOVŠEK, T., PERUŠ, I., KUGLER, G., TURK, R., TERČELJ, M. 15

Development of test rig for thermal fatigue testing – preliminary results

Razvoj testne naprave za študij termičnega utrujanja – preliminarni rezultati

FAZARINC, M., TURK, R., KUGLER, G., MRVAR, P., TERČELJ, M. 33

Pulzno varjenje konstrukcijskih jekel

Pulsed arc welding of structural steels

KEJŽAR, R., KEJŽAR, U. 49

¹⁵N signal of *Aplysina aerophoba* as a tracer of anthropogenic nitrogen in the Murter Sea and Pirovac Bay (Central Adriatic)

¹⁵N v *Aplysini aerophobi* kot sledilo antropogenega dušika v Murterskem morju in Pirovaškem zalivu (srednji Jadran)

ROGAN, N., DOLENEC, T., LOJEN, S., LAMBAŠA, Ž., DOLENEC, M. 63

Rock failures in tunnels

Zruški v predorih

ČARMAN, M. 77

The solution of differential equations of fluid flow by numerical program

YILMAZ, L. 87

Optimization of geo-mechanical-structural drilling with diamond crowns

Optimizacija geomehansko strukturnega vrtnja z diamantnimi kronami

ŠPORIN, J., VUKELIĆ, Ž. 97

Filling-up mine spaces of »Block 1« and »Block 2« in the Uranium mine Žirovski vrh from the surface and remediation of a damaged cementation of well for filling-up mine spaces

Zapolnjevanje jamskih prostorov bloka 1 in 2 rudnika urana Žirovski vrh iz površine in sanacija poškodovane cementacije vrtine za zapolnjevanje jamskih prostorov

ŠPORIN, J., STERNAD, Ž., VUKELIĆ, Ž., LIKAR, B., GANTAR, I. 117

Geotechnical conditions for construction of sanitary disposal site »Luka-vačka rijeka«, B&H

ŠKRPIĆ, N., BAŠAGIĆ, M., LANGOF, Z., SKOPLJAK, F. 127

Author's Index, Vol. 54, No. 1	139
Instructions to Authors	140
Template	143
No. of indexing of RMZ-M&G in singular Databases	
Število indeksiranih člankov iz RMZ-M&G v posameznih bazah	150

Hot forming of AISI D2 tool steel

Vročje preoblikovanje AISI D2 orodnega jekla

TATJANA VEČKO PIRTOVŠEK¹, GORAN KUGLER¹, PETER FAJFAR¹, MATEVŽ FAZARINC¹,
IZTOK PERUŠ², MILAN TERČELJ¹

¹University of Ljubljana, Faculty of Natural Sciences and Engineering, Department of Materials and Metallurgy, Aškerčeva cesta 12, SI-1000 Ljubljana, Slovenia;

E-mail: tpirtovsek@metalravne.com; goran.kugler@ntf.uni-lj.si;

peter.fajfar@ntf.uni-lj.si; matevz.fazarinc@arnes.guest.si; milan.tercelj@ntf.uni-lj.si

²University of Ljubljana, Faculty of Civil and Geodetic Engineering, Department of Civil Engineering, Jamova cesta 2, SI-1000 Ljubljana, Slovenia;

E-mail: iztok.perus@fgg.uni-lj.si

Received: July 4, 2007

Accepted: July 10, 2007

Abstract: Surface cracking during hot forming of AISI D2 tool steel is a serious problem since very frequently charges occur that exhibit decreased hot deformability in comparison to other charges. By means of laboratory hot compression tests the approximate framework of mean technological parameters of hot forming was obtained. The tests for as-cast and for deformed initial state in temperature range 850-1150 °C, strain rate range 0.001-10 °C and strain range 0-9 were carried out. On the base of obtained flow curves the processing maps for both states have been developed. The results obtained indicate that hot forming of as-cast state in initial phase of deformation process is not stable whereas the deformed state did not exhibit any un-stable area. Further improvement of hot deformability was obtained by optimisation of chemical composition based on data of surface cracking from industrial hot forming process. The analysis carried out by CAE neural network revealed the influences of carbide-forming element on occurrence of surface cracking. The results of analyse were additionally supported by THERMOCALC calculations. It was shown that variable nature of chemical composition of tool steel results also in variability of precipitation temperature of eutectic carbides.

Izveleček: Nastanek razpok med vročim preoblikovanjem AISI D2 orodnega jekla je zelo resen problem, saj se zelo pogosto pojavijo šarže, ki izkazujejo nižjo sposobnost plastičnega preoblikovanja v primerjavi z ostalimi šaržami. Z laboratorijskimi testi smo najprej določili okvirne vrednosti parametrov za vroče preoblikovanje. Omenjene teste smo opravili tako za lito, kot tudi za predelano izhodno stanje. Dobljene krivulje tečenja so nam služile za izdelavo procesnih map; ti rezultati kažejo na nestabilnost v začetni fazi preoblikovanja za lite mikrostrukture, medtem ko predelano stanje ne izkazuje nobenih nestabilnih področij. Nadaljnje izboljšanje vročega

preoblikovanja smo dosegli z optimiranjem kemične sestave, s pomočjo CAE nevronske mreže in na osnovi baze podatkov pridobljene v industrijski praksi, saj je bila predhodno opravljena analiza vplivov kemičnih elementov na izplen vročega valjanja. Nekateri rezultati omenjene analize so bili dodatno podkrepjeni tudi z izračuni s pomočjo THERMOCALC-a, ki kažejo na to, da variabilna kemična sestava (karbidotvorni elementi) vpliva na temperaturo izločanja evtektičnih karbidov.

Key words: D2 tool steel, hot deformability, as-cast state, deformed state, hot compression, processing map, chemical composition, CAE neural networks

Ključne besede: D2 orodno jeklo, vroča preoblikovalnost, lito stanje, predelano stanje, vroče stiskanje, procesne mape, kemična sestava, CAE nevronske mreže

INTRODUCTION

Very frequently and unexpected high density of surface cracking (Figure 1a-b) occurring in hot rolling of AISI D2 tool steel, despite the rolling process took place in prescribed technological parameters, is still today insufficient researched area. In order to achieve the desired mechanical properties the steels are alloyed with Cr, V, Mo etc (carbide-forming elements, M_7C_3 , MC , M_6C , $M_{23}C_6$, etc) that results in higher yield strength, better tempering resistance, higher wear and fatigue resistance, and considerably lower hot ductility. Thus the windows of technological parameters for safe hot forming with regards to temperature, strains, strain rates, etc are very narrow. Additionally hot deformability is influenced by previous thermo-mechanical processing parameters, i.e. (casting temperature, cooling rate, soaking temperature, etc) and chemical composition. The mentioned carbides besides other brittle phases precipitated (segregation) on grain boundary accelerate cracking at lower and medium area of temperature range. The effect of carbides on hot ductility depends on their number and size, type,

morphology and distribution. As deformation proceeds voids tend to form around the carbides by decohesion and/or fracture of the particles which, in addition to the usual wedge type cracks at triple points, lead to drastic lowering of the ductility of tool steel. Upper limit of temperature range is determined by begin of incipient melting (eutectic carbides and phases with low melting point) and consequently by extensive grain boundary decohesion^[1-15].

Despite the hot forming of tool steels is of great interest from both fundamental and industrial viewpoints, there has been little research reported in the scientific literature about hot forming of tool steels. The researches are namely predominately focused on deformed state that usually exhibit considerably higher hot deformability in comparison to as-cast state; consequently the results do not approach enough to conditions occurring at initial and very critical phase of hot forming of as-cast microstructure.

AISI D2 tool steel has found his application mainly for cold forming, i.e., rolling threads, trimming tools, cutting

tools, broaches, etc. Due to its relatively low hot deformability it reduces the profitability of the production process as well as the useful mechanical properties of the tool steel because of the defects in the material that can originate from its hot deformation.

For elucidation of occurrence of cracking in initial phase of hot rolling of AISI D2 tool steel the hot compression tests for as-

cast and for deformed state, and analyse (CAE NN) of influences of chemical composition on surface cracking were carried out. Obtained results were additionally supported by THERMOCALC calculations of influences of chemical composition on precipitation temperature of eutectic carbides. Processing maps have been developed in order to reveal area of safer hot forming.

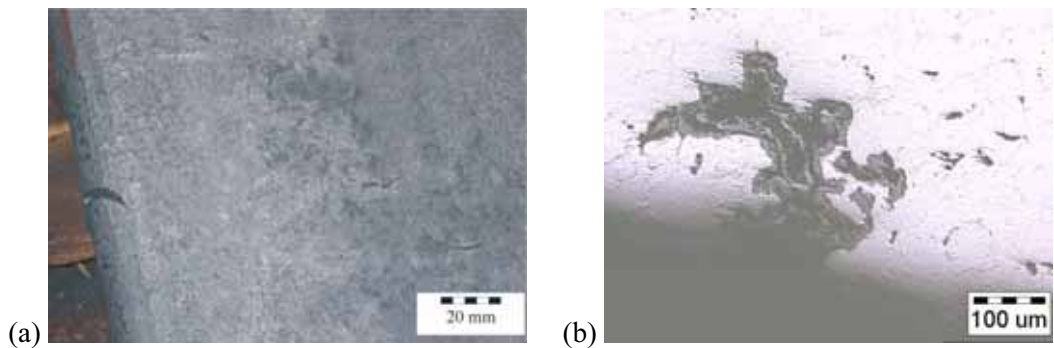


Figure 1. Occurrence of the surface cracks on rolling (AISI D2), macro-view (a), and detailed presentation of crack (b)

Slika 1. Pojav površinskih razpok med vročim valjanjem AISI D2 orodnega jekla, makro posnetek (a), in detajlnější prikaz razpoke (b)

EXPERIMENTAL – LABORATORY TESTING AND MATERIALS

Applied materials and hot compression

Computer controlled servo-hydraulic machine Gleeble 1500 was applied for hot compression testing to study hot forming of as-cast and of deformed initial state of AISI D2 tool steel. The allowable range of chemical composition of AISI D2 tool steel is given in Table 1. Cylindrical hot compression specimens of Rastegew type with dimensions $\phi=10$ mm x 15 mm were

cut from ingot (as-cast state) of cross-sectional 400x400 mm and from rod (deformed state) of cross-sectional $\phi=20$ mm. For reduction of friction between the cylindrical specimen and the tool, and to avoid their mutual welding, graphite lubricant and tantalum follies were used. After deformation the specimens were rapidly quenched with water.

The hot compression tests was performed in the temperature range from 850 °C to 1180 °C, at five different strain rates (0.001, 0.01, 0.1, 1 and 10 s⁻¹) and in strain

range 0 - 0.9 (Figure 3). The heating rate was 3 °C/s, soaking time of 5 min at 1160 °C, followed by cooling at a rate of 2 °C/s down to the deformation temperature and

with a soaking time of 5 min again. The initial microstructure of as-cast state and the deformed state are given in Figure 2a and Figure 2b, respectively.

Table 1. The ranges of permissible variation of chemical composition according to EN ISO 4957 (wt%), D2 tool steel

Tabela 1. Področje dovoljenega variiranja kemične sestave glede na EN ISO 4957 (wt%), D2 orodno jeklo

	C	Si	Mn	Cr	Mo	V	P	S
Range of variation	1.45 1.60	0.10 0.60	0.20 0.60	11.0 12.0	0.70 1.00	0.70 1.00	max 0.030	max 0.030

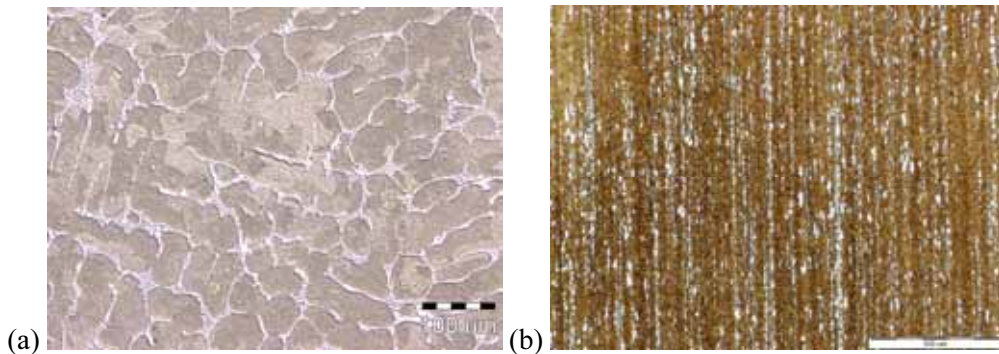


Figure 2. Initial microstructures of applied tool steel (AISI D2), as-cast state (network of eutectic carbides) (a), deformed state (b)

Slika 2. Začetna mikrostruktura uporabljenega orodnega jekla (AISI D2), lito stanje (mreža eutektičnih karbidov) (a), deformirano stanje (b)

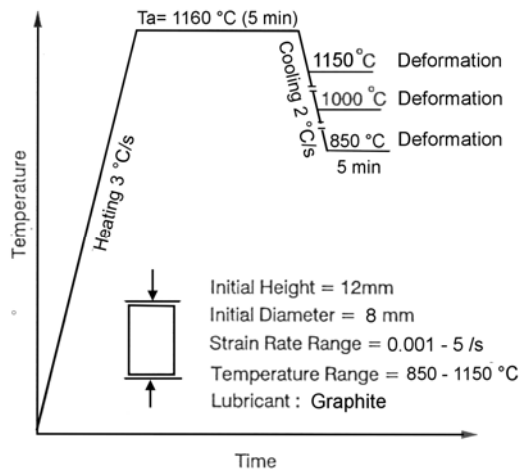


Figure 3. Schematic representation of the time-temperature course for the tested cylindrical specimens

Slika 3. Shematski prikaz poteka temperature vzorcev med vročimi stiskalnimi preizkusi

Flow curves

In such way obtained flow stresses for as-cast and for deformed state at strain rates of 1 s^{-1} and 0.1 s^{-1} are presented on Figure 4a and Figure 4b, respectively.

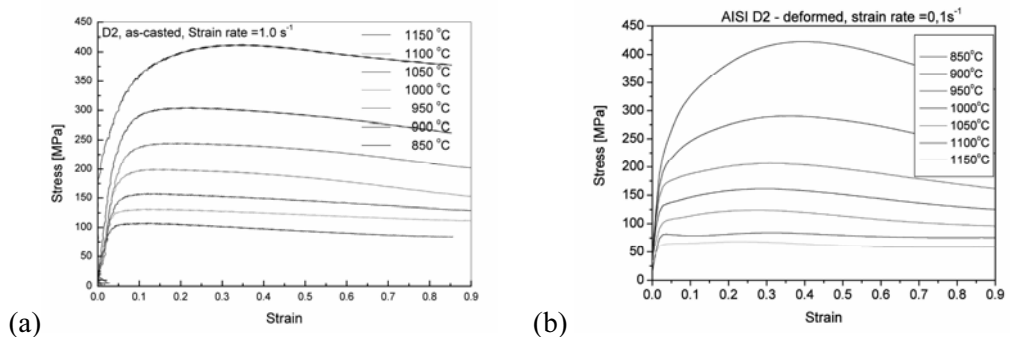


Figure 4. Flow stresses in temperature range 850-1150 °C for as-cast initial state (strain rate of 1 s^{-1}) (a), for deformed initial state (strain rate of 0.1 s^{-1}) (b)

Slika 4. Vroče krivulje tečenja v temperaturnem območju 850-1150 °C, za lito stanje (hitrost deformacije 1 s^{-1}) (a), za predelano stanje (hitrost deformacije $0,1 \text{ s}^{-1}$) (b)

PROCESSING MAPS

Efficiency of power dissipation processing maps

Processing maps are developed on the basis of a dynamic material model (DMM) which has been suggested and widely used by the group of Prasad^[16-17]. The processing map of the material can be described as an explicit representation of its response to the imposed process parameters. It is a superimposition of the efficiency of power dissipation and an instability map.

The work-piece under hot deformation conditions of this model works as an essential energy dissipater. The constituent equation describes the manner in which energy P is converted at any instant into two forms, thermal energy G making temperature increase and microstructural change caused by transform of metallurgical dynamics J , which are not recoverable. In general, most of the dissipation is due to a temperature rise and only a small amount of energy dissipates through microstructural changes. The power partitioning between G and J is controlled by the constitutive flow behaviour of the material and is decided by the strain rate sensitivity m of flow stress as shown in the equation

$$\frac{dJ}{dG} = \frac{\dot{\varepsilon} \frac{d\bar{\sigma}}{d\dot{\varepsilon}}}{\bar{\sigma} \frac{d\dot{\varepsilon}}{d\ln\dot{\varepsilon}}} = \frac{\dot{\varepsilon} \bar{\sigma} \frac{d \ln \bar{\sigma}}{d \ln \dot{\varepsilon}}}{\bar{\sigma} \dot{\varepsilon} \frac{d \ln \dot{\varepsilon}}{d \ln \dot{\varepsilon}}} \approx \frac{\Delta \log \bar{\sigma}}{\Delta \log \dot{\varepsilon}} = m \quad (1)$$

For an ideal dissipater it can be shown that both quantities J and G are equal in their amount, which means that $m = 1$ and $J =$

J_{max} whereas the efficiency of power dissipation η is given by:

$$\eta = \frac{J}{J_{max}} = \frac{2m}{m+1} \quad (2)$$

The variation of η with temperature and ε represents the relative value of energy dissipation occurring through microstructural changes. Microstructural changes, which includes a dynamic recovery and dynamic recrystallization, are predominately stable, and instable, which includes wedge cracking, void formation at hard particles, dynamic strain ageing and macro-structural cracking. As new surfaces are formed during instable changes, more energy is required, while stable changes always take place by grain boundary migration.

Flow instability

The instability map is defined by a stability criterion for a dynamic material, where the differential quotient of its dissipative function has to satisfy an inequality condition, given by Equation 3, to allow a stable flow.

$$\xi \left(\frac{\dot{\varepsilon}}{\varepsilon} \right) = \frac{\partial \ln(m/(m+1))}{\partial \ln \dot{\varepsilon}} + m > 0 \quad (3)$$

Figures 5a-b represents processing maps for temperature range from 850 °C to 1150 °C and strain rates 0.001 s⁻¹ to 10 s⁻¹ at strain 0.6 for as-cast and deformed initial state. The maps are similar at various strains. For as-cast initial state (Figure 5a) the instable zone with $\xi < 0$ appears in the temperature range approx. 1060 °C to 1150 °C at all strain rates

and at temperatures around 900 °C for higher strain rates. On the contrary for deformed initial state (Figure 5b) instable zone appears

in very limited range at strain rates of approx. 0.1 s^{-1} and around temperature 1000 °C.

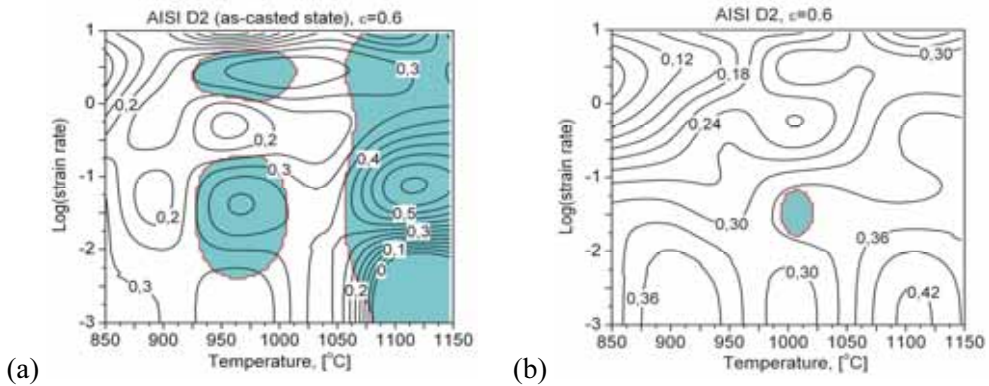


Figure 5. Processing maps for D2 tool steel, for as-cast initial state (a) and for deformed initial state (b), at strain $\varepsilon = 0.6$

Slika 5. Procesne mape za D2 orodno jeklo, za lito stanje (a) in za predelano začetno stanje (b), deformacija $\varepsilon = 0,6$

It is visible from Figure 6b that micro-cracks occurred on specimen edge (see Figure 6a) at average strain 0.8 where also tensile stresses occurred. On the contrary, in the specimen centre (see Figure 6a) micro-cracks free microstructure was obtained since predominately compression

stresses prevail on this spot. Thus as-cast microstructure is very sensitive to micro-cracking at initial deformation on high temperatures (1150 °C) and higher strains (>0.5). No cracks were obtained at lower strains.

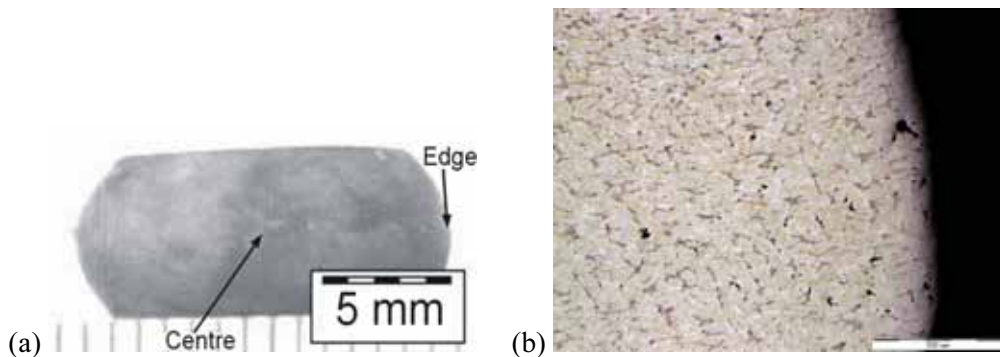


Figure 6. Macro-view of deformed specimen (a), occurrence of micro-cracks on network of eutectic carbides (specimen edge) (b), average strain $\varepsilon = 0.8$, deformation temperature 1150 °C

Slika 6. Makro pogled deformiranega vzorca (a), pojav mikrorazpok na mreži eutektičnih karbidov (rob deformiranega vzorca) (b), deformacija $\varepsilon = 0,8$, temperatura 1150 °C

ANALYSE OF INFLUENCES OF CHEMICAL COMPOSITION ON CRACKING DURING HOT ROLLING

Forming of data base

In the presented study the database contained 80 hot-rolled samples. In comparison, Szilvassy et al.^[13] applied 128 samples with various chemical compositions for the statistical treatment of the influence of chemical composition on the hot deformability of AISI M2 tool steel. All the rolled pieces had the same nominal chemical composition, which varied from charge to charge within certain limits and thus varied also the phenomenon of surface cracking on the rolled stock. The contents of chemical elements (Si, Cr, V, Mn, Mo, W, etc.) was established by the spectrometric method have an error (depending on the element) between 0.01 % and 0.1 %.

The content of carbon is usually determined by specimen ignition in an induction furnace in combination with detection based on infrared spectre absorption. The typical error is around 1%. The random variation of chemical composition easily covered the whole problem space, though the majority of the information was concentrated somewhere in the middle of the permissible intervals of variation for a single element. Therefore, the diagrams of the relationships are shown only for the interval of greater concentration of information. The appearance of surface cracks was observed for rolled pieces with dimensions 200 mm x 200 mm that were rolled (in the temperature range 1170-900 °C) in 20 passes from an ingot with dimensions 400 mm x 400 mm x 1200mm, that were previously soaked for 2 hours at 1200 °C. Thus, the influence of chemical composition on the hot deformability was studied; in our case using information on the variation of industrial charge compositions

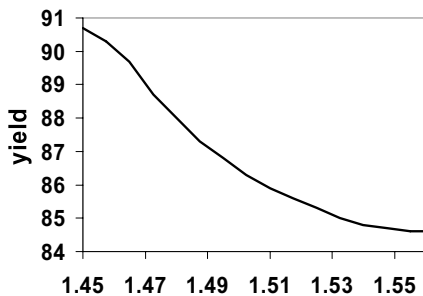
and the formation of surface cracks on the rolled stock. The deformability criterion was thus the yield percentage during hot rolling that varied in the approximate interval 78-95 %. The interval of permissible variations for the most important elements was relatively narrow, and it is given in Table 1.

Influence of the chemical composition on surface cracking

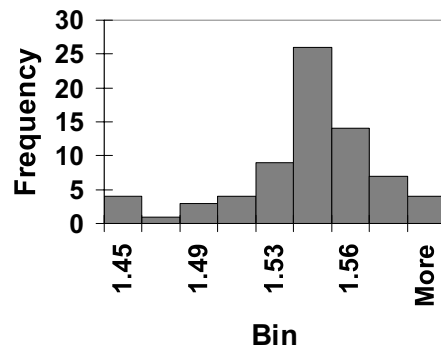
Influence of the carbon

The CAE NN was applied to analyze both the individual and group influences on the phenomenon of surface cracking. Figure 7a

makes it evident that the yield is improved by reducing the carbon content (the distribution frequency is given in Figure 7b). This means that the carbon content must be on the lower limit of the permissible interval of variations. These results correspond to the experimental findings (M2 tool steel) given in reference^[18] where a better hot deformability was obtained with lower carbon contents. Carbon forms carbides with the V, Cr, Mo, Ti, and W present in steel, which in general increases the yield strength and simultaneously reduces the hot deformability very significantly.



(a)



(b)

Figure 7. Yield depending on the carbon content (a), and histogram of the distribution frequency of the data (b)

Slika 7. Izplen v odvisnosti od vsebine ogljika (a), histogram frekvence porazdelitve podatkov (b)

Influence of V/C ratio

The yield as a function of the vanadium / carbon ratio (V/C) is presented in Figure 8a, and the distribution frequency of the data is presented in Figure 8b. It is evident that some of the vanadium data are somewhat outside the interval of permissible variations (up to approximately 0.3 % V). Furthermore, Figure 8a makes it evident

that there is no correlation between the yield and the carbon and vanadium contents for the interval of permissible variations (0.8-1.1 %).

If the data outside the interval of permissible variations are also enclosed in the database, then Figure 8a shows that the yield is increased with lower vanadium

contents. In the interval of permissible variations of the carbon and vanadium contents there is nearly no correlation between the V/C ratios and the yields; the same finding is also given in reference^[18]. If the data outside the permissible interval are also enclosed in the database then it is evident that reduced V/C ratios (V on the lower permissible limit) give better yields. This unclear relationship (i.e., nearly no correlation) in the permissible interval for vanadium (at V/C ratios of about 0.4 or

higher) can be ascribed to the already-mentioned lower accuracy in determining yields and to the relatively narrow interval of the permissible variations of vanadium in the AISI D2 tool steel. Similar relationships, i.e., higher hot-deformability values at lower vanadium contents, were also found by Szilvassy et al.^[13] for the BRM2 tool steel, which had a somewhat wider interval of permissible variations, and by Mohamed^[19], for ordinary steel.

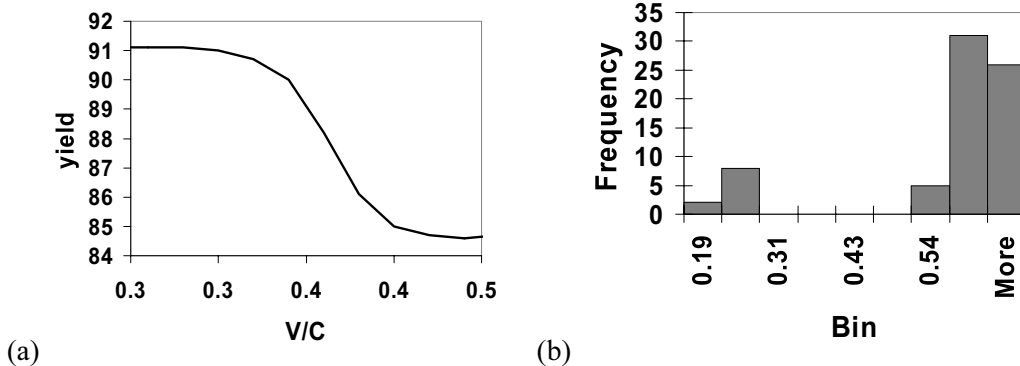


Figure 8. Yield as a function of the V/C ratio for $w_{min} = 0.07$ and $w_{max} = 0.15$ (a) with the frequency distribution (b)

Slika 8. Izplen v odvisnosti od razmerja V/C za $w_{min} = 0,07$ in $w_{max} = 0,15$ (a) s frekvenco porazdelitve podatkov (b)

Influence of the Cr/C ratio

The results of the analysis of the chromium's/carbon ratio influence are given in Figure 9a (the chromium/carbon distribution is given in Figure 9b). The yield is improved with higher chromium contents in the tool steel. However, this could be explained by the following:

- Vanadium tends to form carbides of the MC type, which are extremely hard and thus they hinder the movements of dislocations; chromium, which has a

similar affinity for carbon as vanadium (i.e., a similar Gibbs free energy) tends to form carbides of the $M_{23}C_6$ type, which are softer and thus they hinder movement of dislocations to a lesser extent, since they can be crushed during the working. Thus, chromium competes with vanadium to bind with carbon. The chromium content on the upper limit would thus increase the volume portion of softer $M_{23}C_6$ carbides and therefore reduce the

portion of harder MC carbides. This results in a higher workability of the tool steel and thus a higher yield^[4-5].

- Higher Cr content could increase the temperature (above 1150 °C) of pre-

cipitation of eutectic carbides (M_7C_3) on grain boundaries and thus could influence on deformability at the initial deformations of ingots.

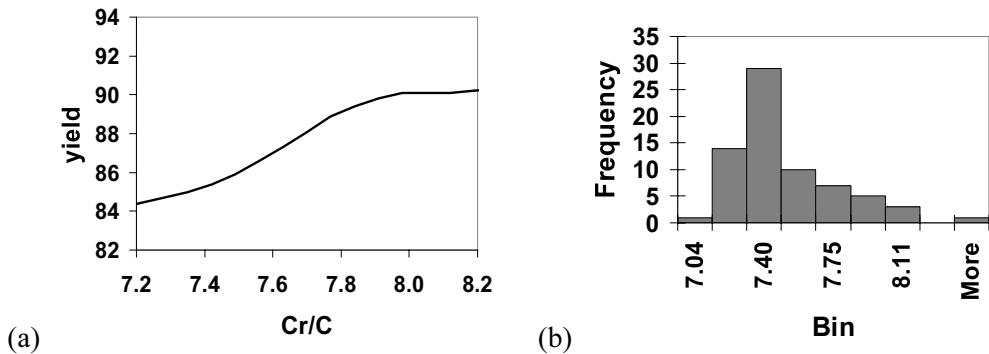


Figure 9. Yield as a function of the Cr/C ratio (a), and histogram of the corresponding frequency distribution of the Cr/C ratio (b)

Slika 9. Izplen v odvisnosti od razmerja Cr/C (a) s frekvenco porazdelitve podatkov (b)

Influence of the Mo/C ratio

There also exists a clear relationship between the molybdenum/carbon ratio and yield: the smaller molybdenum content increases the yield (Figure 10a), Figure 10b shows the frequency distribution. Molybdenum forms carbides of the M_6C type, which have a detrimental influence on the hot deformability.

As already mentioned, the analysis of the influence of vanadium content in the interval of its permissible variations within the V/C ratios did not show any clear relationship with the yield. Therefore, unclear relationships occur between the

yield and the groups of elements enclosing vanadium. On the other hand, there is a very clear relationship between the Cr/Mo ratio and the yield. This indicates that chromium and molybdenum are competitors in reactions with carbon and thus in the formation of carbides. It can be concluded that carbides formed with chromium are less detrimental to the hot deformability.

Hwang et al.^[20-21] obtained in high speed steels used for rolls a reduced quantity of MC carbides at higher chromium concentrations if vanadium was simultaneously present.

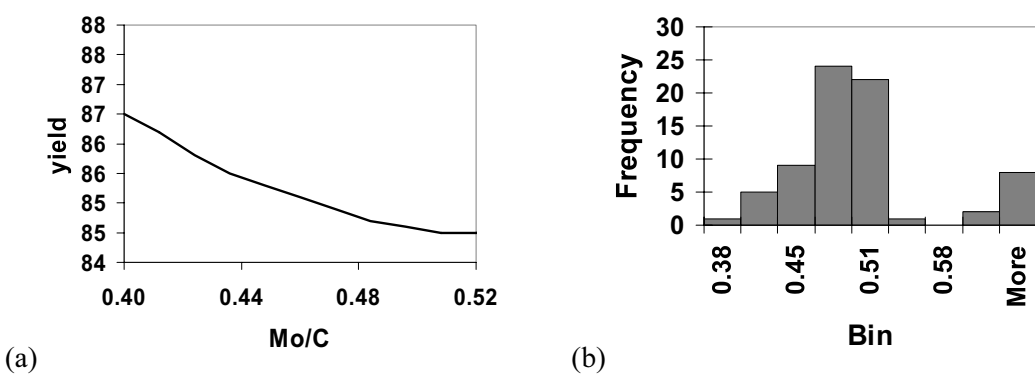


Figure 10. Yield as a function of the Mo/C ratio (a), and the corresponding frequency distribution (b)

Slika 10. Izplen v odvisnosti od razmerja Mo/C (a) s frekvenco porazdelitve podatkov (b)

Calculation of equilibrium phase diagram THERMOCALC for various V, Mo, Cr and C content (lower and upper allowable limit) confirmed the results of the CAE

NN analysis. In the case that Cr content is on upper limit it results in increasing of temperature of precipitation of eutectic carbides.

CONCLUSIONS

In order to increase the hot deformability of AISI D2 tool steel hot compression tests for as-cast and for deformed state in temperature range 850-1150 °C, strain rate range 0.001 - 10 s⁻¹ and strain range 0-0.9 were carried out. Hot deformation behaviours have been also studied by using Prasad's processing maps (efficiency of power dissipation and instability maps) developed on the basis of dynamic materials model. The result revealed that deformation of specimens in as-cast state in the temperature range approximately above cca 1060 °C is not stable due to the occurrence of micro-cracks on network of eutectic carbides.

Additionally influence of chemical composition on appearance of surface cracking during hot rolling by means of CAE NN was obtained. It was found that carbon, vanadium and molybdenum should be on the lower limits of the intervals of permissible variations, whereas the chromium content should be on the upper limit in order to improve the yield. Calculations with THERMOCALC confirm that higher Cr content increase the temperature of precipitation of eutectic carbides and thus elucidate the one of the possible reasons for occurrence of cracks in initial stage of deformation of ingots when as-cast microstructure prevails. We can conclude that to each chemical composition of AISI D2 tool steel also corresponds optimal temperature range of the initial deformations.

POVZETKI

Vročje preoblikovanje AISI D2 orodnega jekla

Da bi izboljšali vročo preoblikovalnost AISI D2 orodnega jekla smo izvedli vroče stiskalne preizkuse v temperaturnem območju 850-1150 °C, v območju hitrosti deformacij 0,001-5 s⁻¹ ter deformacijskem območju 0-0,9. Obnašanje materiala med preoblikovanjem je bilo proučevano tudi s Prasadovimi procesnimi mapami (učinkovitost porazdelitve energije in mape nestabilnosti). Mape nestabilnosti nam kažejo na nestabilnost v začetni fazi preoblikovanja lite mikrostrukture (1150-1080 °C) saj pride v vzorcu na mestih s pretežno nateznim napetostnim stanjem do nastanka mikrorazpok. Posledično se

moramo pri liti mikrostrukturi izogibati nateznim napetostnim stanjem v deformacijski coni in temu ustrezno izbrati tudi optimalni preoblikovalni postopek.

S pomočjo CAE nevronske mreže in na osnovi podatkov o izplenu iz industrijske proizvodnje smo analizirali vpliv kemične sestave na zvišanje preoblikovalnosti. Rezultati analize kažejo na to, da morajo biti ogljik, V in Mo na spodnji meji, medtem ko pa Cr na zgornji meji območja dopustnega variiranja. Ti rezultati so bili potrjeni tudi z izračuni s pomočjo THERMOCALC-a, ki kažejo na variabilnost temperature izločanja evtektičnih karbidov v odvisnosti od kemične sestave. Vsaki kemični sestavi tako ustreza neko optimalno področje začetnih deformacij.

REFERENCES

- [1] ERVASTI, E., STÄHLBERG, U. (2000): Transversal cracks and their behaviour in the hot rolling of steel slabs. *Journal of Materials Processing Technology.*; Vol. 101, No. 1-3, pp. 312-321.
- [2] IMBERT, C.A.C., MCQUEEN, H.J. (2001): Hot ductility of tool steels. *Canadian Metallurgical Quarterly.*; Vol. 40, pp. 235-244.
- [3] RODENBURG, C., KRYZANOWSKI, M., BEYNON, J.H., RAINFORTH, W.M. (2004): Hot workability of spray-formed AISI M3:2 high speed steel. *Materials Science and Engineering.*; Vol. 386, pp. 420-427.
- [4] IMBERT, C.A.C. and MCQUEEN, H.J. (2000): Dynamic recrystallisation of D2 and W1 tool steels. *Materials Science and Technology.*; Vol. 16, No. 5, pp. 532-538.
- [5] IMBERT, C.A.C. and MCQUEEN, H.J. (2000): Flow curves up to peak strength of hot deformed D2 and W1 tool steels. *Materials Science and Technology.*; Vol. 16, No. 5, pp. 524-531.
- [6] KOPP, R. and BERNRATH, G. (1999): The determination of formability for cold and hot forming conditions. *Steel Research.*; Vol. 70, pp. 147-153.
- [7] KLEBER, S. and WALTER, M. (2003): Physical Simulation and Analysis of the Hot Workability of a New Powder Metallurgical "Micro.Clean" HS-Steel Grade. *Materials Science Forum.*; Vol. 426-432, pp. 4173-4178.
- [8] HUCHTEMANN, B. and WULFMAIER, E. (1998): Begleitelemente in Edelbaustählen und ihr Einfluss auf die Verarbeitungseigenschaften. *Stahl und Eisen.*; Vol. 118, No. 11, pp. 129-135.

- [9] THOME, R. and DAHL, W. (1995): On the crack susceptibility of high alloyed tool steels during continuous casting and in the temperature region of hot working. *Steel Research.*; Vol. 66, pp. 63-70.
- [10] MINTZ, B. (1999): The influence of Composition on Hot Ductility of Steels and the Problem of Transverse Cracking. *ISIJ International.*; Vol. 39, No. 9, pp. 833-855.
- [11] IMAI, N., KOMATSUBARA, N., KUNISHIHE, K. (1997): Effect of Cu and Ni on Hot Workability of Hot-rolled Mild Steel. *ISIJ International.*; Vol. 37, No. 3, pp. 224-231.
- [12] IMAI, N., KOMATSUBARA, N., KUNISHIHE, K. (1997): Effect of Cu, Sn and Ni on Hot Workability of Hot-rolled Mild Steel. *ISIJ International.*; Vol. 37, No. 3, pp. 217-223.
- [13] SZILVASSY, C.C. and WONG, W.C.K. (1992): Statistical classification of chemical composition and microstructure as a function of tool-steel deformability. *Journal of Materials Processing Technology.*; Vol. 29, pp. 191-202.
- [14] MATSUOKA, H., OSAWA, K., ONO, M., OHMURA, M. (1997): Influence of Cu and Sn on Hot Ductility of Steels with various C Content. *ISIJ International.*; Vol. 37, No. 3, pp. 255-262.
- [15] MILOVIC, R., MANOJLOVIC, D., ANDJELIC, M. and DROBNJAK, D. (1992): Hot workability of M2 type High-speed steel. *Steel Research.*; Vol. 63, pp. 78-84.
- [16] PRASAD, Y.V.R.K., SASIDHARA, S. (1997): Hot Working Guide, Compendium of Processing Maps. *ASM – International.*; pp. 1-24, OH, USA.
- [17] NARAYANA MURTY, S.V.S., NAGESWARA RAO, B., KASHYAP, B.P. (2000): Instability criteria for hot deformation of materials. *International Materials Reviews.*; Vol. 45, No. 1, pp. 15-26.
- [18] SPITTEL, M., WEISS, C., SPITTEL, T. (1991): Einfluss der chemische Zusammensetzung und der Umformbedingungen auf das Warmumformvermögen von Schnellarbeitsstählen der Typen S6-5-2 und S6-5-2-5. *Neue Hütte.*; Vol. 36, No. 8, pp. 284-289.
- [19] MOHAMED, Z. (2002): Hot ductility behaviour of vanadium containing steels. *Materials Science and Engineering.*; Vol. 326, pp. 255-260.
- [20] HWANG, K.C., LEE, S., LEE, H.C. (1998): Effect of alloying elements on microstructure and fracture properties of cast high speed steel rolls, Part I: Microstructural analysis. *Materials Science and Engineering.*; Vol. 254, pp. 282-295.
- [21] HWANG, K.C., LEE, S., LEE, H.C. (1998): Effect of alloying elements on microstructure and fracture properties of cast high speed steel rolls, Part II: Fracture behaviour. *Materials Science and Engineering.*; Vol. 254, pp. 296-304.

Flow stresses of the AISI A2 tool steel

Krivulje tečenja za AISI A2 orodno jeklo

TATJANA VEČKO PIRTOVŠEK¹, IZTOK PERUŠ², GORAN KUGLER¹, RADO TURK¹, MILAN TERČELJ¹

¹University of Ljubljana, Faculty of Natural Sciences and Engineering, Department of Materials and Metallurgy, Aškerčeva cesta 12, SI-1000 Ljubljana, Slovenia;

E-mail: tpirtovsek@metalravne.com; goran.kugler@ntf.uni-lj.si; rado.turk@ntf.uni-lj.si; milan.tercelj@ntf.uni-lj.si

²University of Ljubljana, Faculty of Civil and Geodetic Engineering, Department of Civil Engineering, Jamova cesta 2, SI-1000 Ljubljana, Slovenia;

E-mail: iperus@siol.net

Received: June 21, 2007 **Accepted:** July 10, 2007

Abstract: The hot deformation behaviour of the AISI A2 tool steel was examined with hot compression tests carried out in the Gleeble 1500D thermomechanical simulator in wide range of temperatures (900-1200 °C), of strain rates (0.001-10 s⁻¹) and of true strains (0-0.7). Due to the increased demands for the accuracy in predicting various parameters for the needs of optimization of hot forming technologies, it is nowadays reasonable to employ artificial intelligence for this purpose. Thus the obtained experimental database of flow stresses (curves) was used for such predictions with the CAE NN (Conditional Average Estimator Neural Network). Regardless of the scarcity of databases for strain rates (experimental data only for each decade) the mentioned approach enables to predict the flow stresses also for their intermediate states. The activation energy for the entire examined temperature range was calculated. The obtained value was compared with the reference data that had been acquired from the analysis of the hot torsion experiment.

Izvleček: Termomehanski simulator Gleeble 1500D je bil uporabljen za študij toplega preoblikovanja AISI A2 orodnega jekla. Stiskalni preizkusi v vročem so bili izvedeni v deformacijskem območju 0-0,7, temperaturnem območju 900-1200 °C in hitrostih deformacije 0,001-10 s⁻¹. Zaradi povečanih zahtev po natančnosti napovedovanja krivulj tečenja za današnje potrebe optimiranja tehnologij toplega preoblikovanja, je za te namene dandanes običajna uporaba nevronske mreže. V našem primeru smo uporabili CAE nevronske mreže s katerimi smo lahko napovedovali krivulje tečenja tudi za vmesna (nemerjena) stanja tako za temperature kot tudi hitrosti deformacije. Izračunana je bila tudi aktivacijska energija za celotno temperaturno območje in primerjana z dobljeno vrednostjo na osnovi torzijskih preizkusov.

Key words: A2 tool steel, hot compression, flow stress, CAE neural network, hyperbolic sine function

Ključne besede: A2 orodno jeklo, vroče stiskanje, krivulje tečenja, CAE nevronske mreže, funkcija sinus hiperbolikus

INTRODUCTION

During the hot deformation many factors (Figure 1) influence the flow stresses of metal. The effects of these factors are very complex and the relationship between the flow stresses and the mentioned factors is a non-linear one, and spatially disordered^[1-4]. The flow stresses during the hot metal forming cannot be in all cases accurately described with phenomenological or empirical mathematical models resulting from experiments. The accuracy is still unsatisfactory and it ranges from 2 to 60 %^[5-10]. Hodgson and Kong^[11-12] report that the accuracy needed for the prediction of flow stresses should be within 5 % for an efficient optimization of hot rolling technologies. Physically-based models have been improved quite a lot, but they

are still limited more or less to rather pure metals and are not yet used in industrial applications^[13], thus the development of constitutive equations from a purely empirical basis to a more physical-basis remains an important long term scientific objective. In spite of constantly new constitutive models for describing flow stress, there has not been any substantial improvement in accuracy as far as prediction is concerned. In recent time researchers began to use BP neural networks (BP NN) as an efficient predictive tool for flow stress predictions^[3-4]. In this study we intentionally deal with the so-called CAE NN (Conditional Average Estimator Neural Network) which is, according to the author's opinion and experience, easier for use.

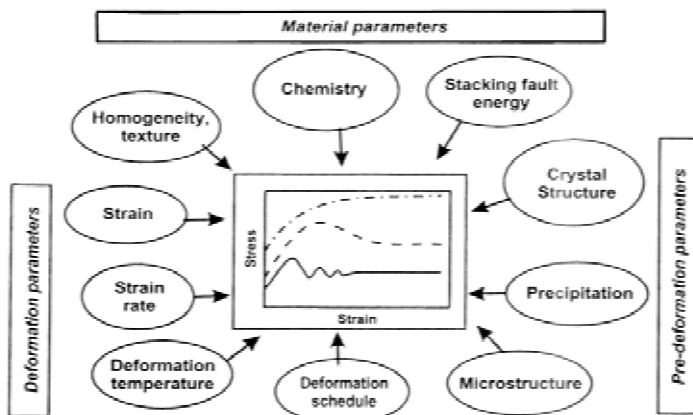


Figure 1. Parameters influencing hot flow stress curves^[2]
Slika 1. Parametri, ki vplivajo na tople krivulje tečenja^[2]

AISI A2 tool steel is conventionally hot forged (or hot rolled) after casting into ingots, and after the intermediate reheating the hot rolling process is continued to obtain the required dimensions. Increase of the productivity is oriented towards the hot forming of ingots with higher initial dimensions (cross sections and lengths) and toward the rolling to smaller dimensions (even below $\phi = 18\text{mm}$); and for that an optimal determination of rolled billet cross-section reductions (roll pass design) with the regard to the loading capacities of the rolling mill itself, to the strength characteristics of the rolls, to the appropriate microstructures, etc is needed to be achieved. In the available references, the characterization of the working properties of the AISI A2 tool steel (generally applied for cold-working) refers

to the hot torsion tests^[14-15], while there are no available data on the hot compression tests.

In this paper hot compression tests were carried out in the Gleeble 1500D thermomechanical simulator to obtain experimental flow stress curves for the AISI A2 tool steel in a wide range of temperatures and strain rates. The flow stress curves were predicted also for intermediate states of influential parameters (strain rates, temperatures and strain) using CAE neural networks, for both, constant and non-constant smoothness parameters. The peak stresses were predicted with the hyperbolic sine function, and the constitutive equation constants were determined.

EXPERIMENTAL PROCEDURE

Specimens and material

The chemical composition of the AISI A2 tool steel is given in Table 1. Cylindrical specimens of the Rastegew type with

dimensions $\phi = 8\text{ mm} \times 12\text{ mm}$ were cut from the rod with cross section of $\phi = 90\text{ mm}$ which had been previously forged from a round (circular) ingot of $\phi = 400\text{ mm} \times 1000\text{ mm}$. The initial microstructure of the specimens is given in Figure 2.

Table 1. Chemical composition of the AISI A2 tool steel (wt %)

Tabela 1. Kemična sestava za AISI orodno jeklo (wt %)

C	Si	Mn	P	S	Cr	Mo	V
1.01	0.30	0.55	0.02	0.02	5.20	1.40	0.20

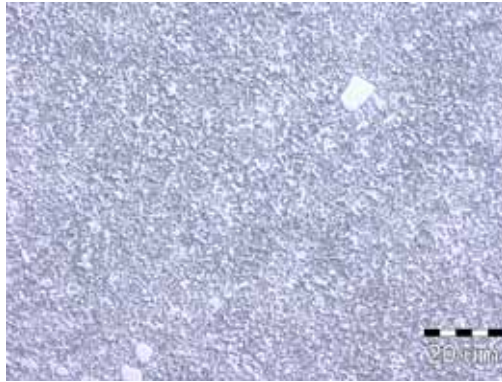


Figure 2. Initial microstructure of the applied tool steel (AISI A2), (soft annealed microstructure - spheroidal pearlite and carbides)

Slika 2. Začetna mikrostruktura orodnega jekla (AISI A2), (mehko žarjena, kroglasti perlit in karbidi)

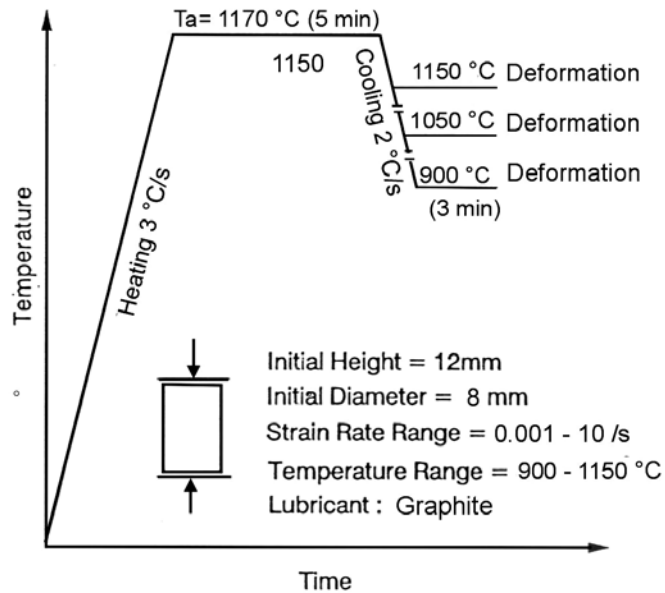


Figure 3. Schematic representation of the time-temperature relationship for the tested cylindrical specimens

Slika 3. Shematski prikaz časovnega poteka temperature vzorca med preizkusom

Procedure and testing conditions

A computer controlled Gleeble 1500 servo-hydraulic machine was used for compression tests. In order to reduce the friction between the cylindrical specimen and the tool, and to avoid sticking, graphite lubricant was used.

The testing conditions for the hot compression tests of cylindrical specimens are given in Table 2. Testing was performed at seven temperatures in the temperature range of 900 to 1150 °C (Figure 3), and with five different strain rates (0.001, 0.01, 0.1, 1, 10 s⁻¹). The heating rate was 3 °C/s, soaking (austenitizing) time 5 min at 1170 °C, followed by cooling at a rate of 2 °C/s down to the deformation temperature; with a further soaking time of 3 min.

It should be stressed here that hot compression at higher temperatures (1200 °C) was not reasonable due to incipient melting; the grain boundary decohesion resulted macro-cracks on the deformed specimens (Figure 4). Figures 5 a-d show the stress-strain relations at different temperatures, between 900 and 1150 °C, with 50 °C intervals, and for five different strain rates, i.e. for 0.001 - 10 s⁻¹, respectively.

The flow stress curves have shapes typical for dynamic recovery (and recrystallization at lower strain rates), while the values of flow stresses are slightly higher in comparison with the results of flow stress curves that were obtained from the hot torsion tests (Imbert et al.^[15-16]). They made tests only at four temperatures and with three strain rates.

Table 2. Values of the main parameters of the test

Tabela 2. Vrednosti glavnih testnih parametrov

Tool steel	Ta	Temp. range	Strain rate
AISI A2	1170 °C	900 -1150 °C	0.001- 10 s ⁻¹

Ta Temperature of austenitizing



Figure 4. Appearance of macro-cracks on the compressed specimen, T = 1200 °C, strain rate = 1 s⁻¹

Slika 4. Pojav razpok na površini deformiranega vzorca, T = 1200 °C, deformacijska stopnja = 1 s⁻¹

APPLICATION OF A CAE NEURAL NETWORK FOR PREDICTION OF HOT FLOW STRESS CURVES

Derived equations

The problem analyzed in this paper is how to estimate the flow stress curves as a function of known parameters (data), i.e. temperature, strain, and strain rate. The first and the second set of variables will be called the output and the input variables, respectively.

Our aim is to demonstrate the potential applicability of the proposed method. In order to determine unknown output variables from the known input variables, a database containing sufficient number of well-distributed and reliable empirical data is needed. The database should include both, the measured values of output variables and the corresponding input variables. One particular observation that is included in the database can be described by a model vector. The input and output variables correspond to the components of this vector. For example, if the corresponding measured stress at the temperature $T = 950$ °C, strain 0.3 and strain rate 5 s^{-1} , is 350 MPa, then the model vector is defined as $\{950, 0.3, 5; 350\}$. The data base consists of a finite set of model vectors. A scheme of the structure of the CAE neural network is presented in references^[16-17].

According to the CAE method, each of the output variables, corresponding to the vector under consideration (i.e. a vector with known input variables and output variables to be predicted), can be estimated by the expressions^[18-22]:

$$\hat{r}_k = \sum_{n=1}^N C_n \cdot r_{nk} \quad (1)$$

where

$$C_n = \frac{c_n}{\sum_{j=1}^N c_j} \quad (2)$$

and

$$c_n = \exp \left[\frac{-\sum_{i=1}^L (p_i - p_{ni})^2}{2w^2} \right] \quad (3)$$

Here, \hat{r}_k is the estimated (predicted) k -th output variable (e.g. *stress*), r_{nk} is the same output variable corresponding to the n -th vector in the database, N is the number of vectors in the database, p_{ni} is the i -th input variable of the n -th vector in the database (e.g. temperature, strain, strain rate), p_i is the i -th input variable corresponding to the vector under consideration, and L is the number of input variables.

Equation 1 suggests that the estimate of an output variable is computed as a combination of all output variables in the database. Their weights depend on the similarity between the input variables p_i of the vector under consideration, and the corresponding input variables p_{ni} pertinent to the sample vectors stored in the database. C_k is a measure of similarity. Consequently, the unknown output variable is determined in such a way that the computed vector composed of the given and estimated data is the most

consistent with the sample vectors in the database.

The parameter w is the width of the Gaussian function and is called the smoothness parameter. It determines how fast the influence of data in the sample space decreases with the increasing distance from the point whose co-ordinates are determined by the components (input variables) of the vector under consideration. The larger is the value of w , the more slowly this influence decreases. Large w values exhibit an averaging effect. In principle, a proper value of w should correspond to the typical distance between data points. In this case the CAE method flows a smooth interpolation of the functional relation between the input and the output variables.

In some applications, as it will be shown later, a non-constant value of w flows more reasonable results than a constant value. When using non-constant w values, Equation 1 can still be used, but proper, locally estimated values of w_i should be taken into account. The expression for c_n (see Equation 3) can be rewritten as

$$c_n = \exp \left[- \sum_{i=1}^L \frac{(p_i - p_{ni})^2}{2w_i^2} \right] \quad (4)$$

in which different values of w_i correspond to different input variables.

It should be stressed that Equations 1 to 3 were derived mathematically^[18-20], based on the assumption of a constant uncertainty in the input data. The extension of the applicability of these equations to non-constant w values (Equation 4) is,

however, based on physical considerations. Whereas a constant w corresponds to a sphere in an L -dimensional space (L is the number of input variables), a non-constant w value corresponds to a multi-axial ellipsoid in the same space^[21-22].

The choice of an appropriate value of w depends not only on the distribution of data, but also on the latter's accuracy, and on the sensitivity of the output variables to change into the input variables. Some engineering judgment, based on knowledge of the investigated phenomenon, and a trial and error procedure, are needed to determine appropriate value(s) for w .

Training process

The originally proposed procedure^[18] that is called CAE in its extended form and is presented here, consists of two parts. The first part corresponds to the so-called self-organisation of the neurons. When using relatively small databases, this part is not needed. The second part represents the mathematical description of different phenomena, using an optimal estimator, as described in previous section. From this point of view training represents a simple presentation of the data to the CAE neural network. In addition, compared to the conventional back-propagation neural networks (BP NN), testing the model is much simpler. Instead of using approximately 70 % of the data for training and the remaining 30 % of the data for testing, a different approach was used. The predicted parameter, i.e. stress of the stress-temperature-strain-strain rate curve, was predicted for each point. In this process the model vector under consideration was temporarily removed from the database. By several trials

optimal values of the smoothness parameter were obtained. Recently, tests on phenomenon^[28], very different from that presented here, show that such an estimation of the efficiency of the proposed model in general gives more conservative estimates than the conventional approach.

To estimate quantitatively the accuracy of the CAE method for predicting the flow stress curves, the following equation, that enables calculations of the root mean sum of the squared deviations (RMSSD) for each deformation condition, is used:

Results for the A2 tool steel show relatively good agreement between the experimental and CAE predicted results (Figures 5). As the relations between the input and the output variables are relatively simple, a constant smoothing parameter can be used (Equation 3). Greater deviations may be observed at smaller strains, where large gradients of the stress curves exist. It should be noted that smaller values of the smoothness parameter w may

$$RMSSD = \sqrt{\frac{\sum_{i=1}^N (\hat{r}_k - r_k)^2}{N}} \quad (5)$$

The prediction is considered good if the RMSSD value is within 5 % of the mean flow stress for that experimental condition^[11-12]. The mean flow stress σ_{mfs} is calculated according to

$$\sigma_{mfs} = \frac{1}{\varepsilon} \int \sigma \, d\varepsilon \quad (6)$$

be used, which will produce better results, but then the interpolation in the strain rate direction will result in a poor overall behaviour of the proposed model. The accuracy attained with the training data ranges from 1.2 % to 6 %, with an average error of 3.6 %. The accuracy of the prediction based on the testing data ranges from 1.4 % to 7.6 %, with an average error of 4.1 %. The errors arising are in general within the required accuracy limits.

The obtained flow stress curves and their CAE predictions with a constant smoothness parameter

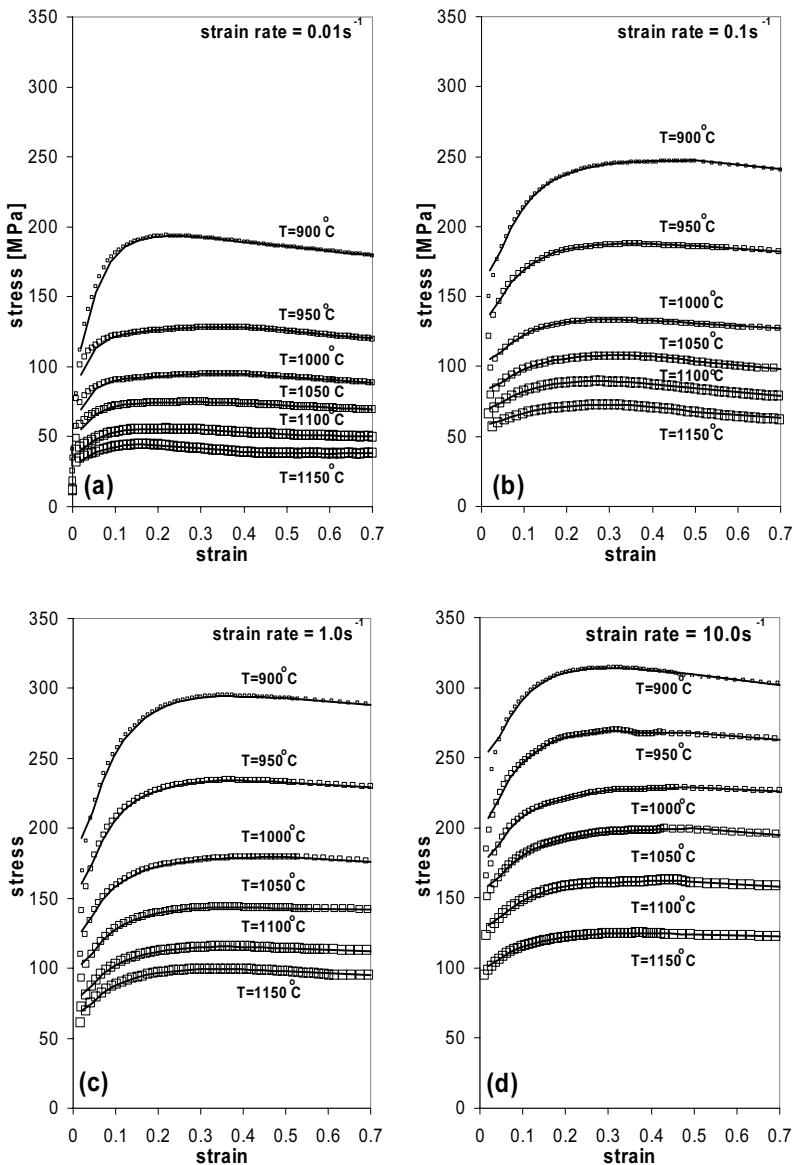


Figure 5. Hot flow stress curves of the AISI A2 tool steel - experimental (\square), and the CAE predicted results ($-$), using a constant smoothing parameter ($w = 0.05$)
Slika 5. Tople krivulje tečenja za orodno jeklo AISI A2 - experimentalne oz. merjene (\square) in CAE napovedane vrednosti ($-$), uporaba konstantnega parametra gladkosti ($w = 0,05$)

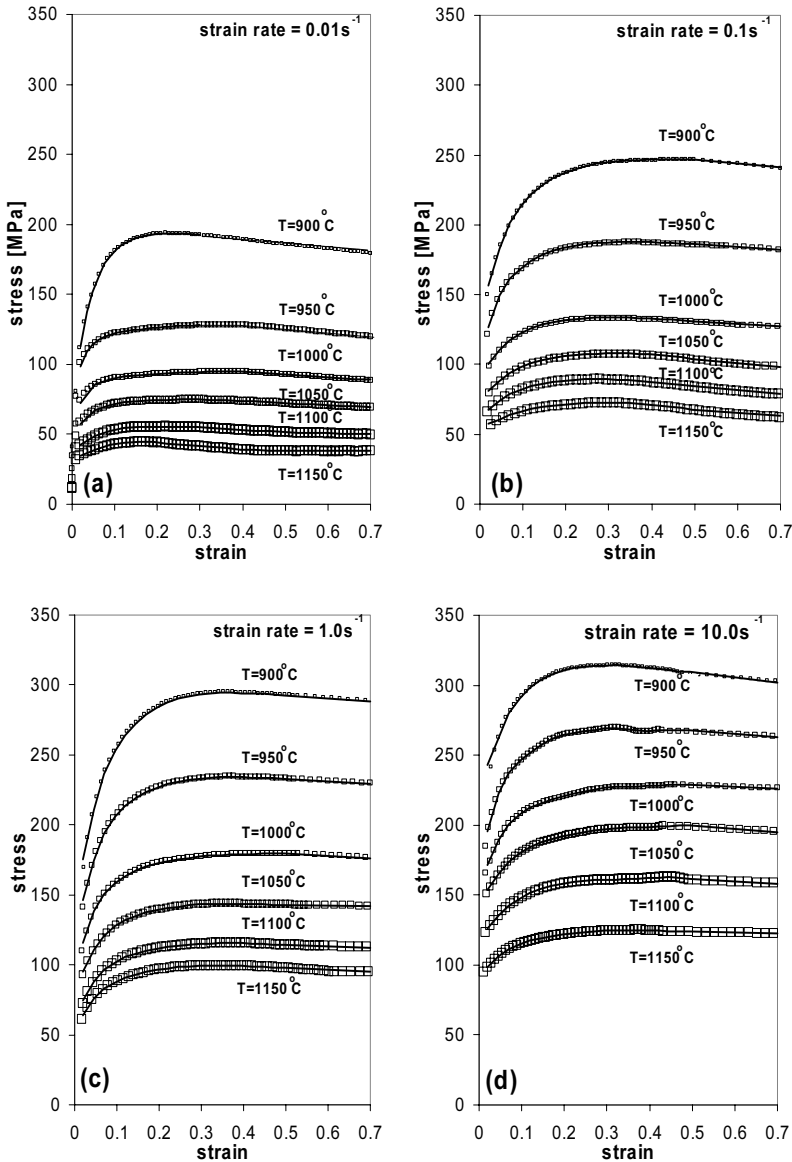


Figure 6. Hot flow stress curves for the AISI A2 tool steel - experimental (\square), and the CAE predicted results ($-$), using a non-constant smoothing parameter ($w_\epsilon = w_T = 0.03$, $w_{\epsilon(\epsilon=0.02)} = 0.01$, $w_{\epsilon(\epsilon=0.52)} = 0.03$)

Slika 6. Tople krivulje tečenja za orodno jeklo AISI A2 - experimentalne oz. merjene (\square) in CAE napovedane vrednosti ($-$), uporaba nekonstantnega konstantnega parametra gladkosti ($w_\epsilon = w_T = 0,03$, $w_{\epsilon(\epsilon=0,02)} = 0,01$, $w_{\epsilon(\epsilon=0,52)} = 0,03$)

CAE prediction with a non-constant (elliptical) smoothness parameter

Figures 6 a-d clearly show great improvements in the strain, ranging from 0.02 to 0.1. The results suggest that modelling the flow stress curves may be improved by using a non-constant smoothing parameter (Equation 4). The accuracy achieved with the training data ranges from 0.1 % to 4.3 %, with an average error of around 2.2 %. The accuracy of predictions based on the testing data ranges from 0.2 % to 5.8 %, with an average error of up to 3 %. The errors arising are in general within the required accuracy limit^[11-12], and are smaller than that obtained with conventional BP neural networks^[3-4].

The ability of CAE NN to interpolate is demonstrated by predicting flow stresses at temperatures and strains over the entire domain in which the model is trained.

Predicting flow stresses for the intermediate input parameters

The real power of the methods for prediction of hot flow stress curves can be clearly recognized from the prediction of the intermediate values of the input parameters. Figure 7a shows the results of the prediction of hot flow stress curves in the direction of the strain rate for $\varepsilon = 0.05$ and $T = 900$ °C. “Experimental” results were calculated from the existing experimental results using linear interpolation

(i.e. data points in the neighbourhood of $\varepsilon = 0.05$ for hot flow stress curves at $T = 900$ °C for different strain rates 0.001 s⁻¹, 0.01 s⁻¹, 0.1 s⁻¹, 1 s⁻¹ and 10 s⁻¹). Figure 7b shows the results of the prediction of hot flow stress curves in the direction of the strain rate for $\varepsilon = 0.3$ at $T = 925$ °C. Experimental results for temperatures 900 and 950 °C at the strain $\varepsilon = 0.3$ are presented as comparison. CAE prediction seems to be a fair estimate of real hot flow stress curve. Note the semi-logarithmic scale, being logarithmic in the direction of the strain rate.

Figure 7c shows the results of the prediction of hot flow stress curves in the direction of strain for the strain rate 1 s⁻¹ and temperature $T = 1025$ °C. Experimental results for temperatures 1050 and 1000 °C at the strain rate 1 s⁻¹ are shown as comparison.

Thus this study confirmed the good predictive power of the CAE NN to predict flow stress curves also for intermediate temperatures and strain rates where experimental data existed only for each decade. However, due to the fairly linear relationship between the strain rates and the stresses that might be observed from the “experimental” results, linear rule might be adopted for better agreement. A so called hybrid CAE model for prediction of hot flow stress curves, considering aforementioned rule, was studied and would be applied in the future.

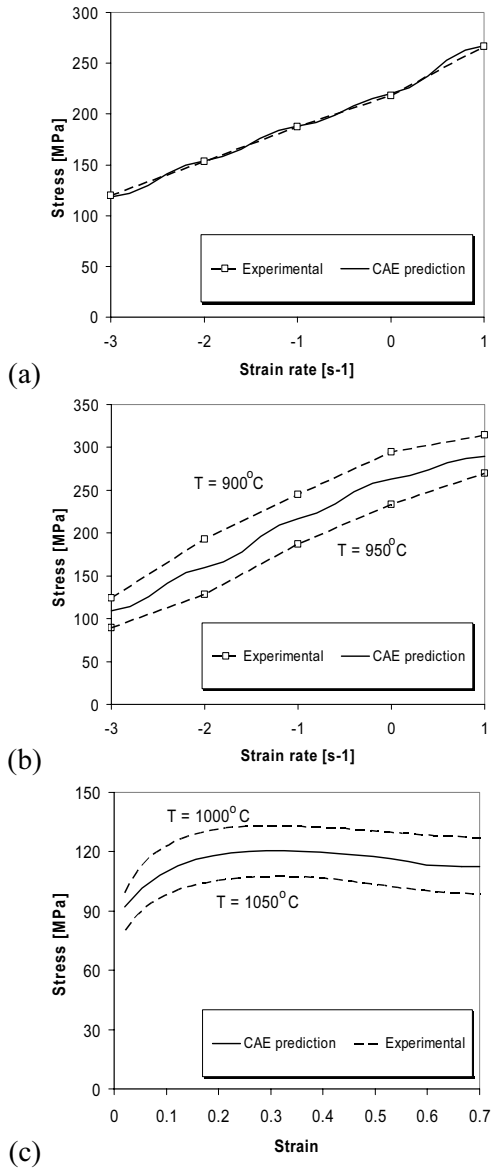


Figure 7. Prediction of hot flow stress curves for material AISI A2 as a function of strain rate for (a) $\varepsilon = 0.05$, $T = 900$ °C, (b) $\varepsilon = 0.3$, $T = 925$ °C and (c) as function of strain for $\dot{\varepsilon} = 0.1$ s⁻¹, $T = 1025$ °C. Non-constant smoothing parameter was used ($w_{\dot{\varepsilon}} = 0.1$, $w_T = 0.05$, $w_{\varepsilon(\varepsilon=0.02)} = 0.01$, $w_{\varepsilon(\varepsilon=0.52)} = 0.03$).

Slika 7. Napovedovanje krivulj tečenja za orodni material AISI A2 za (a) $\varepsilon = 0,05$, $T = 900$ °C, (b) $\varepsilon = 0,3$, $T = 925$ °C in (c) kot funkcija deformacije za $\dot{\varepsilon} = 0,1$ s⁻¹, $T = 1025$ °C. Uporabljen je bil nekonstantni parameter gladkosti ($w_{\dot{\varepsilon}} = 0,1$, $w_T = 0,05$, $w_{\varepsilon(\varepsilon=0,02)} = 0,01$, $w_{\varepsilon(\varepsilon=0,52)} = 0,03$).

DISCUSSION

Imbert and McQueen^[14-15] carried out hot torsion tests on a material of the same grade. These authors obtained somewhat lower values for the flow stress curves. This was expected, since flow stress curves were obtained with torsion tests. The reasons for this discrepancy were firstly a slightly different chemical composition of the tested material, though it was still within permitted limits for the given grade, secondly a different initial microstructure, further, unstable testing conditions, and finally a different heat generation during deformation of the two types of tests.

The constants were calculated from the maximum flow stresses for different temperatures and strain rates with the hyperbolic sine equation^[23-25]

$$Z = \dot{\epsilon} \exp(Q/RT) = A(\sinh \alpha\sigma)^n \quad (7)$$

For this purpose, the function χ^2 which determined the difference between measured and calculated values of maximum flow stresses was defined first:

$$\chi^2 = \sum_{i=1}^N \frac{(z_i - a_1 x_i - a_2 y_i - a_3)^2}{e_i^2} \quad (8)$$

where N was the number of measurements, $z_i = \ln(\sinh \alpha\sigma_i)$, $x_i = \ln \dot{\epsilon}_i$ and $y_i = 10^4 T^{-1}$. Parameter $a_1 = n^{-1}$, $a_2 = 10^{-4} Q n^{-1} R^{-1}$ and $a_3 = n^{-1} \ln A$. When errors were calculated only measurement errors of the parameter z_i , given by $e_i = \alpha e_i^\sigma \coth \alpha\sigma_i$, where e_i^σ were the measurement errors of the flow stresses were taken in account. The

details of the minimization procedure of the above expression (8) are given elsewhere^[26]. χ^2 had a minimum for $Q = 497.5 \text{ kJ mol}^{-1}$, $\alpha = 0.0056 \text{ MPa}^{-1}$, $n = 6.0$ and $A = 7.06 \cdot 10^{19} \text{ s}^{-1}$. The value of the activation energy was higher than that obtained by Imbert and McQueen^[14-15]; they obtained the value of 399 kJ mol^{-1} ($\alpha = 0.012 \text{ MPa}^{-1}$, $n = 3.6$). It is also generally known that hot compression tests flow little higher values of activation energies in comparison to the hot torsion tests. Thus, contrary to the claims of some authors^[27] that it was not easy to calculate factors α directly from the experimental data, we managed it. For these parameters a comparison between the calculated and the measured relationship between peak stresses and temperatures for five different strain rates is shown in Figure 8a and a comparison between the calculated and the measured peak stresses in Figure 8b. McQueen^[13-14] proposed use of an universal value for the coefficient α ($\alpha = 0.012 \text{ MPa}^{-1}$) for steels. In our case and for the value of $\alpha = 0.012 \text{ MPa}^{-1}$ ^[18-19], it flowed $Q = 496 \text{ kJ mol}^{-1}$, $n = 4.0$, and $A = 3.5 \cdot 10^{15} \text{ s}^{-1}$, but we got worse agreement ($\chi^2 = 3.5\text{E-}001$) between the measured and the calculated maximum flow stresses since in our case χ^2 was $1.08\text{E-}001$.

It is clearly seen From Figure 8a that experimental peak values of flow stress curves at testing temperature $900 \text{ }^\circ\text{C}$ are higher than the predicted ones. The mean reason is probably precipitation of carbide particles as a very frequent phenomenon in tool steel at temperatures below $1000 \text{ }^\circ\text{C}$ ^[27]. It means that activation energies should be determined for two temperature ranges, i.e. $900 - 1000 \text{ }^\circ\text{C}$ and $1000 - 1150 \text{ }^\circ\text{C}$, respectively.

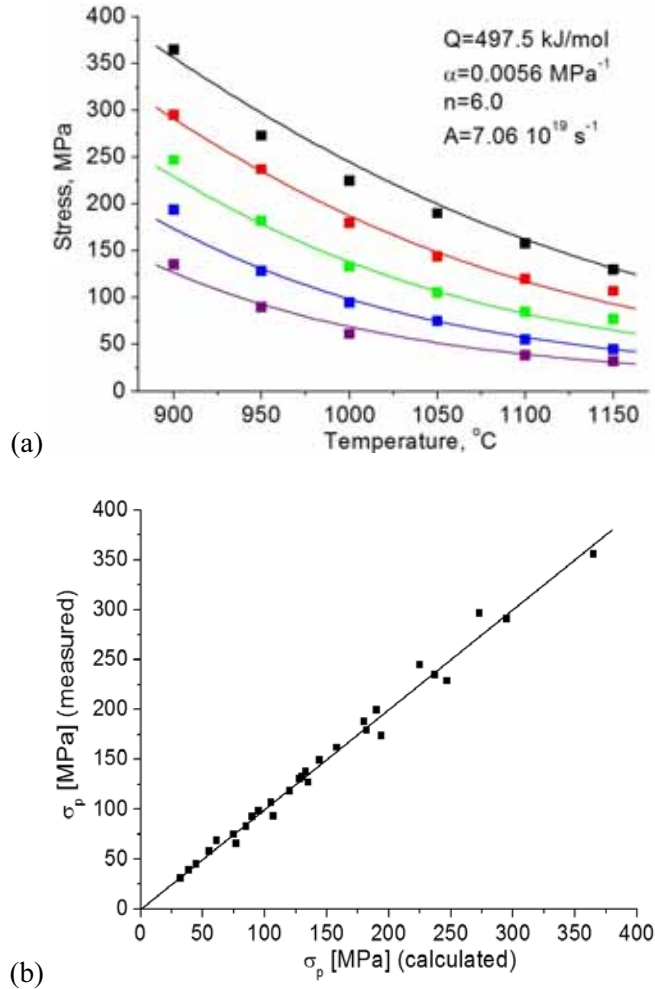


Figure 8. Relationship between peak stresses and temperature of deformation for five different strain rates (from top to bottom: 10 s⁻¹, 1.0 s⁻¹, 10^{-1} s⁻¹, 10^{-2} s⁻¹ and 10^{-3} s⁻¹), squares present measured data and full lines the calculated ones (a). Comparison between the measured and the calculated peak stresses (b).

Slika 8. Zveza med maksimumi napetosti in temperaturo deformacije za pet različnih hitrosti deformacije (od spodaj navzgor: 10 s⁻¹, $1,0$ s⁻¹, 10^{-1} s⁻¹, 10^{-2} s⁻¹ in 10^{-3} s⁻¹), kvadrati predstavljajo merjene vrednosti, polna črta pa izračunane vrednosti (a). Primerjava med merjenimi in izračunanimi maksimumi vrednosti (b).

CONCLUSIONS

For the needs to optimize the hot forming of the AISI A2 tool steel the hot compression tests in the Gleeble 1500D thermo-mechanical simulator were carried out; the test temperatures were in the range (900 - 1150 °C), strain rates (0.001 - 10 s⁻¹) and strains (0 - 0.7). Due to incipient melting, deformations at higher temperatures (1200 °C) should be avoided. This study confirmed the good predictive power of the CAE NN to predict flow stress curves also for the intermediate temperatures and strain rates where experimental data existed only at each decade. Two approaches, namely the method of a constant smoothness parameter and the method of a non-constant smoothness parameter, were examined. The latter gave better results.

POVZETKI

Krivulje tečenja za AISI A2 orodno jeklo

Za potrebe optimiranja tehnologije toplega preoblikovanja, so bili na termomehanskem simulatorju Gleeble 1500D izvedeni stiskalni preizkusi v vročem. Zaradi taljenja eutektičnih karbidov (na višjih temperaturah (cca. 1200 °C)) na kristalnih mejah, preoblikovanje v tem temperaturnem območju zaradi nastanka razpok ni možno. S pomočjo CAE nevronske mreže so bile zelo uspešno napovedane vrednosti za krivulje tečenja, tako za merjena kot tudi za vmesna (nemerjena) stanja. Dobra prediktivna moč je izkazana tudi za vmesna stanja v polju hitrosti deformacij,

Hyperbolic sine equation was additionally applied to predict the peak values of flow stresses. Good agreement between the measured and the predicted values was obtained with an exception at the lowest temperature (900 °C, precipitation of carbides). The calculated activation energy (temperature range 900 - 1150 °C) for the AISI A2 was about $Q = 497 \text{ kJ mol}^{-1}$. That was a higher value, compared with the values ($Q = 399 \text{ kJ mol}^{-1}$, that were obtained with the tangent method based on results of torsion experiments. In cases when precipitation of the carbides at lower temperature range could occur, an activation energy for two temperature ranges should be determined.

saj so tu eksperimentalni podatki samo na vsako dekadno.

Preizkušeni sta bili dve metodi napovedovanja krivulj tečenja z nevronskimi mrežami in sicer metoda s konstantnim ter metoda z nekonstantnim parametrom gladkosti. Slednja daje boljše rezultate. Izračunana je bila tudi aktivacijska energija ($Q = 497 \text{ kJ mol}^{-1}$) za celotno temperaturno območje preizkušanja, ki je nekoliko višja kot dobljena iz torzijskih preizkusov ($Q = 399 \text{ kJ mol}^{-1}$). Izmerjeni ter izračunani (funkcija sinus hiperbolikus) maksimumi krivulj tečenja se dobro ujemajo na celotnem temperaturnem območju, razen na temperaturi 900 °C. Vzrok za to je verjetno v izločanju sekundarnih karbidov pod temperaturo 1000 °C.

REFERENCES

- [1] KOOP, R., LUCE, R., LEISTEN, B., WOLSKE, M., TSCHIRNICH, M., REHRMANN, T. and VOLLES, R. (2001): Flow stress measuring by use of cylindrical compression test and special application to meta forming processes. *Steel Research.*; Vol. 72, pp. 394-401.
- [2] SCHOTEN, K., BLECK, W., and DAHL, W. (1998): Modelling of flow curves for hot deformation. *Steel Research.*; Vol. 69, pp. 193-197.
- [3] LIU, J., CHANG, H., HSU, T.Y., RUAN, X. (2000): Prediction of the flow stress of high speed steel during hot deformation using a BP artificial neural network. *Journal of Materials Processing Technology.*; Vol. 103, pp. 200-205.
- [4] WU, R.H., LIU, J.T., CHANG, H.B., HSU, T.Y., RUAN, X.Y. (2001): Prediction of flow stress of 0.4C-1.9Cr-1.5Mn-1.0Ni-0.2Mo steel during hot deformation. *Journal of Materials Processing Technology.*; Vol. 116, pp. 211-218.
- [5] HATA, N., KAKADO, J.I., KIKUCHI, S., TAKUDA, H. (1985): Modelling on flow stress of plain carbon steel at elevated temperatures. *Steel Research.*; Vol. 56, No. 11, pp. 575-582.
- [6] RAO, K.P. and HAWBOLT, E.B. (1992): Development of constitutive relationships using compression testing of medium carbon steel. *Trans. ASME.*; Vol. 114, pp. 116-123.
- [7] KLIBER, J., SCHINDLER, I. (1997): Mathematical description of stress-strain curve in metal forming processes. *Metallurgija.*; Vol. 36, No. 1, pp. 9-13.
- [8] DAVENPORT, S.B., SILK, N.J., SPARKS, C.N., SELLARS, C.M. (2000): Development of constitutive equations for modelling of hot rolling. *Materials Science and Technology.*; Vol. 16, pp. 539-546.
- [9] LIU, J., CHANG, H., WU, R., HSU, T.Y., RUAN, X. (2000): Investigation on hot deformation behaviour of AISI T1 high-speed steel. *Materials Characterization.*; Vol. 45, pp. 175-186.
- [10] MCQUEEN, H.J., RYAN, N.D. (2002): Constitutive analysis in hot working. *Materials Science and Engineering.*; Vol. 322, pp. 43-63.
- [11] HODGSON, P.D., KONG, L.X., DAVIES, C.H.J. (1999): The prediction of the hot strength of steels with an integrated phenomenological and artificial neural network model. *Journal of Materials Processing Technology.*; Vol. 87, pp. 131-138.
- [12] KONG, L.X., HODGSON, P.D. (1999): The application of constitutive and artificial neural network model to predict the hot strength of steels. *ISIJ Int.*; Vol. 39, No. 10, pp. 991-998.
- [13] KUGLER, G., TURK, R. (2004): Modelling the dynamic recrystallization under multi-stage hot deformation. *Acta Materialia.*; Vol. 52, pp. 4659-4668.
- [14] IMBERT, C.A.C., MCQUEEN, H.J. (2001): Dynamic Recrystallisation of A2 and M2 tool steels. *Materials Science and Engineering.*; Vol. 313, pp. 104-116.
- [15] IMBERT, C.A.C., MCQUEEN, H.J. (2001): Peak strength, strain hardening and dynamic restoration of A2 and M2 tool steels in hot deformation. *Materials Science and Engineering.*; Vol. 313, pp. 88-103.
- [16] TERČELJ, M., PERUŠ, I., TURK, R. (2003): Suitability of CAE neural network and FEM for predicting of wear on die radii in hot forging. *Tribology International.*; Vol. 36, pp. 573-583.
- [17] TURK, R., PERUŠ, I. and TERČELJ, M. (2004): New starting points for prediction of tool wear in hot forging. *International Journal of Machine*

- Tools & Manufacture.*; Vol. 44, No. 12-13, pp. 1319-1331.
- [18] GRABEC, I., SACHSE, W. (1997): *Synergetics of Measurement, Prediction and Control*. ISBN 3-540-57048-9, Springer-Verlag.
- [19] GRABEC, I. (1990): Self-Organization of Neurons Described by the Maximum-Entropy Principle. *Biol.Cybern.*; Vol. 63, pp. 403-409.
- [20] PERUŠ, I., FAJFAR, P. and GRABEC, I. (1994): Prediction of the seismic capacity of RC structural walls by non-parametric multidimensional regression. *Earthquake Eng. Struct. Dyn.*; Vol. 23, pp. 1139-1155.
- [21] FAJFAR, P., PERUŠ, I. (1997): A non-parametric approach to attenuation relations. *Journal of Earthquake Engineering.*; Vol. 1, No. 2, pp. 319-340.
- [22] PERUŠ, I., FAJFAR, P. (1997): A non-parametric approach for empirical modelling of engineering problems. *Engineering Modelling.*; Vol. 10, No. 1-4, pp. 7-16.
- [23] SELLARS, C.M., TEGART, W.J. MCG. (1966): La relation entre la resistance et la structure dans la deformation a chaud. *Mem. Sci. Rev. Metal.*; Vol. 63, pp. 731-746.
- [24] SELLARS, C.M., TEGART, W.J. MCG. (1972): *Int. Metall. Rev.*; Vol. 17, pp. 1-24.
- [25] JONAS, J.J., SELLARS, C.M., TEGART, W.J. MCG. (1969): *Metall. Rev.*; Vol. 130, pp. 1-24.
- [26] KUGLER, G., KNAP, M., PALKOWSKI, H., TURK, R. (2004): Estimation of activation energy for calculating the hot workability properties of metals. *Metallurgia.*; Vol. 43, No. 4, pp. 267-272.
- [27] LIU, J., CHANG, H., WU, R., HSU, T.Y., RUAN, X. (2000): Investigation on hot deformation behaviour of AISI T1 high-speed-steel. *Materials Characterization.*; Vol. 45, pp. 175-186.
- [28] ORETA, A.W.C., KAWASHIMA, K. (2003): Neural Network Modeling of Confined Compressive Strength and Strain of Circular Concrete Columns. *Journal of Structural Engineering.*; Vol. 129, pp. 554-561.

Development of test rig for thermal fatigue testing – preliminary results

Razvoj testne naprave za študij termičnega utrujanja – preliminarni rezultati

MATEVŽ FAZARINC¹, RADO TURK¹, GORAN KUGLER¹, PRIMOŽ MRVAR¹, MILAN TERČELJ¹

¹University of Ljubljana, Faculty of Natural Sciences and Engineering, Department of Materials and Metallurgy, Aškerčeva cesta 12, SI-1000 Ljubljana, Slovenia;

E-mail: matevz.fazarinc@guest.arnes.si; rado.turk@ntf.uni-lj.si; goran.kugler@ntf.uni-lj.si; primoz.mrvar@ntf.uni-lj.si; milan.tercelj@ntf.uni-lj.si

Received: June 21, 2007 **Accepted:** July 10, 2007

Abstract: In this study preliminary results of a new developed test rig for simulation of thermal fatigue/shocks are presented. The rig has computer guided heating and quenching of the specimen that enables constant thermal loading and gathering of reliable experimental data. At the same maximal testing temperature it is possible to generate different and higher temperature gradients in comparison to other tests. Verification of the abilities of the rig was carried out with specimens (AISI H11 tool steel) which had different wall thicknesses (2.75 - 4 mm) and different surface qualities (heat treated, gas nitrided). The gas nitrided specimens exhibited lower thermal fatigue resistance. The shape of cracks was a grid, which is a typical characteristic of tools subjected to thermal fatigue (tools for hot forming of materials, etc.). Some specimens were additionally mechanically loaded and cracks obtained that were at right-angled to the direction of the compression force were essentially detained; their nucleation and growth were suppressed. The measured temperatures in the surface layer were used to calculate the initial stress field using the Finite Element Method (FEM).

Izveček: V tem prispevku so prikazani preliminarni rezultati novo razvite testne naprave za študij termičnega utrujanja kovinskih materialov. Testna naprava ima računalniško vodeno ogrevanje in gašenje testnega vzorca, kar omogoča konstantnost termičnega (temperaturnega) obremenjevanja in pridobivanje zanesljivih eksperimentalnih podatkov. Pri isti maksimalni testni temperaturi, je v primerjavi z ostalimi testi opisanimi v literaturi, mogoče generirati različne in višje temperaturne gradiente. Verifikacija sposobnosti testne naprave je bila napravljena na preizkušancih (AISI H11 orodno jeklo) z različnimi debelinami sten (2,75 - 4 mm) in različnimi kvalitetami površine (toplotno obdelan, plinsko nitriran). Plinsko nitrirani izkazujejo nižjo odpornost na termično utrujanje. Na površini nastane mrežasta oblika razpok,

ki je značilna za orodja, ki jih uporabljamo za vroče preoblikovanje kovin. Nekateri preizkušanci so bili med termičnim utrujanjem še dodatno mehansko obremenjevani pri čemer so razpoke pravokotno na smer obremenjevanja skoraj popolnoma izginile. Izmerjene temperature na površinski plasti preizkušanca so služile za izračun napetostnega polja z uporabo metode končnih elementov (MKE).

Key words: thermal fatigue, test rig, tool steel AISI H11, FEM analysis

Ključne besede: termično utrujanje, testna naprava, orodno jeklo AISI H11, analiza z MKE

INTRODUCTION

Thermal shock and/or fatigue resistance are very important characteristics of a material. The laboratory test rig (equipment) for their evaluation must be capable of carrying out such tests at various temperatures and have the capability, at the same testing temperature, to generate various temperature (stress) fields in order to better evaluate the usage of materials for a specific application. The tests that can be found in the literature cannot fulfil the above mentioned tasks satisfactorily. Poor knowledge of the temperature field within the specimen and consequently also poor knowledge of the stress/strain field results in an inaccurate estimation of the influence of parameters that are responsible for the nucleation and growth of cracks. In the past years an increased demand for improvement experimental data for better numerical modelling of crack growth can be found in the literature. Quenching in water is a very popular method to measure of thermal shock or thermal fatigue resistance but it has some weaknesses due to the unknown (unstable) heat transfer coefficient as a consequence of the

vaporisation of water in the vicinity of the tested specimen surface^[1-4]. Some authors designed special nozzles in order to minimize the effect of water vaporisation^[5]. Marsh et al.^[6], Amiabe et al.^[4] and Hadder et al.^[7] applied the so-called SPLASH test that also utilises water quenching of samples to generate temperature fields. Although they made great progress in modelling of crack growth on the basis of the experimental data further experimental improvements in this research area are desired.

Therefore the goal of this paper was to present a new test rig for better evaluation of thermal shock or thermal fatigue resistance of materials. This test rig enables generation of high thermal stress with well defined thermal boundary conditions which allows the study of the temperature and thermal stress distribution in order to better evaluate the thermal shock or fatigue resistance of the tested material. An especially desirable characteristic of the test should have be the ability to generate various stress fields in the tested sample at the same maximal temperature.

EXPERIMENTAL SET-UP

Test rig and testing parameters

For obtaining reliable test data it is of a great importance that the test is computer controlled and thus highly repeatable. Thus it was found helpful to carry out the tests on a thermo-mechanical simulator of metallurgical states, the Gleeble 1500D, in order to utilize the possibility of computer guided resistance heating of specimens and movement of the working jaws, simultaneously. The main idea was that the specimens would be rapidly heated to the maximum holding temperature and then the surface would be quenched with water. It was estimated that the cracks would form earlier than in 1000 cycles (for tool steel); this would shorten the testing time of a given specimen.

Circular and hollow shaped specimen were applied for testing (Figure 1). The thermocouple (type K) needed for temperature control and guidance was welded inside the specimen in the middle of its testing area, as shown on Figure 1. The outer testing part of the specimen was placed in a cooling chamber (Figure 2). The cooling and emptying process was optimized by a pair of magnetic computer controlled valves. One valve controlled the water quench and the other controlled the air compression to empty the cooling chamber. The valves were guided using the Gleeble 1500D control computer that was programmed simultaneously with the program for thermal and mechanical loading of the specimen.

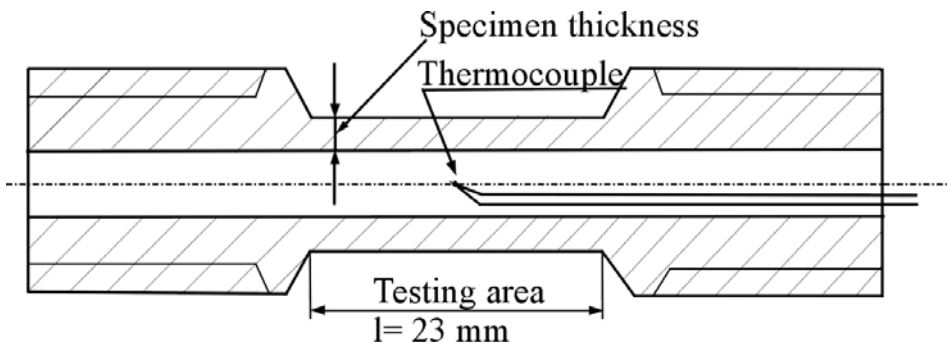


Figure 1. Cross section of the testing specimen with welded wires

Slika 1. Shematski prikaz prečnega preseka preizkušanca s privarjenim termoelementom

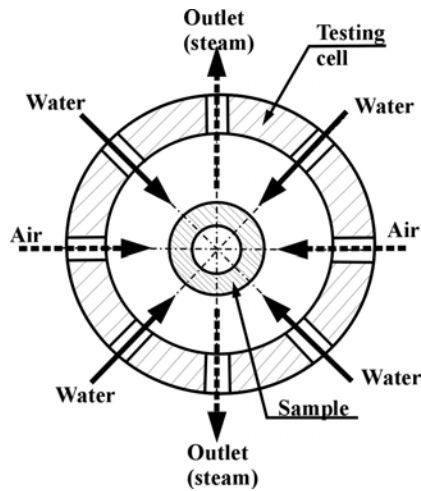


Figure 2. The cooling chamber with water quenched sample
Slika 2. Hladilna komora z vodno gašenim preizkušancem

The setup of the test rig, without working jaws, is shown in Figure 3a and its positioning in the Gleeble load cell is shown in Figure 3b.

For proving the test's abilities of the test rig, nine different specimens (made from AISI H11 tool steel) with various characteristics given in Table 1 were tested. Two different types of specimens were compared, i.e. five were heat treated (I - IV and IX, initial microstructure on Figure 4a) and four were heat treated plus gas nitrided (V-VIII, initial microstructure on Figure 4b). Further, the specimens differed also in specimen thickness (2.75 - 4 mm). Two specimens of each mentioned types were also mechanically loaded during testing by applying a compression force (0-19 kN) equal to 90 % of the yield stress at 650 °C corresponding to a value around 150 MPa.

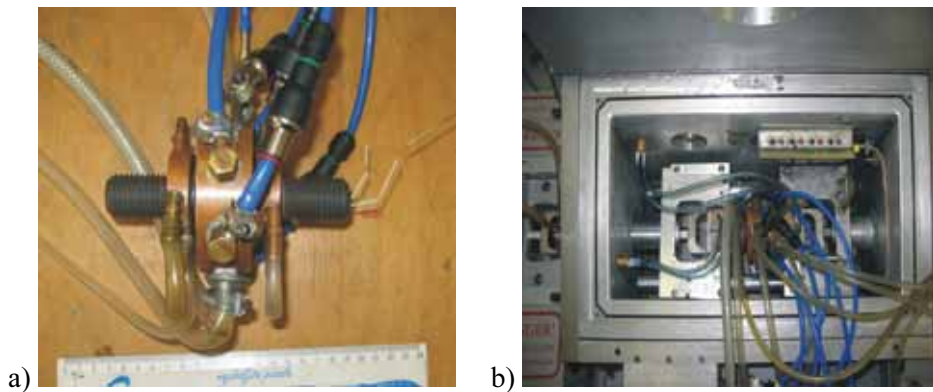
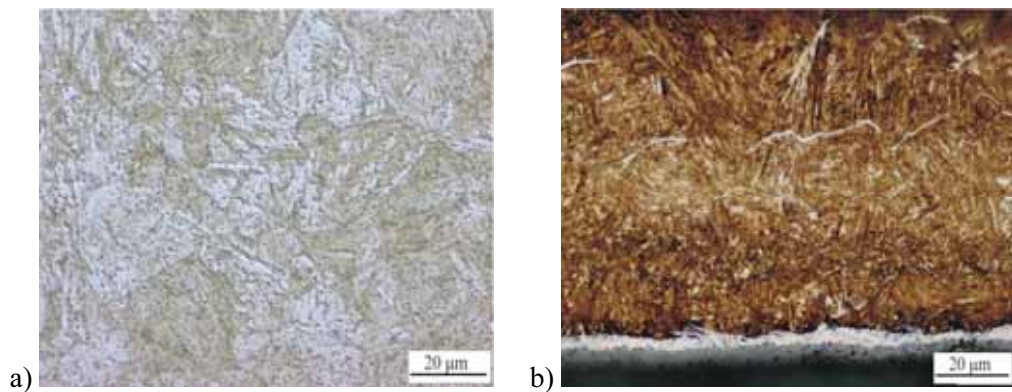
The program used for thermal and mechanical loading (see Figure 5 a-b) of the specimen was written in the applicative program QuickSim and was composed in following way:

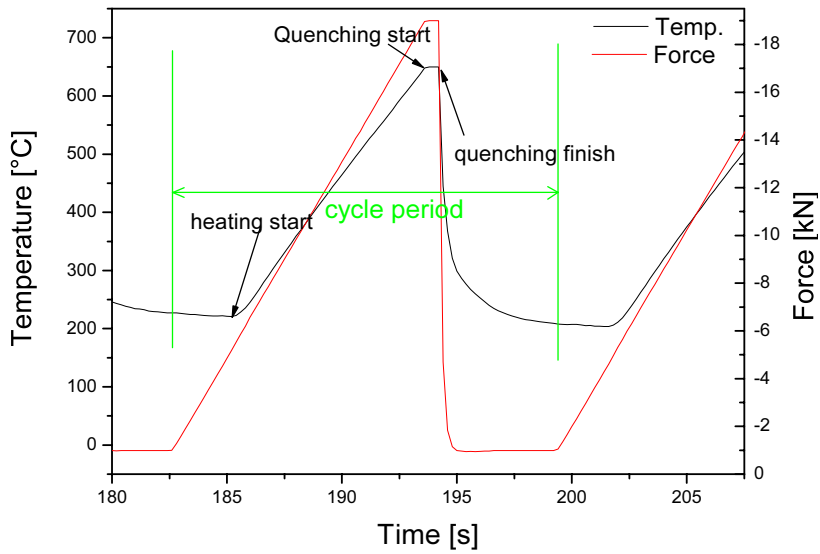
- resistance heating of the sample to the holding temperature of 650 °C with increasing mechanical loading (0 to 19 kN, see Figure 5 a-b),
- water quenching (0-0.50 s) during maintenance of the programmed temperature and mechanical loading,
- interruption of heating and quenching (and mechanical unloading),
- blowing of compressed air into the chamber (3 s).

After 500 cycles the tested surface was examined visually and after 1000 cycles the specimens were cut and metallographically prepared for microscopic analysis.

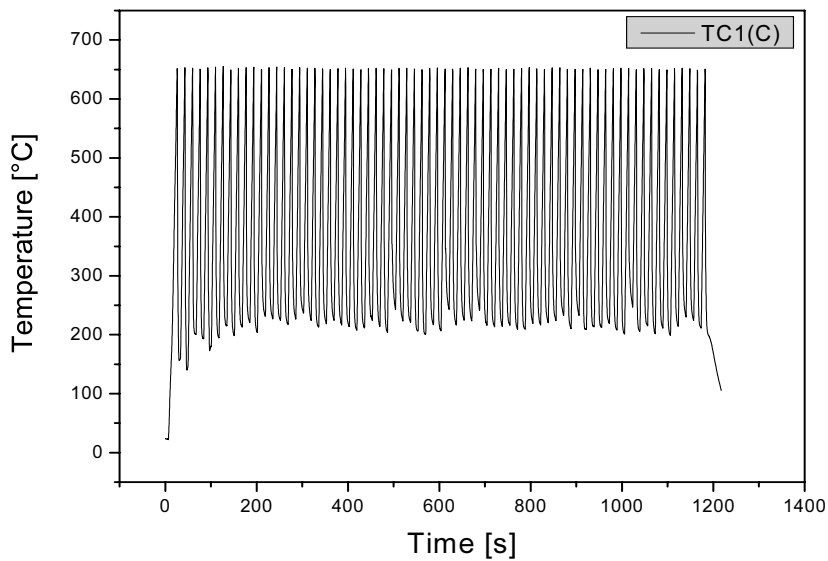
Table 1. Characteristics of specimens (AISI H11) and loadings (Thickness in mm)**Tabela 1.** Karakteristike testiranih vzorcev (AISI H11) in mehanskega obremenjevanja (debelina v mm)

Surface treatment	Heat treated		Heat treated		H.T. + nitrided		H.T. + nitrided		Heat treated
	I	II	III	IV	V	VI	VII	VIII	
Specimen									
Thickness	2.75	3.25	2.75	3.25	2.75	3.25	2.75	3.25	4
T_{\max} (°C)	650		650		650		650		650
F_{\max} (kN)	0		-19.0		0		-19.0		0

**Figure 3.** a) Testing device with specimen, b) Inserted test rig in testing cell of Gleeble 1500D**Slika 3.** a) Testna naprava s preizkušancem, b) Vsatvitev testne naprave v testno celico Gleebla 1500D**Figure 4.** Microstructure, a) Heat treated specimens, b) Nitrided specimens**Slika 4.** Mikrostrukture, a) Toplotno obdelanega preizkušanca, b) Nitriranega preizkušanca



a)



b)

Figure 5. a) The thermal and mechanical loading in one cycle, b) 50 temperature cycles

Slika 5. a) Potek temperature in mehanske obremenitve med enim ciklom, b) 50 temperaturnih ciklov

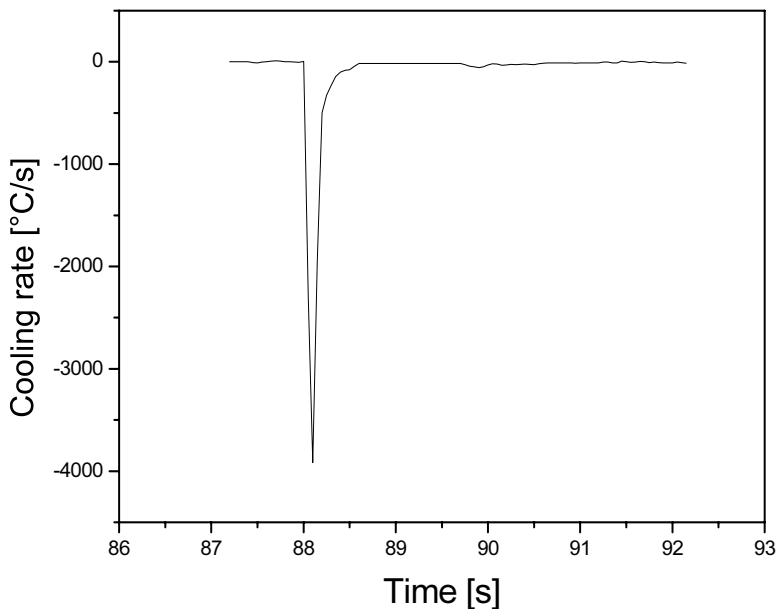
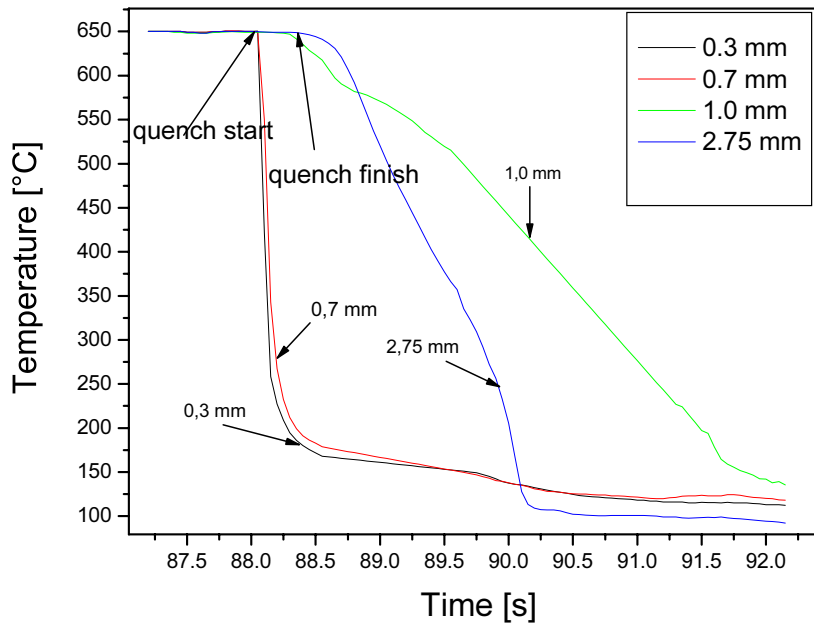


Figure 6. a) Measured temperatures at different depths during the quenching sequence, b) Cooling rate at the depth of 0.30 mm

Slika 6. a) Merjene temperature na različnih globinah med fazo gašenja površine, b) Hitrost ohlajanja na globini 0,30 mm

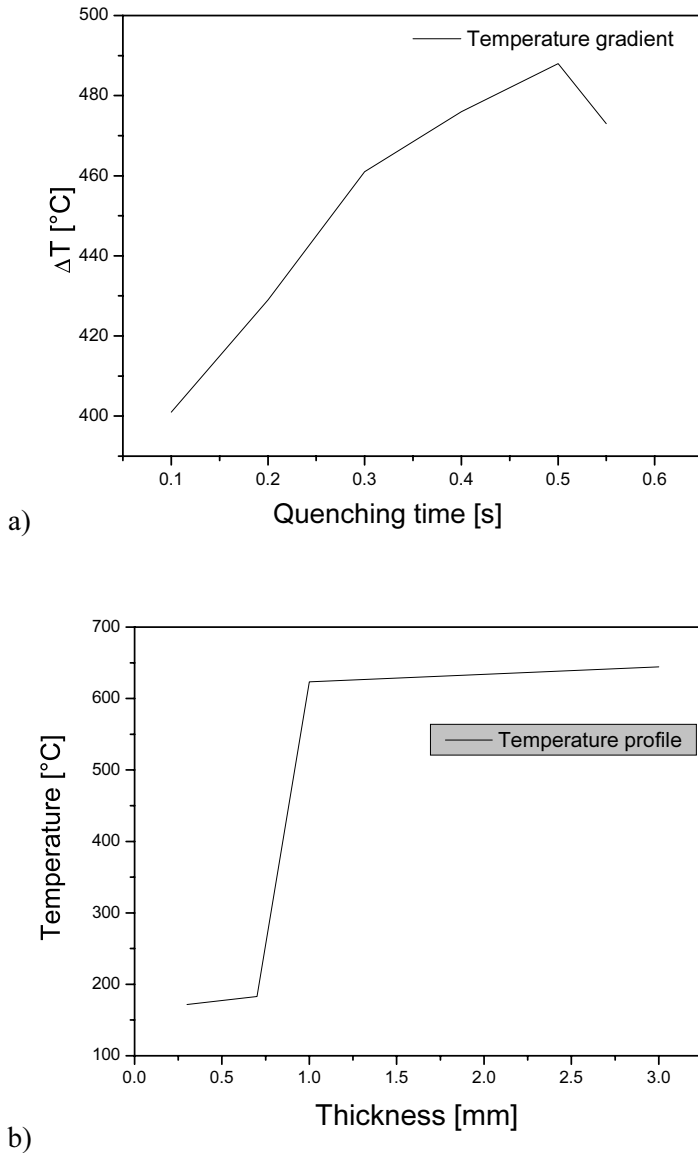


Figure 7. a) Measured temperature gradient in the specimen at various quenching times, b) Measured minimal temperature (temperature profile) in various depths at quenching time of 0.5 s

Slika 7. a) Merjeni temperaturni gradienti v preizkušancu pri različnih časih gašenja, b) Merjene minimalne temperature (temperaturni profil) v različnih globinah pri času gašenja 0,5 s

RESULTS

Measurements of temperature in the specimen

A typical example of a thermal and mechanical cycle is shown in Figure 5a. The simultaneous increasing of temperature and mechanical loading of the tested specimen is visible, while during quenching both of them maintain the programmed (same) value. The repetitiveness of the testing cycles obtained is presented on Figure 5b. The temperature of the specimen was controlled by the thermocouple, as presented in Figure 1. In order to determine (measure) the temperature field on the tested surface, a specially made specimen was applied in which inside had welded three additional highly responsive thermocouples (wire diameter 0.2 mm, type K) on various distances (0.30 mm, 0.70 mm, 1 mm) below quenched surface, while the fourth thermocouple (Figure 1) served for computer guidance and control of temperature. Their measured values are shown in Figure 6a. It is apparent that the temperature of the fourth and computer guided thermocouple remained at the programmed value of 650 °C also during quenching. After the quenching period the temperature fall of the fourth thermocouple was higher in comparison to the third thermocouple, since the heat transfer on the outer surface in the hollow specimen is also higher. The highest temperature gradient was registered at the quenching time of 0.5 s where the measured temperature difference between the first and the fourth thermocouple was 473 °C. The cooling rate was determined by differentiating the temperature/time curve at the depth of 0.30 mm from the quenched

surface. Using this technique the maximum cooling rate was determined (3918 °C/s, Figure 6b). At the specimen surface these rates were certainly higher. Thus with a combination of simultaneously controlled cooling and resistance heating of the specimen, greater thermal gradients in relatively thin specimen surface layer were achieved, while the remaining depth of the specimen kept approximately the same value (see Figures 5a and 6a). This reduced the number of cycles needed for crack nucleation and resulted in faster crack growth. For comparison Hadder et al.^[7] and Marsh et al.^[6] report cooling rates between 500 and 1000 °C/s. The minimal measured temperature for the first thermocouple and various quenching times (0.1 - 0.55 s) are shown in Figure 7a while Figure 7b shows the temperature profile (field) in the tested specimen at a quenching time of 0.5 s. With the possibility of generation of various thermal gradient, the test can also simulate various thermal loading conditions in an applicative environment.

Estimation of initial stress field by FEM

When the entire temperature profile was known the FEM was applied in order to estimate initial stress field (thermal stress) for different quenching times and specimen thicknesses. The MSC Super Forge 2005 code was used for this. The results of these analyses are shown in Figure 8. The analyses show that the maximum stresses are obtained after 0.5 s of quenching and are roughly 140 MPa for a specimen thickness of 2.75 mm. At 0.12 s of quench time the stresses reached the values around 125 MPa. This shows that the temperature and consequently the stress field can be varied by changing the quenching time. The stress obtained also

depends on specimen thickness; thus they reached values of cca 160 MPa and 175 MPa for specimen thicknesses of 3.25 mm and 4 mm, respectively. Furthermore the

temperature can be varied by changing the quenching liquid (nitrogen, air, etc) and changing its pressure.

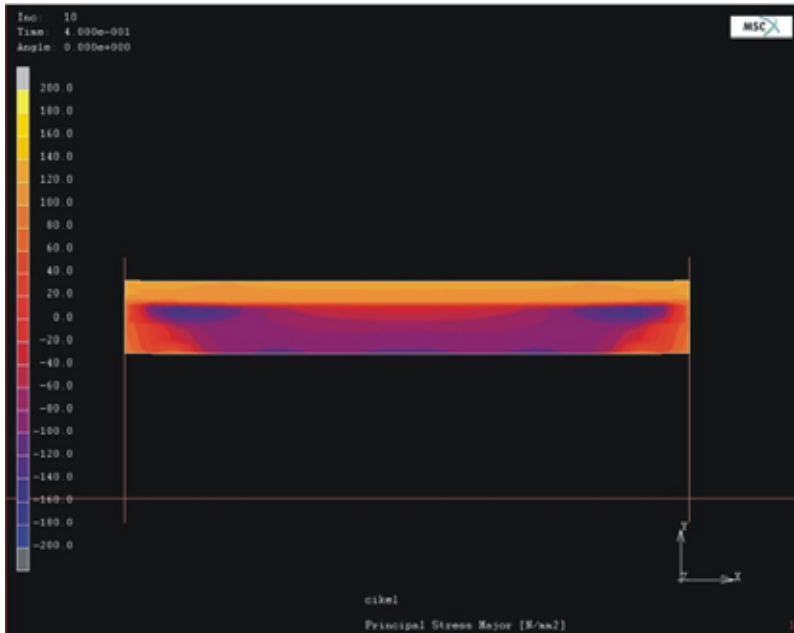


Figure 8. Estimated stress field simulated by FEM method, $t = 0.5$ s, wall thickness 2.75 mm, $T = 650$ °C

Slika 8. Ocenjeno napetostno polje z MKE, $t = 0,5$ s, deblina stene 2,75 mm, $T = 650$ °C

Appearance of surface cracking

From the estimated stress field it could be predicted that cracks would appear in thicker specimens sooner than in thinner specimens. The next batch of pictures were taken by an optical microscope after 1000 cycles of testing. The results are given in sequences according to thickness.

Wall thickness 2.75 mm

Estimated initial maximal stresses for the wall thickness of 2.75 mm were namely around 140 MPa that is lower as yield stress of AISI H11 tool steel at 650 °C (cca 150 MPa). This fact explain why on heat treated no cracks occurred but on contrary on gas nitrated specimens network of cracks was observed after 1000 cycles; the depth of obtained crack was in range 20 - 60 μm (Figure 9).

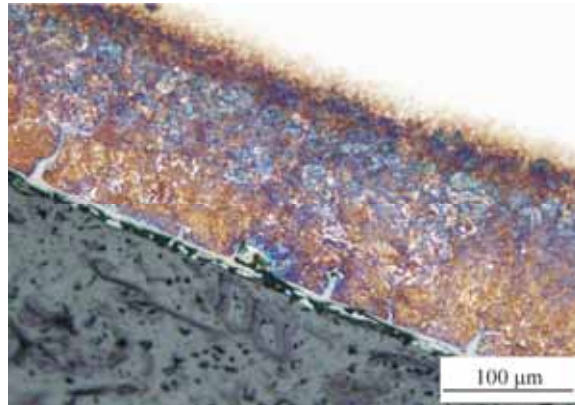


Figure 9. Appearance of surfaces of nitrided specimens after 1000 cycles, axially unloaded specimen; quenching time 0.5 s, thickness 2.75 mm, radial cross-section
Slika 9. Pojav površinskih razpok nitriranega vzorca po 1000 ciklih, aksialno neobremenjen vzorec, čas gašenja 0,5 s, debelina stene 2,75 mm, radialni presek

Wall thickness 3.25 mm

The next batch of pictures was taken on nitrided specimens after 1000 cycles where the thickness of the specimens was 3.25 mm. Estimated maximal stress using the FEM wall thickness of the specimen 3.25 mm amounted around 160 MPa. Consequently the cracks appearing were deeper and denser. Figure 10a shows the surface of nitrided specimen after 1000 cycles. The cracks here are clearly visible and they are appearing in both directions (radial and axial). As expected, the axial loading of the specimen restricted the nucleation of cracks in the radial direction. The maximal compression force during

cooling was 19 MN corresponding cca 140 MPa. Thus it means that maximal stresses in axial direction of the specimen were close to zero and consequently no cracks appeared in the radial direction (Figure 10b). The depths of the obtained cracks in the radial direction for an axially unloaded specimen are presented on Figure 11a and for an axially loaded specimen on Figure 11b. The crack depth obtained was cca 180 μm in the radial direction and cca 120 μm in the axial direction. The same phenomenon also occurred on heat treated specimen, only the depth of the cracks were lower (cca 20-30 μm).

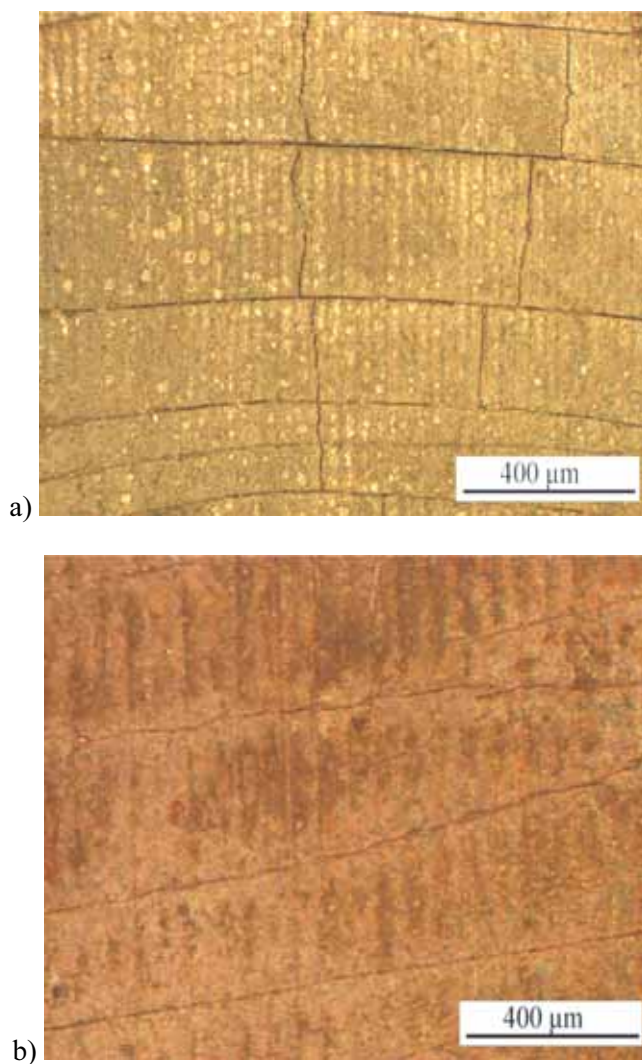


Figure 10. Appearance of surface of nitrided specimens after 1000 cycles, a) Axially unloaded specimen, b) Axially loaded, ← direction of axial loading; quenching time 0.3 s, and thickness 3.25 mm

Slika 10. Pojav površinskih razpok na nitriranemu vzorcu po 1000 ciklih, a) Aksialno mehansko neobremenjen preizkušaneec, b) Aksialno mehansko obremenjen, ← smer mehanskega obremenjevanja, čas gašenja 0,3 s, debelina stene 3,25 mm

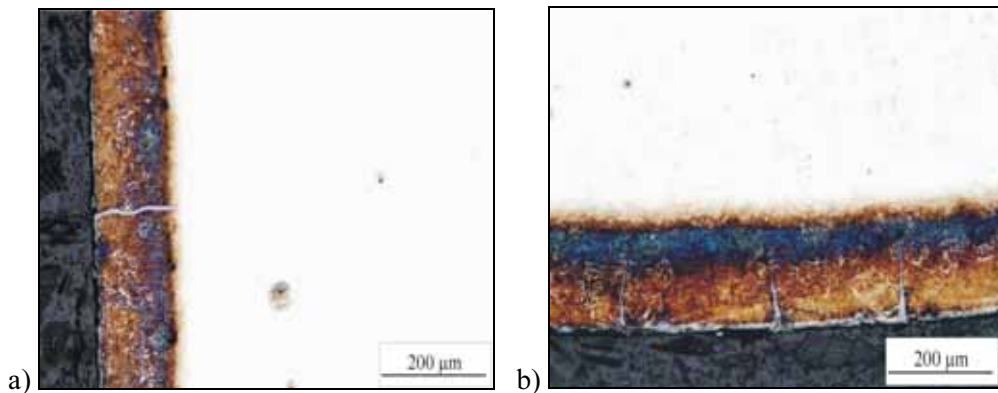


Figure 11. Cross-section of nitrided specimen and axially loaded nitrided specimens, a) Axial section, b) Radial section; quenching time 0.3 s, wall thickness 3.25 mm.

Slika 11. Prečni presek nitriranega in aksialno mehansko obremenjevanega vzorca, a) aksialni presek, b) radialni presek, čas gašenja 0,3 s, debelina stene 3,25 mm

Wall thickness 4 mm

As was expected denser cracks were obtained in thicker specimen and at a quenching time of 0.5 s since the estimated maximal stress (for the specimen thicknesses of 4.0 mm) amounted around 170 MPa. On Figure 12 a-b the cracks network on heat treated specimen is visible. Mentioned cracks were visible still after 500 quenching cycles and after 1000 quenching cycles the crack net obtained was denser. The depth of the cracks was around 40 µm.

Discussion

The test enables to vary all important parameters which influence the experimental results. These are the heating rate, maximum specimen temperature, quenching time, quenching medium, pressure of the quenching medium, specimen wall thickness, and the external specimen loading (tensile - compressive, cyclic - constant). The appearance of

cracks on tested specimen was very similar to those obtained on a hot working surface of rolls as presented on Figure 13. Namely, after its contact with heated specimen the roll surface is subjected to rapid water cooling leading to surface cracking.

In the literature we can find contradictory result regarding to the thermal fatigue resistance of some nitrided surfaces. Thus Pellizari et al.^[8] claim that nitrided surfaces decreased the fatigue resistance on the contrary Spies et al.^[9] claim that the nitrided surface increased fatigue resistance. The authors did not present the temperature field and consequently they also could not calculate (asses) the stress field (predominately tensile or compression stresses) on the tested specimens from which the reason for the appearance of cracks based. Therefore, different results should be carefully compared according to the specific test conditions.

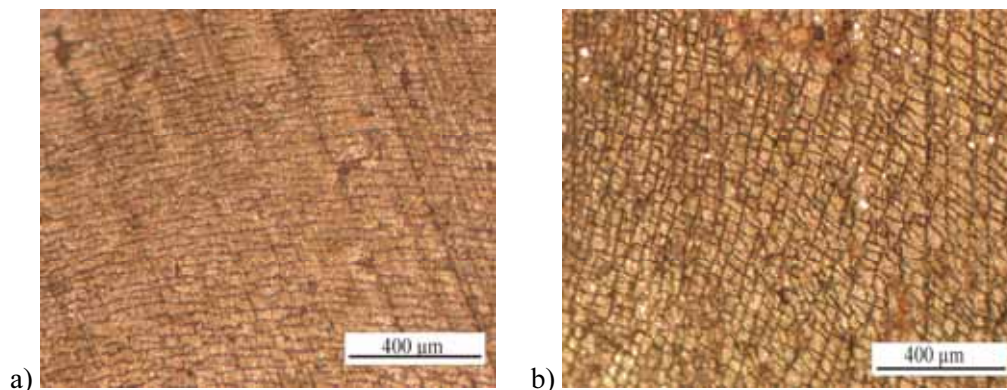


Figure 12. Appearance of the surface of heat treated specimens, a) After 500 cycles, b) After 1000; axially unloaded specimen, quenching time 0.5 s, wall thickness 4 mm

Slika 12. Prikaz površine toplotno obdelanega preizkušanca, a) po 500 ciklih, b) po 1000 ciklih; aksialno mehansko neobremenjen preizkušavec, čas gašenja 0,5 s, debelina stene 4 mm

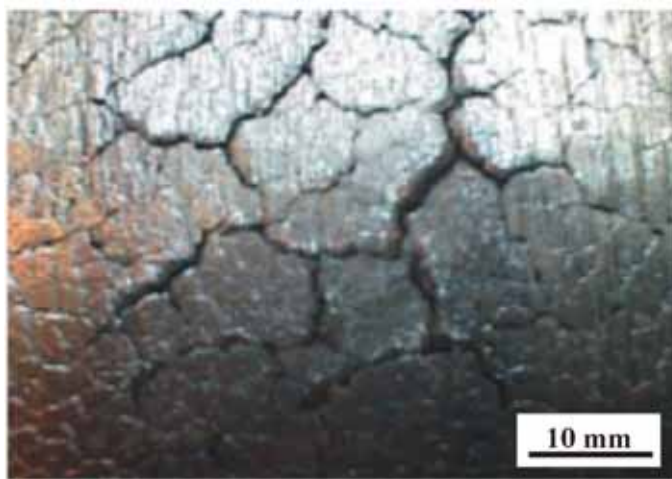


Figure 13. Appearance of cracks on the surface of hot roll
Slika 13. Pojav razpok na površini valjev za vroče valjanje

CONCLUSIONS

A new thermal fatigue test was developed for testing materials. It is based on computer guided heating and quenching of the specimen. The specific shape of the specimen and special execution of the program enables the achievement of very high temperature gradients that are greater than those found in the literature. In combination with mechanical loading different stress states on specimens can be achieved (mechanical pre-loading of forging tools, etc.). The test can generate a wide range of conditions to which the real parts can be subjected. Calculation of the

stress field using the FEM showed the highest stresses in the thicker walls of the specimen. Thus on specimens with thicker walls and longer cooling times, the cracks nucleated earlier and are denser. A comparison of two differently treated materials (heat treated or heat treated + gas nitrated) showed that the nitrated layer is brittle and rapidly cracks under tensile thermal stresses. The newly developed test with its proven characteristics will contribute to better understanding of crack nucleation and their growth. This is the basis for better modelling of the processes involved.

POVZETKI

Razvoj testne naprave za študij termičnega utrujanja – preliminarni rezultati

Razvit je bil nov test za termično utrujanje kovinskih materialov, ki ima računalniško vodeno, tako ogrevanje kot tudi gašenje preizkušanca. S testom je tako mogoče simulirati različne primere termičnega utrujanja, ki so jim podvrženi predmeti med svojo uporabno dobo. Specifična oblika preizkušanca ter posebna izvedba njegovega ogrevanja in ohlajanja omogočata doseganje visokih temperaturnih gradientov, ki so višji glede na znane podatke v literaturi. To zmanjšuje število ciklov, ki so potrebni za nukleacijo razpok in s tem krajša trajanje preizkusov. V

kombinaciji z mehanskim obremenjevanjem lahko še dodatno simuliramo različna obremenitvena stanja predmetov med njihovo uporabno dobo (npr. dodatno mehansko obremenjevanje površine orodij za toplo preoblikovanje zaradi trenja med preoblikovancem in orodjem); na ta način lahko pospešimo ali zavremo rast razpok. Na preizkušancih z večjo debelino stene je prišlo do pojava razpok prej, prav tako so bili razpokam bolj podvrženi preizkušanci z nitrirano površino kot samo toplotno obdelani preizkušanci iz orodnega jekla AISI H11. Pri primerjavi dveh različnih materialov (toplotno obdelan + nitriran UTOPMO1, toplotno obdelan UTOPMO1) se je izkazalo, da je nitrirana plast krhka in pod nateznimi napetostmi hitro razpoka.

REFERENCES

- [1] WEROŃSKI, A., HEJWOWSKI, T. (1991): *Thermal fatigue of metals*. Marcel Dekker.
- [2] HADDER, N., FISSOLO, A., MAILLOT, V. (2005): Thermal fatigue crack networks: an computational study. *International Journal of Solids and Structures.*; Vol. 42, pp. 771-788.
- [3] PERSSON, A., HOGMARK, S., BERGSTRÖM, J. (2004): Simulation and evaluation of thermal fatigue cracking of hot work tool steel. *International Journal of Fatigue.*; Vol. 26, pp. 1095-1107.
- [4] AMIABLE, S., CHAPULIOT, S., CONSTANTINESCU, A., FISSOLO, A. (2006): A comparison of life time prediction methods for a thermal fatigue experiment. *International Journal of Fatigue.*; Vol. 28, pp. 692-706.
- [5] ABSI, J., GLANDUS, J.C. (2004): Improved methods for severe thermal shocks testing of ceramics by water quenching. *Journal of European Ceramic society.*; Vol. 24, pp. 2835-2838.
- [6] MARSH, D.J. (1981): A thermal shock fatigue study of type 304 and 316 stainless steels. *Fatigue of Engineering Materials and Structures.*; Vol. 4, No. 2, pp. 179-195.
- [7] HADDER, N., FISSOLO, A. (2005): 2D simulation of the initiation and propagation of crack array under thermal fatigue. *Nuclear Engineering and Design.*; Vol. 235, pp. 945-964.
- [8] PELLIZZARI, M., MOLINARI, A., STRAFFELINI, G. (1983): Thermal fatigue resistance of gas and plasma nitrided 41CrAlMo7 steel. *Materials Science & Engineering.*; Vol. 352, pp. 186-194.
- [9] SPIES, H.J., VOGT, F., SVENNSON, M. (1983): *Neue Hütte* 8, pp. 281-287.

Pulzno varjenje konstrukcijskih jekel

Pulsed arc welding of structural steels

RAJKO KEJŽAR¹, UROŠ KEJŽAR²

¹Univerza v Ljubljani, Fakulteta za strojništvo, Aškerčeva cesta 6, 1000 Ljubljana, Slovenija;

E-mail: rajko.kejzar@fs.uni-lj.si

²ISKRA VARJENJE, Stegne 21c, 1000 Ljubljana, Slovenija;

E-mail: uros.kejzar@iskra-varjenje.si

Received: July 6, 2007

Accepted: July 10, 2007

Izveček: Konstrukcijska jekla lahko zelo ekonomično varimo z žicami VAC 60 v zaščiti plina CO₂. Varilni proces je zelo kaotične narave in ne zagotavlja lepega izgleda površine (brizganje) in visoke kakovosti vara. Že z zamenjavo zelo oksidativnega plina CO₂ z manj oksidativno plinsko mešanico Ar + 18 vol.% CO₂ dobimo lepši izgled površine in tudi višjo kakovost vara. Še boljše kakovost varov lahko dobimo s pulznim varjenjem konstrukcijskih jekel. Pri študiju in razvoju obstoječega varilnega procesa smo posebno pozornost usmerili na prehajanje materiala. To poteka pri pulznem varjenju z žico VAC 60 v zaščitni mešanici Ar + 18 vol.% CO₂ zelo mirno in enakomerno v zelo širokem območju varilnih parametrov. Zaradi nizke oksidativnosti plinske mešanice Ar + 18 vol.% CO₂ in zelo kratkega časa nastajanja kapljice pri pulznem varjenju prihaja do pomembnih kemičnih procesov v kapljici šele pri varjenju z višjo povprečno jakostjo varilnega toka (281A). Manj legirane navare s silicijem in manganom, ki so bolj kakovostni, dobimo zato le zaradi razredčenja navara, ki je posledica taljenja osnovnega materiala – uvarjanja. Na velikost uvara pa lahko pri pulznem varjenju zelo učinkovito vplivamo z izbiro oblike in energije pulza ter jakosti osnovnega toka.

Abstract: Structural steels can be welded very cost-effectively with VAC 60 wires in CO₂ shielding gas. Welding process is very chaotic and does not guarantee a nice appearance of the weld face and a high weld quality. With the replacement alone of a highly oxidizing gas, i.e. CO₂, with a less oxidizing gas mixture, i.e. Ar + 18 vol.% CO₂, a nicer appearance of the weld face and a higher weld quality may be obtained. Still higher quality of welds may be accomplished by employing pulsed arc welding of structural steels. In the study and development of the existing welding process special attention was paid to the metal transfer. In pulsed arc welding with VAC 60 wire in the protective gas mixture of Ar + 18 vol.% CO₂, the metal transfer is very smooth and uniform in a very wide range of welding parameters. Because of the low oxidizing capability of Ar + 18 vol.% CO₂ gas mixture and a very short time of droplet formation, however, in pulsed arc welding

major chemical processes in the droplet will occur only in welding with a higher average welding current (281A). Less alloyed surfacing welds with silicon and manganese will provide higher quality only due to the surfacing weld dilution resulting from the parent-metal fusion, i.e. penetration. In pulsed arc welding the degree of penetration may be efficiently affected by a pulse shape and energy and base current.

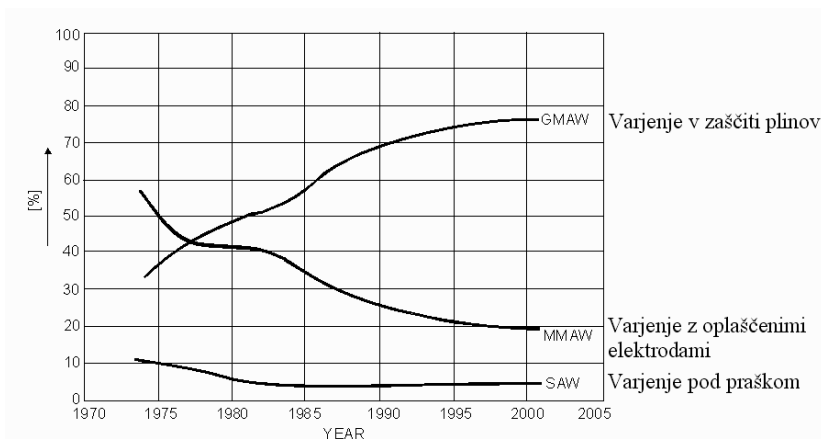
Ključne besede: MIG/MAG-varjenje, pulzno varjenje, žica VAC 60, konstrukcijsko jeklo H2, zaščitni plini: (CO₂, Ar + 18 vol.% CO₂), prehajanje materiala, odtaljevanje, uvarjanje, kvaliteta vara

Keywords: MIG/MAG welding, pulsed arc welding, VAC 60 wire, H2 structural steel, shielding gases: (CO₂, Ar + 18 vol.% CO₂), metal transfer, melting-off, penetration, weld quality.

UVOD

V praksi konstrukcijska jekla običajno varimo po MAG-postopku z masivnimi varilnimi žicami in v zaščiti CO₂. MAG – postopek varjenja je produktiven in ekonomičen ter zelo prilagodljiv. Ta postopek omogoča polavtomatsko varjenje tudi na terenu ter je zelo primeren za avtomatizacijo in robotizacijo varilnega procesa v industriji. Zaradi njegove

vsestranske industrijske uporabnosti se je delež varjenj različnih materialov v zaščiti plinov zelo povečal. V zadnjih dvajsetih letih se je predvsem zaradi zmanjšanja deleža ročno obločnega varjenja z oplaščenimi elektrodami delež tega načina varjenja v zaščiti plinov celo podvojil. Na sliki 1 je prikazana zastopanost najpomembnejših elektroobločnih postopkov varjenja^[1].



Slika 1. Zastopanost elektro-obločnih postopkov varjenja v zahodni Evropi^[1]
Figure 1. Shares of most important arc welding processes in Western Europe^[1]

Pospešeno povečevanje uporabe postopkov elektro obločnega varjenja v zaščiti plinov je sprožilo vrsto raziskav, ki so vplivale na hitrejši razvoj MIG/MAG postopka varjenja^[1-3].

Z uporabo najnovejših dosežkov moderne elektronike in računalništva se je znatno pospešil tudi razvoj varilnih naprav. Ker je varilni proces zelo kompleksen, je razvoj izvorov toka usmerjen v mikroračunalniško krmiljenje parametrov varjenja^[4-7].

Klasičen varilni proces pri varjenju konstrukcijskih jekel z varilno žico VAC 60 (oznaka po EN 440 je G3Si)^[8] pod oksidativnim zaščitnim plinom CO₂^[9-11] je zelo kaotične narave in ne zagotavlja visoke kakovosti vara^[12]. Tako poteka kratkostično varjenje tankih pločevin neenakomerno z vidika prehajanja materiala. Še bolj neenakomeren prehod materiala je zaslediti pri zelo produktivnem pršečem varjenju debelih pločevin. Pršeče prehajanje materiala temelji na eksplozijah odtaljenih kapljic, zaradi nastajanja ogljikovega monoksida (CO) v raztaljeni kovini varilne žice. Tako varjenje je zelo dinamično ter ga spremlja zelo pogosto tudi brizganje taline, kar pa daje slab

KRATKOSTIČNO IN PRŠEČE VARJENJE PO MAG-POSTOPKU

Pri varjenju konstrukcijskih jekel zelo pogosto kot dodajni material uporabljamo masivno žico VAC 60. Namenjena je

izgled vara in njegove okolice. Z zamenjavo zelo oksidativnega plina CO₂ z bolj inertno plinsko mešanico Ar + 18 vol.% CO₂ postane varjenje bolj mirno, ker zaradi zmanjšane oksidativnosti atmosfere obloka v kapljicah ne nastaja več ogljikov monoksid (CO). Proces poteka zelo enakomerno in brez brizganja in s prehajanjem materiala v finokapljičasti obliki^[13].

Še bolj enakomeren proces varjenja in bolj umirjene razmere med varjenjem, pa se doseže s pulznim prehajanjem materiala, ki zagotavlja znatno boljšo kakovost varov. Pulzno varjenje lahko dosežemo s tiristorskimi^[14], kot tudi tranzistorskimi izvori varilnega toka. Zadnji so izjemno primerni za mikroračunalniško krmiljenje varilnega procesa^[4-7,15].

Pulzno varjenje z digitalnimi izvori toka zagotavlja kakovosten nadzor nad procesom varjenja v zelo širokem območju varilnih parametrov. Zaradi izjemnih možnosti vplivanja na uvarjanje je ta način varjenja primeren tako za varjenje tankih kot tudi debelih pločevin in prav tako tudi za oplemenitenje konstrukcijskih jekel z navarjanjem^[16].

varjenju pod CO₂, zato je legirana z 0,9 % Si in 1,5 % Mn. Zaradi oksidativnosti zaščitnega plina CO₂ silicij in mangan med varjenjem delno odgorita^[11]. Odgorevanje je prikazano v tabeli 1.

Tabela 1. Odgor in prigor elementov ter nastajanje čistega vara (navara) in varilne žindre pri varjenju z žico VAC 60 v oksidativnem zaščitnem plinu CO₂. Osnova za izračun je 100 g masivne varilne žice.

Table 1. Burn-off and pick-up of elements and formation of the deposited metal and the welding slug in CO₂ welding with VAC 60 solid wire. The calculations are based on 100 g of the wire.

Dodajni material	Kovine					Oksidi			
	C	Si	Mn	Fe	Σ	SiO ₂	MnO	FeO	Σ
VAC 60 (g)	0,06	0,90	1,50	97,54	100	-	-	-	/
Odgor/Prigor (g)	+0,03	-0,33	-0,22	-0,16	-0,68	+0,71	+0,28	+0,21	+1,20
Čisti var/Žindra (g)	0,09	0,57	1,28	97,38	99,32	0,71	0,28	0,21	1,20
Sestava (%)	0,09	0,57	1,29	98,05		59,2	23,3	17,5	
Sestava navara (%) 45 % uvara	0,099	0,417	0,979						

Opomba: Navarjamo na konstrukcijsko jeklo H II (1.0452; 0,11 % C, 0,23 Si in 0,60 % Mn).

Zaradi oksidativnosti CO₂ pri visokih temperaturah varjenja, se vzpostavlja ravnotežje med oksidi v nastajajoči žindri in kovinami v varu:

$$\frac{(\% FeO)}{[\% Fe]} = 0,178$$

$$\frac{(\% MnO)}{[\% Mn]} = 18,1$$

$$\sqrt{\frac{(\% SiO_2)}{[\% Si]}} = 10,2$$

ki ustreza dezoksidaciji vara z okoli 0,1 mas.% O₂ [11].

Na kakovost varov varjenih po MAG-postopku v zaščitnem plinu CO₂ s kratkostičnim in pršičim prehajanjem materiala z varilno žico VAC 60, pomembno vpliva pogosto pojavljanje mikroporoznosti na mejah med posameznimi varki. Dosežena žilavost varov je

zato nekoliko slabša, vendar v večini primerov varjenja konstrukcijskih jekel še vedno zadovoljiva, saj dobimo kakovosten varjen spoj z žilavostjo okoli 100 J po metodi Charpy V notch pri 20 °C ter s sestavo in s trdotami okoli 140 HV 0,3. Nasprotno pa pri varjenju v plinski zaščitni mešanici sestavljeni iz Ar + 18 vol.% CO₂ dobimo nekoliko višje legirane in trše vare, če kot dodajni material uporabimo varilno žico VAC 60. Vzrok je manjše odgorvanje silicija in mangana iz varilne žice, kot v primeru varjenja pod zaščito CO₂. Zaradi drobno kapljicastega prehoda materiala in bolj enakomernega odtaljevanja so vari zelo čisti, skoraj brez nekovinskih vključkov in brez poroznosti. Ne glede na razmeroma veliko trdoto je žilavost varov varjenih v plinski mešanici Ar + 18 vol.% CO₂ presenetljivo dobra – celo boljša od varov varjenih v zaščiti plina CO₂. V tabeli 2 so podani rezultati kemične analize ter meritev trdot in žilavosti varov, ki smo jih varili po MAG-postopku z žico VAC 60 v zaščiti plina CO₂ in plinske mešanice Ar + 18 % CO₂.

Tabela 2. Kemične sestave, trdote in žilavosti varov, ki smo jih varili z varilno žico VAC 60, Φ 1,2 mm po MAG-postopku v zaščiti plina CO₂ in plinske mešanice Ar + 18 vol.% CO₂

Table 2. Chemical composition, hardness, and toughness values for MAG welds, welded in CO₂ and Ar + 18 vol.% CO₂ with VAC 60 welding wire, with diameter of 1.2 mm

Vzorec	Kemična sestava [%]			Trdote [HV 0,3]				Žilavost [J, Charpy Vnotch]		
	Št.	C	Si	Mn	Koren	Sredina	Teme	O.M.	+20°C	0°C
1	0,096	0,47	0,86	136	130	143	145	149	128	88
2	0,093	0,49	0,89	136	138	177	134	157	132	107
3	0,064	0,69	1,20	150	168	184	136	205	157	156

Legenda:

1. Kratkostično pod CO₂ (130A, 22V)
2. Pršeče pod CO₂ (210A, 24V)
3. Finokapljičasto v zaščiti mešanice plinov Ar + 18 vol.% CO₂ (220A, 24V)

Iz podatkov o kemični sestavi varov lahko ugotovimo, da je odgorevanje dezoksidantov (Si in Mn) pri varjenju pod zaščitnim plinom CO₂ tako na nataljeni žici, kot tudi na nastali kapljici zelo intenzivno. Znižanje vsebnosti silicija od 0,9 % v žici na 0,49 % v varu in mangana od 1,5 % v žici na 0,89 % v varu med varjenjem lahko pripišemo istočasno vplivu, ki ga ima na sestavo vara odgorevanje dezoksidantov in razredčenje čistega vara zaradi uvarjanja, ki je okoli 40 do 50 %-no, če varimo po MAG-postopku v zaščitnem plinu CO₂.

Pri varjenju pod zaščitnim plinom CO₂ se zaradi skoraj popolne disociacije CO₂ ($2\text{CO}_2 \rightarrow 2\text{CO} + \text{O}_2$) na temperaturi obloka, ki je pri MIG/MAG varjenju nad 5000 °C, zviša vsebnost ogljika v varih. Prigor ogljika v var je posledica reakcije $[\text{C}] + [\text{O}] \leftarrow \{\text{CO}\}$, ki zaradi visokega parcialnega tlaka ogljikovega monoksida v obloku pri varjenju v zaščiti CO₂ poteka v levo.

Pri varjenju z manj oksidativno plinsko mešanico Ar + 18 vol.% CO₂ pa je tako odgorevanje dezoksidantov (Si in Mn) kot tudi prigor ogljika v var neznatni. Kemična sestava vara je odvisna predvsem od razredčenja čistega vara zaradi uvarjanja v osnovno konstrukcijsko jeklo.

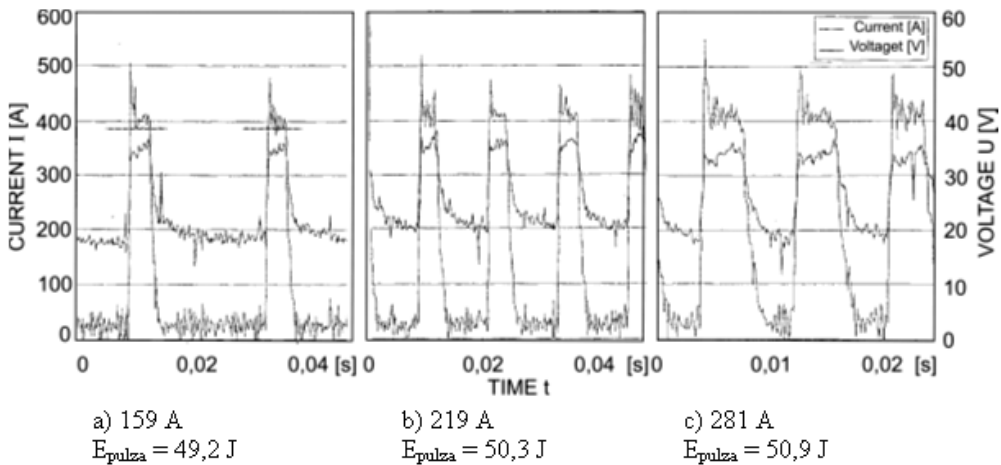
Velikost uvarjanja je pri varjenju v zaščiti plinske mešanice Ar + 18 vol.% CO₂ okoli 35 %-na, kar povzroči delno znižanje silicija od 0,9 % v žici na 0,69 % v varu in mangana od 1,5 % v žici na 1,20 % v varu, kar pa je bistveno manj kot pri varjenju v zaščiti plina CO₂. Zato imajo vari varjeni v zaščiti plinske mešanice Ar + 18 vol.% CO₂ kljub nižji vsebnosti ogljika (0,064 % C), še vedno nekoliko višjo trdoto. Boljša žilavost teh varov pa je posledica večje homogenosti in čistoče. Vari varjeni v zaščiti plinske mešanice Ar + 18 vol.% CO₂ so skoraj brez napak, to je brez mikroporoznosti in prav tako brez nekovinskih vključkov.

PULZNO VARJENJE PO MAG-POSTOPKU

Iz primerjave kakovosti varov, ki so bili varjeni po MAG-postopku v zelo oksidativnem zaščitnem plinu CO₂, in varov, ki smo jih varili v manj oksidativni mešanici plinov Ar + 18 vol.% CO₂ smo ugotovili, da enakomerno odtaljevanje dodajnega materiala zelo ugodno vpliva tako na izgled vara, kot tudi na njegovo kakovost. Najlepše in najbolj kakovostne vane pa dobimo pri pulznem varjenju.

Pri pulznem varjenju z varilno napravo SYNERGIC 450 MIG PULSE pri jakostih varilnega toka nad 150 A v plinski zaščitni

mešanici Ar + 18 vol.% CO₂ poteka odtaljevanje dodajnega materiala v obliki drobnih kapljic. Pri izbrani nastanitvi varilnih parametrov, ko je povprečna in pulzna (maksimalna) jakost in napetost varilnega toka usklajena s hitrostjo varilne žice in frekvenco pulziranja, smo dosegli popolnoma enakomerno odtaljevanje kapljic. Potek pulziranja varilnega toka in napetosti je prikazan na sliki 2, v tabeli 3 pa so podani varilni parametri in meritve odtaljevanja kapljic za pulzno varjenje z žico VAC 60 premera ϕ 1,2 mm v zaščitni plinski mešanici Ar + 18 vol.% CO₂.



Slika 2. Časovno spreminjanje toka in napetosti pri pulznem MAG-varjenju različnih povprečnih jakosti toka: a) 159 A, b) 219 A in c) 281 A

Figure 2. Time variation of welding current and voltage in pulsed MAG welding with different average currents: a) 159 A, b) 219 A in c) 281 A

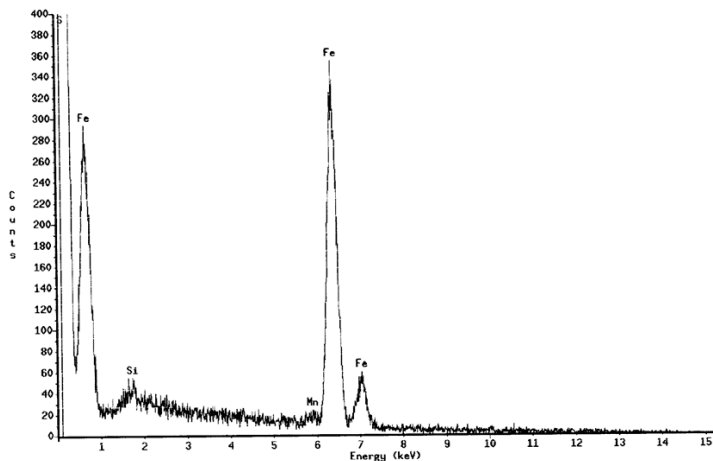
Tabela 3. Varilni parametri in podatki o odtaljevanju za pulzno MAG varjenje z žico VAC 60, premera ϕ 1,2 mm v zaščitni plinski mešanici Ar + 18 vol.% CO₂

Table 3. Welding parameters and information's of melting-off for pulsed MAG welding with 1.2 mm VAC 60 wire and using Ar + 18 vol.% CO₂ gas mixture

Vzorec	Jakost toka I (A)		Varilna napetost U (V)		Hitrost pomika varilne žice [m/min]	Frekvenca pulziranja Hz [s ⁻¹]	Odtaljevanje	
	Povprečna	Pulzna	Povprečna	Pulzna			Masa povprečne kapljice [g]	
Zap. št.	Povprečna	Pulzna	Povprečna	Pulzna			Izmerjena	Izračunana
1	159	385	16,3	33,6	3,0	42	0,0118	0,0106
2	219	386	21,4	34,3	5,0	80	0,0118	0,0092
3	281	392	24,9	32,7	6,7	130	0,0041	0,0075

Iz rezultatov študija odtaljevanja kapljic (prehajanje materiala) se lepo vidi, da se pri vsakem pulzu odtali samo ena kapljica. Le pri varjenju št. 3 (povprečna jakost toka je 281 A) prihaja do eksplozije kapljic (izmerjene kapljice so manjše od izračunanih).

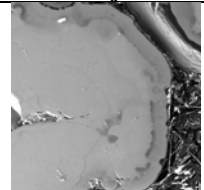
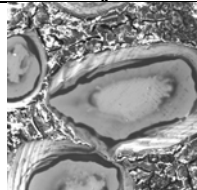
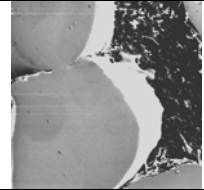
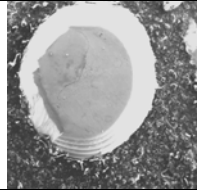
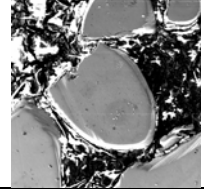
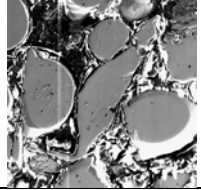
Intenzivnost in potek kemičnih procesov dezoksidacije vara med pulznim varjenjem smo ocenjevali na osnovi analize silicija in mangana v odtaljenih kapljicah. Na sliki 3 je prikazana izvedba meritev, v tabeli 4 pa rezultati določitev vsebnosti Si in Mn v kapljicah in izgled presekov kapljic.



Slika 3. Diagram določitve Si in Mn v kapljici po metodi EDS na elektronskem mikroskopu (št. 1; povprečna jakost toka 159A-manjša kapljica)

Figure 3. Diagram of determination of Si and Mn in droplet from method EDS on the electronic microscope (no. 1; average current 159 A – smaller droplet)

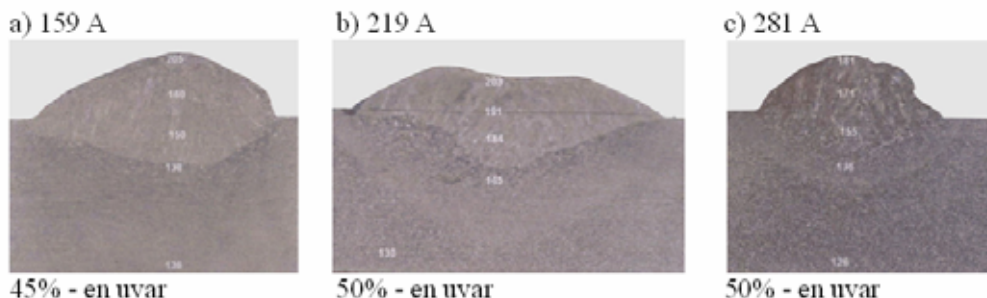
Tabela 4. Vsebnosti Si in Mn v kapljici in mikrostruktura na prerezu kapljic
Table 4. Contents of Si and Mn in the droplet and microstructure on cross section of droplet

Vzorec št. varjenja	Velikost kapljic	Kemična sestava kapljic		Mikrostruktura na prerezu kapljic (pov. 25x)	
		[mas.% Si]	[mas.% Mn]	večje	manjše
1 (159 A)	▪ večje	0,65 ± 0,33	2,05 ± 0,77		
	▪ manjše	0,96 ± 0,33	1,99 ± 0,81		
2 (219 A)	▪ večje	1,12 ± 0,24	1,65 ± 0,75		
	▪ manjše	0,88 ± 0,24	1,33 ± 0,44		
3 (281 A)	▪ večje	0,35 ± 0,21	0,43 ± 0,38		
	▪ manjše	0,82 ± 0,22	1,29 ± 0,40		

Iz kemične analize kapljic, ki je podana v tabeli 4, lahko zaključimo, da pri pulznem varjenju v zaščitni mešanici Ar + 18 % CO₂, ki je rahlo oksidativna, pri nizkih jakostih varilnega toka (pod 200 A) skoraj ni odgorevanja dezoksidantov, kot sta silicij in mangan. Intenzivnejše odgorevanje nastopi šele pri višjih jakostih varilnega toka (nad 250 A) in to le v večjih kapljicah.

Pri pulznem varjenju v rahlo oksidativni mešanici plinov Ar + 18 vol.% CO₂ je

odgorevanje dezoksidantov in legirnih elementov neznatno. Kemična sestava navara je zato odvisna le od razredčenja (razmešanja) čistega vara zaradi uvarjanja v osnovni material. Iz presekov navarov na sliki 4 vidimo, da je uvarjanje v vseh primerih navarjanja skoraj povsem enako. Trdote navarov in njihove kemične sestave se zato malo razlikujejo. Podatki o kemični sestavi navarov in njihovi trdoti so prikazani v tabeli 5.



Slika 4. Makrostruktura navarov pri pulznem MAG varjenju pri različnih povprečnih jakosti toka: a) 159 A, b) 219 A in c) 281 A

Figure 4. Macrostructure of surfacing welds in pulsed MAG welding with different average currents: a) 159 A, b) 219 A in c) 281 A

Tabela 5. Kemične sestave in trdote navarov po pulznem varjenju z žico VAC60 v zaščitni plinski mešanici Ar + 18 vol.% CO₂ na konstrukcijsko jeklo s parametri varjenja podanimi v tabeli 3

Table 5. Chemical composition and hardness of surfacing welds after pulsed MAG welding in an Ar + 18 vol.% CO₂ gas mixture with VAC 60 wire on structural steel employing the welding parameters given in Table 3

Vzorec	Povprečni tok	Kemična sestava navarov [%]			Trdota navarov [HV 0,3]		
		C	Si	Mn	Koren	Sredina	Teme
št.	I [A]						
1	159	0,073	0,51	0,91	138	160	206
2	219	0,084	0,52	0,93	145	181	203
3	281	0,094	0,44	0,78	136	171	181

Pulzno varjeni navari z žico VAC 60 v zaščitni plinski mešanici Ar + 18 vol.% CO₂ so visoko kakovostni in lepega videza. Tudi po detaljnem pregledu na preseku večvarkovnih navarov nismo zasledili mikroporoznosti in vključkov. Proces varjenja poteka zelo mirno in enakomerno, tako da se pri vsakem pulzu odtali le ena kapljica. Varjenje poteka brez brizganja, kar zagotavlja zelo lep izgled površine navara.

Zaradi znatno večjega uvarjanja v osnovno konstrukcijsko jeklo, so navari pri pulznem varjenju z varilno žico VAC 60 celo manj

legirani, kot pri finokapljicastem varjenju v zaščitni plinski mešanici Ar + 18 vol.% CO₂ (tabela 1). Legiranje navarov z ogljikom narašča z jakostjo varilnega toka. Parametri varjenja imajo močan vpliv na disociacijo CO₂ ter s tem tudi na parcialni tlak ogljikovega monoksida v obloku ($2 \text{ CO}_2 \rightarrow 2 \text{ CO} + \text{O}_2$) in oksidativnost atmosfere v okolici obloka. Zato pri nizkih jakostih varilnega toka (159 A) silicij in mangan skoraj ne odgorevata med varjenjem. Pri višji jakosti varilnega toka (281 A) pa povečana oksidativnost plinske atmosfere povzroči intenzivnejše odgo-

revanje dezoksidantov. Proces odgorevanja vpliva na znižanje vsebnosti Si in Mn v varu 3, kar je zelo lepo vidno v tabeli 3.

Pri danih pogojih pulznega varjenja z varilno žico VAC 60 v zaščitni plinski mešanici Ar + 18 vol.% CO₂ je bilo uvarjanje v osnovno konstrukcijsko jeklo okoli 50 %-no. Tako uvarjanje smo dosegli

SKLEPI

Z žico VAC 60 (0,06 % C; 0,9 % Si in 1,5 % Mn), ki jo proizvajajo ELEKTRODE Jesenice za varjenje po MAG postopku pod CO₂, dobimo zelo kakovostne vare z žilavostjo preko 150 J tudi v primeru, ko varimo v zaščitni plinski mešanici Ar + 18 vol. % CO₂. Varjenje poteka mirno, enakomerno in skoraj brez brizganja. Zaradi šibke oksidativnosti zaščitne plinske mešanice Ar + 18 vol.% CO₂ skoraj ni odgorevanja dezoksidantov med procesom taljenja dodatnega materiala pri varjenju. Razredčenje navara zagotavlja le intenzivnost taljenja osnove oziroma velikost stopnje uvarjanja, kar pa ne zadostuje, da ne bi bili navari višje legirani in trši. Dobre žilavosti so posledica visoke čistoče in kakovosti varov.

Še kakovostnejše vare in navare z dobrim videzom dobimo s pulznim varjenjem, v zaščitni plinski mešanici Ar + 18 vol. % CO₂. Ker vsak pulz odtali le eno kapljico, tudi brizganja ni, kar zagotavlja zelo lep izgled varov ali navarov. Zaradi zelo intenzivnega uvarjanja v osnovno konstrukcijsko jeklo so navari kljub varjenju z žico VAC 60 celo manj legirani, kot pri finokapljičastem varjenju v zaščiti Ar + 18 vol. % CO₂. Pri pulznem varjenju

pri varjenju z jakostjo osnovnega toka 30 A in energijo pulza, ki je bila pri vseh varjenjih okoli 50 J. S spreminjanjem jakosti osnovnega toka in energije pulza lahko vplivamo na uvarjanje, to je taljenje osnovnega materiala, kar je zelo pomembno pri varjanju, še pomembnejše pa je pri navarjenju legiranih nanosov na nelegirano konstrukcijsko jeklo^[16].

z nizkimi povprečnimi jakostmi varilnega toka skoraj ne pride do odgorevanja silicija in mangana med taljenjem dodatnega materiala. Na vsebnost silicija in mangana v navaru vpliva torej le stopnja uvarjanja, ki povzroči razredčenje čistega vara zaradi taljenja osnovnega konstrukcijskega jekla. Šele pri višjih povprečnih jakostih varilnega toka (281 A), nastane zaradi intenzivne disociacije CO₂ ($2\text{CO}_2 \rightarrow 2\text{CO} + \text{O}_2$) povečana oksidativnost obločne atmosfere, kar vpliva tudi na znatnejše odgorevanje dezoksidantov (Si in Mn). Ti navari zato vsebujejo najmanj silicija in mangana.

Stopnja disociacije CO₂ v obločni atmosferi ima pri pulznem varjenju v zaščitni plinski mešanici Ar + 18 vol. % CO₂ posebno pri višjih povprečnih jakostih varilnega toka (nad 250 A) pomemben vpliv na kemično sestavo navara. Vsebnost ogljika v navaru se zvišuje, če povečujemo povprečno jakost varilnega toka.

Pri pulznem varjenju v zaščitni plinski mešanici Ar + 18 vol. % CO₂ je kemična sestava varov in navarov, ki pomembno vpliva na njihovo kakovost, najbolj odvisna od stopnje uvarjanja v osnovno konstrukcijsko jeklo. Na velikost uvarjanja pa lahko uspešno vplivamo z izbiro oblike in energije pulza ter jakostjo osnovnega

toka. Velikost uvara je izredno pomembna za uspešno varjenje tankih pločevin, katerih brez nadzorovanega taljenja osnovnega materiala ne moremo pro-

duktivno variti, in pri navarjanju legiranih nanosov na nelegirano konstrukcijsko jeklo.

SUMMARY

Pulsed arc welding of structural steels

In practice structural steels are usually MAG welded using solid welding wires and CO₂ shielding gas. MAG welding is a productive, cost-effective and very adaptable welding process. It may be used as a semi-automatic process also on site. It is also very suitable for automation and robotization of the welding processes in industrial applications^[1-7]. Because of its versatile industrial applicability, the share of shielding gas arc welding applications for various materials has considerably increased. In the last 20 years its share has doubled mainly at the expense of the manual metal arc welding with covered electrodes. Figure 1 shows the shares of the most important arc welding processes^[1].

In welding of structural steels usually as filler material using solid wires VAC 60 (0.9 % Si and 1.5 % Mn)^[8]. Because welding with of the very oxidising shielding gas CO₂ are intense burn-off of silicon and manganese (Table 1).

A common welding process in welding of structural steels using VAC 60 wire (EN 440 - G3Si)^[8] and CO₂ oxidizing shielding gas^[9-11] is very chaotic and does not guarantee a high weld quality^[12]. Thus short-circuiting welding of thin sheets will be irregular in terms of metal transfer. A still more irregular metal transfer can be

found in high-productivity spray arc welding of thick sheets. Spray metal transfer consists in the explosions of the droplets melting off due to the formation of carbon monoxide (CO) in the molten pool of the melted wire.

The quality of the welds made with MAG welding in CO₂ with VAC 60 wire, and with short-circuiting and spray metal transfers, is essentially affected by the frequent occurrence of microporosity at bead boundaries. The weld toughness achieved is, therefore, somewhat lower, but still satisfactory in most cases of structural-steel welding. Thus a quality welded joint with a toughness of around 100 J according to a Charpy V-notch test at 20 °C and with a composition and hardness values of around 140 HV 0.3, which is very close to the quality of the parent metal, i.e. structural steel, is still satisfactory (Table 2).

With VAC 60 wire (0.06 % C; 0.9 % Si and 1.5 % Mn), product of Slovenian firm ELEKTRODE Jesenice, for CO₂ welding high-quality welds with toughness of over 150 J are obtained also in case welding is carried out in Ar + 18 vol. % CO₂ gas mixture. Welding is calm, uniform and almost without spatter. Because of a low oxidizing capability of Ar + 18 vol. % CO₂ gas mixture there is almost no burn-off of the deoxidizers during melting of the filler material. The surfacing-weld dilution can

be ensured only by intense melting of the parent metal, i.e., the degree of penetration respectively. This, however does not suffice to obtain higher-alloyed surfacing welds with higher hardness. Favourable toughness is a result of high purity and quality of surfacing welds (Table 2).

Surfacing welds of still higher quality and nice appearance can be obtained in pulsed arc welding in the gas mixture of Ar + 18 vol. % CO₂. There is no spatter because each pulse will melt only one droplet, which provides nice appearance of the surfacing welds or weld (Figure 2 and Table 3)^[13-15]. Due to intense penetration into the parent metal, i.e. structural steel, the surfacing welds are, in spite of welding with VAC 60 wire, even lower alloyed than in welding in fine-droplet welding in Ar + 18 vol. % CO₂. In pulsed welding with low average welding currents there is almost no burn-off of silicon and manganese during melting of the filler material (Figure 3 and Table 4). The contents of silicon and manganese in the surfacing welds are thus affected only by the degree of penetration, which produces the dilution of the all-weld metal due to melting of the parent metal (Figure 4 and Table 5). It is only at higher average welding currents (281 A) that, because of intense dissociation of CO₂ ($2\text{CO}_2 \rightarrow 2\text{CO} + \text{O}_2$), the oxidizing capability of the arc atmosphere will occur, which, in turn, will provide stronger burn-off of the deoxidizers Si and Mn. Consequently, these surfacing welds will contain the least

silicon and manganese (Figure 4 and Table 5)^[15, 16].

The degree of dissociation of CO₂ in the arc atmosphere in pulsed welding in Ar + 18 vol. % CO₂ gas mixture thus essentially affects the chemical composition of the surfacing weld. The carbon content in the surfacing weld will be increasing with the average welding current increasing as well (Figure 4 and Table 5).

In pulsed arc welding in Ar + 18 vol. % CO₂ gas mixture, the chemical composition of the welds and surfacing welds, which essentially affects their quality, is mostly dependent on the degree of penetration into the parent metal, i.e., structural steel. The degree of penetration can be affected efficiently by the pulse shape and energy and the base current. The degree of penetration is very important to accomplish efficient welding of thin sheets, which cannot be accomplished without controlled melting of the parent metal, and in surfacing of deposits on unalloyed structural steel.

All experimental pulsed welding and surfacing was carried out with a Synergic 450 MIG pulse welding device, product of ISKRA-Varjenje, which permits controlled energy input during welding and a choice of the base current and the pulse shape and energy. In setting of the degree of penetration, the pulse energy is more important than the base current.

VIRI

- [29] KÖVEŠ, A. (2003): Nadaljni razvoj varilnih postopkov in varilnikov s posebnim ozirom na povečanje produktivnosti varjenja. *Dan varilne tehnike: zbornik*. Maribor, pp. 66-69.
- [30] CHURCH, J.G., IMAIZUMI, H. (1990): Welding characteristics of a new welding Process, T.I.M.E. – Process. *IIW Doc. XII – 1199-90*.
- [31] BAUM, L., KNOCH, R. (1997): Höhere Wirtschaftlichkeit durch MAG-Hochleistungsschweiss-verfahren. *DVS-Berichte Band 183.*; pp. 50-55.
- [32] MITA, S., HARADA, S. (2004): Trends and Perspective of Welding Power Source in Japan. *IIW Doc. XII – 1824-04*.
- [33] UEYAMA, T., TONG, H., HARADA, S. (2000): Improve Sheet Metal Welding Quality & Productivity with AC Pulsed MIG Welding System. *IIW Doc. XII – 1629-00*.
- [34] SUZUKI, R., NAKANO, T. (2001): Development of MAG Welding Wires for Thin Steel Sheets in Automotive Industry. *IIW Doc. XII-1679-01*.
- [35] YAMAMOTO, H., TAKANO, Y., HIRAKAWA, M., TAKATANI, T., SENZAKI, M., IKEGAMI, Y. (2001): Development of a Double Wire MAG Welding System for Robots. *IIW Doc. XII-1682-01*.
- [36] Catalogue of filler materials produced by ELEKTRODE Jesenice d.o.o., Welding Consumables, (1999).
- [37] EN 439: *Dodajni materiali za varjenje – Zaščitni plini za obločno varjenje in rezanje* (EN 439: Welding consumables-shielding gases for arc welding and cutting), 1994.
- [38] SHACKLETON, D.N., SMITH, A.A. (1984): Standardisation of shielding gas mixtures for MIG/MAG welding, *IIW Doc. XII-832-84*.
- [39] KEJŽAR, R. (2001): Deoxidation of the weld in active gas welding. *IIW Doc. XII-1686-01*.
- [40] SUBAN, M. (2001): Kaotično obnašanje prehoda materiala pri MAG/MIG načinu varjenja (The chaotic behaviour of material transfer in MAG/MIG welding). *Varilna tehnika.*; Vol. 50 No. 1, pp. 16-20.
- [41] LANCASTER, J.F. (1986): *The physics of welding.*; IIW-Pergamon Press, Oxford.
- [42] LANGUS, D., KRALJ, V. (2005): Optimiranje varilnih parametrov pri impulznem varjenju MIG/MAG s sinusnimi, širinsko krmiljenimi impulzi toka. *Dan varilne tehnike: zbornik*. Novo mesto, pp. 127-136.
- [43] KEJŽAR, U., KLOBČAR, D., KEJŽAR, R. (2005): Prednosti pulznega varjenja konstrukcijskih jekel. *Dan varilne tehnike: zbornik*. Novo mesto, pp. 119-126.
- [44] KEJŽAR, R. (2003): Študij legiranja navara pri navarjanju obrabno obstojnih nanosov pod legiranimi varilnimi praški (Study of the alloying of a surfacing weld in the surfacing of wear-resistant deposits with alloyed welding fluxes). *Materiali in tehnologije.*; Vol. 37, No. 3-4, pp. 167-172.

^{15}N signal of *Aplysina aerophoba* as a tracer of anthropogenic nitrogen in the Murter Sea and Pirovac Bay (Central Adriatic)

^{15}N v *Aplysini aerophobi* kot sledilo antropogenega dušika v Murterskem morju in Pirovaškem zalivu (srednji Jadran)

NASTJA ROGAN¹, TADEJ DOLENEC^{1,2}, SONJA LOJEN², ŽIVANA LAMBAŠA³, MATEJ DOLENEC¹

¹University of Ljubljana, Faculty of Natural Sciences and Engineering, Department of Geology, Aškerčeva cesta 12, SI-1000 Ljubljana, Slovenia;

E-mail: nastja.rogan@ntfgeo.uni-lj.si, tadej.dolenec@ntfgeo.uni-lj.si, matej.dolenec@s5.net

²Jožef Stefan Institute, Jamova cesta 39, SI-1000 Ljubljana, Slovenia;

E-mail: sonja.lojen@ijs.si

³Šibenik-Knin County, 22000 Šibenik, Croatia

Received: June 21, 2007 **Accepted:** July 10, 2007

Abstract: Stable nitrogen isotopes were used to study the environmental impact of sewage-discharge and fish-farming-derived nitrogen in the Murter Sea and in the semi-enclosed Pirovac Bay (Central Adriatic). The results suggested that the effluents from the septic systems of Murter Island and the coastal part of Pirovac Bay discharged into the adjacent coastal ecosystems, which together with the fish-farm-derived fecal material and the feed wastage affected the stable nitrogen isotopic composition of the marine sponge *Aplysina aerophoba*. Furthermore, the $\delta^{15}\text{N}$ signature of *Aplysina aerophoba* can be useful in tracing the untreated municipal and other sewage-derived nitrogen flow in marine coastal ecosystems and the dispersion of ^{15}N loadings generated by the inflows from fish farms.

Izvleček: Članek obravnava izotopsko sestavo dušika v morski spužvi *Aplysina aerophoba* iz Murterskega morja in Pirovaškega zaliva (srednji Jadran). Rezultati raziskave kažejo, večje vrednosti parametra $\delta^{15}\text{N}$ v *Aplysini aerophobi* iz priobalnih delov Murterskega morja in Pirovaškega zaliva, ki so posledica vnosa izotopsko težjega dušika ^{15}N z netretiranimi komunalnimi in drugimi odplakami ter izpustov iz ribjih farm. Dobljeni podatki nakazujejo tudi možnost uporabe omenjene spužve za monitoring vpliva odpadnih voda na obalne ekosisteme.

Key words: *Aplysina aerophoba*, municipal sewage, fish farming activities, nitrogen isotope composition, Murter Sea, Pirovac Bay, Central Adriatic

Ključne besede: *Aplysina aerophoba*, komunalne odplake, ribje farme, izotopska sestava dušika, Murtersko morje, Pirovški zaliv, srednji Jadran

INTRODUCTION

Increased nitrogen loadings have been implicated in eutrophication occurrences worldwide. A significant component of marine eutrophication in many near shore environments can be attributed to the inputs of anthropogenic nitrogen from untreated domestic sewage, as well as municipal and industrial effluents (BACHTIAR, et al., 1996; COSTANZO, et al., 2001; LEE and OLSEN, 1985; NIXON, et al., 1986). In the past decade, the increasing number of fish-culture industries in the Mediterranean and Adriatic area has also begun to create environmental problems due to the impact caused by fish-farming waste. Many papers have shown how fish-farm biodeposition products can negatively affect the sediment chemistry and the community dynamics of seagrass benthic macrofauna, meiofauna, and benthic bacteria (DOLENEC, et al., 2007; 2006; HOLMER, 1991; LA ROSA, et al., 2001; MIRTO, et al., 2002; PERGENT, et al., 1999; RUIZ, et al., 2001; SARA, et al., 2004).

The near-shore environments of the Murter Sea and the semi-closed Pirovac Bay are among the most impacted areas in northern Dalmatia. The area is exposed to and affected by municipal and industrial sewage from Murter Island and the coastal parts of Pirovac Bay. The aquaculture located near Vrgada Island (Murter Sea) is an additional source of the increased

amounts of dissolved and particulate nutrient loads, especially of organic phosphorus (P) and nitrogen (N).

Stable isotopes of biogenic elements (C, N, S) have been used successfully for assessing and monitoring aquatic ecosystem quality. Stable isotope ratios can provide information about trophic structure, resource partitioning, habitat usage and species migration (FRY et al., 1977; KNEIB and STIVEN, 1980; ZIEMAN et al., 1984; MUSCATINE et al., 1989; THOMAS and CAHOON, 1993; NEWELL et al., 1995; DEEGAN AND GARRITT, 1997; MONCREIFF and SULLIVAN, 2001; VIZZINI et al., 2002; VIZZINI and MAZZOLA, 2002) and determine major nutrient sources in natural food webs (SHEARER and KOHL, 1993; COFFIN et al., 1994).

The aim of this study was to assess the anthropogenic effects on the marine sponge *Aplysina aerophoba* in the Murter Sea and Pirovac Bay by using nitrogen isotope analysis. *Aplysina aerophoba* is one of the most abundant sponges; it is very widespread on the shoal rocky bottom in the coastal part of the Adriatic Sea and therefore very representative of the investigated area. As a benthic sessile invertebrate the sponge is relatively non-mobile and thus tends to be representative of the area being sampled (REYNOLDS et al., 1995).

MATERIALS AND METHODS

Study area

The study area of about 380 km² is located in the northern Dalmatia Adriatic, Croatia.

It represents the inshore and offshore parts of the Murter Sea, the semi-enclosed Pirovac Bay, the archipelago of the Kornati Islands and the offshore islands of the main islands Žirje and Žut (Figure 1).

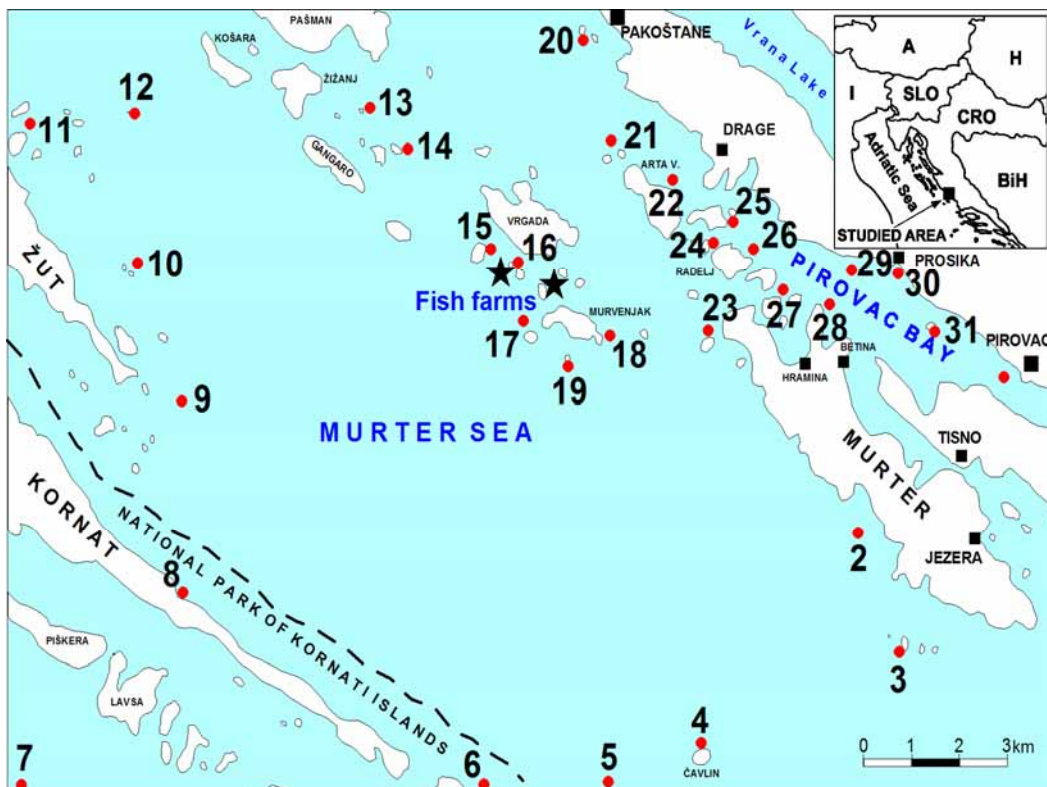


Figure 1. Map of the study area in the Murter Sea and Pirovac Bay (Central Adriatic) showing sites of *Aplysina aerophoba* sampling (★Fish farms)

Slika 1. Geografska karta vzorčnih točak *Aplysine aerophobe* v Murterskem morju in Pirovaškem zalivu - srednji Jadran (★Ribje farme)

The open sea around the Kornati Islands and the islands Žirje and Žut is relatively free from anthropogenic impact, while the coastal part of Murter Sea and Pirovac Bay are exposed to untreated municipal, industrial and to a lesser extent to

agricultural pollution from the nearest small cities, such as Pirovac, Tisno, Jezera, Betina and Murter, which increased the amount of nitrogen loading in the particulate organic matter (POM) and the sediments of this region. Marinas in Jezera,

Betina and Hramina provide additional inputs of anthropogenic nitrogen from untreated faecal sewage and industrial effluents.

Around Vrgada Island are the fish cages with European sea bass (*Dicentrarchus labrax*), gilt-head sea bream (*Sparus aurata*) and Atlantic blue fin tuna (*Thunnus thynnus*). The annual production is approximately 450 tons of *Dicentrarchus labrax* and *Sparus aurata*, as well as 1000 tons of *Thunnus thynnus*. The amount of food consumed each year is about 900 tons of pelleted food for the sea bass and sea bream and about 7200 tons of fresh and frozen fish for the blue fin tuna. Fish-farming activities are the source of N-rich inputs such as fish excreta and uneaten food.

As the reference site we chose Lumbarda reef flat, which is situated in the open sea, 3 km west of the island Sedlo (Figure 1). Results from previous research confirmed that the ecosystems around Lumbarda are not affected by environmental pollution (DOLENEC et al., 2006).

Sample collection

The individuals of *Aplysina aerophoba* were collected by scuba diving from 26 locations at depths of approximately 2-5 m. To obtain the strongest possible $\delta^{15}\text{N}$ signal, the sampling period was limited to the peak of the summer tourist season (the last two weeks in August 2005). A strong light intensity, high temperatures and efficacious nutrients ensure that the increased primary production is high in August. As a result of intensive tourist activities, the input of untreated human and industrial sewage is also at its highest

during that period. The sampling sites were located in the Murter Sea and the semi-enclosed Pirovac Bay (sampling sites PB) as well as around the Vrgada Island, close to the fish farms (sampling sites FF) and in the coastal parts of the small isolated Islands of Kornati, Žut and Žirje (sampling sites ROFF). The reference site was selected in the Lumbarda reef flat. Between five and eight individuals were sampled at each location.

Sample preparation and stable nitrogen isotope analysis

Fresh *Aplysina aerophoba* samples were placed in plastic bags and refrigerated immediately after collection to await further processing. All the *Aplysina aerophoba* individuals were size and weight matched (basal diameter 1.5 cm; height 10 cm) in order to avoid possible isotope effects caused by ontogenetic dietary shifts (DENIRO and EPSTEIN, 1981; MUSCATINE and KAPLAN, 1994, LOJEN et al., 2005) or differences in age (OWENS, 1987), which could also affect the nitrogen isotopic composition. For the isotope analyses only the topmost 1-cm part of five different individuals of *Aplysina aerophoba* from each sampling site were chosen. The selected parts of all the samples were carefully examined with a binocular microscope for the presence of other sponge-dwelling organisms (small worms and crabs), which were separated from their host. Located in a higher trophic level, worms and crabs have different nitrogen isotopic composition than sponges, and their presence in *Aplysina aerophoba* distorts the original nitrogen isotopic signal. *Aplysina aerophoba* samples thus represent the combined tissues of the topmost 1-cm part of five

individuals and the associated micro-organisms.

In the laboratory the sponge samples were first rinsed with deionized water to remove salts and sediment particles and then freeze-dried for a minimum duration of 72 h. Lyophilized samples were crushed and homogenised in an agate mortar to avoid heavy-metal contamination. Powder samples packed in tin capsules were preserved in desiccators at room temperature prior to the isotope analysis. The samples from each location were analysed individually.

The nitrogen isotopic composition of the *Aplysina aerophoba* samples was measured using a Europa 20-20 continuous-flow isotope-ratio mass spectrometer with an ANCA SL preparation module (PZD Europa Ltd., U.K.). The results are expressed in the standard $\delta^{15}\text{N}$ notations as the relative per mille (‰) difference between the sample and the nitrogen standard (atmospheric

nitrogen, $\delta^{15}\text{N} = 0$ ‰). The analytical precision (1 standard deviation) of triplicate analyses of IAEA N-1 and N-2 standards was better than ± 0.16 ‰. The precision (1 standard deviation) of the duplicate isotopic analyses of samples was within ± 0.2 ‰.

Data analysis

The differences between the sampling sites from Pirovac Bay and the coastal part of the Murter Sea (PB group) as well as the reference and other offshore-location sampling sites (ROFF group) and fish farms (FF group) were initially tested using an analyses of variance (one-way ANOVA) followed by Tukey's Honest Significant Difference (HSD) test to compare the data between the nitrogen isotope composition of the *Aplysina aerophoba* from among the sampling-site groups. The results were accepted as significant when $p < 0.05$.

RESULTS

The results of the $\delta^{15}\text{N}$ determination in *Aplysina aerophoba* are shown in Table 1 and represent the average nitrogen composition of the topmost 1-cm part of the *Aplysina aerophoba* individuals collected in August 2005. The mean, minimum and maximum $\delta^{15}\text{N}$ values together with the variance for Pirovac Bay and the coastal part of the Murter Sea (PB group) and the fish farms (FF group), as well as the reference and offshore (ROFF group) samples are shown in Table 2 and Figure 2. The data from Tukey's HSD test are summarized in Table 3.

The *Aplysina aerophoba* samples can be divided into two statistically different groups: the reference and offshore sites (ROFF sampling sites 3-12 and 18, 19) and the Murter Sea and Pirovac Bay sites (PB sampling sites 2 and 20-28) together with the fish-farm sites (FF sampling sites 13-17). The division was made on the basis of the mean $\delta^{15}\text{N}$ values of the group members (1.38, 3.95 and 4.78 ‰ for the ROFF, PB and FF groups, respectively). Tukey's HSD test showed a statistically significant difference between the ROFF and PB and/or the FF sites, while no

significant difference could be observed between the PB and FF sites (Table 3).

The results shown in Table 1 indicate that the $\delta^{15}\text{N}$ values of the *Aplysina aerophoba* tissues varied between -0.7 and $+5.7$ ‰, with a spread of 6.4 ‰ and a mean value of $+2.96$ ‰. The first group of *Aplysina aerophoba* samples (ROFF sites) included individuals from the unaffected Lumbarda reference site (**sampling site 7), from the open-sea locations in the Murter Sea (sampling sites 4-6), as well as from the reef flats near the offshore Kornati Islands (sampling site 8) and the Žut Island (sampling sites 8-12). The $\delta^{15}\text{N}$ values of this group vary between -0.7 and $+3.0$ ‰, with a mean value of $+1.38$ ‰. The

second group (PB sampling sites) represents the *Aplysina aerophoba* individuals with slightly elevated $\delta^{15}\text{N}$ values in the range of $+3.0$ to $+5.1$ ‰ and a mean of $+3.95$ ‰. These samples were mostly collected from the coastal part of Murter Island and from Pirovac Bay. However, in the inner part, the most impacted part of Pirovac Bay, the marine sponge *Aplysina aerophoba* was not present. We can find *Aplysina aerophoba* only near the inner side of the islands, which separate Pirovac Bay from the Murter Sea. The third group (FF sampling sites) consists of *Aplysina aerophoba* individuals with the highest $\delta^{15}\text{N}$ values, which vary from $+4.1$ to $+5.7$ ‰, while the mean is $+4.78$ ‰ (Table 1, Figure 1).

Table 1. $\delta^{15}\text{N}$ values of *Aplysina aerophoba* collected in the Murter Sea and Pirovac Bay - Central Adriatic in August 2005 (average sample of the topmost 1-cm part of five different individuals)

Tabela 1. Vrednosti $\delta^{15}\text{N}$ v *Aplysini aerophobi* v avgustu 2005, na območju Murterskega morja in Pirovaškega zaliva - srednji Jadran (vzorec predstavljajo najvišji, 1 cm veliki deli petih različnih prstastih tvorbo)

Sample No.	Sampling site	Sample group	$\delta^{15}\text{N}$ (‰)	$\sigma \pm$
1	Pirovac (coast)		-	-
2	Murter Island SE	3 PB	+ 3.5	0.1
3	Kukuljari Islands	1 ROFF	+ 2.0	0.1
4	Reef Flat Čavlin	1 ROFF	+ 1.5	0.3
5	Nozdra Island	1 ROFF	+ 0.4	0.2
6	Reef Flat Puh	1 ROFF	+ 0.4	0.1
7*	Reef Flat Lumbarda**	1 ROFF	- 0.7	0.1
8	Bikarijca (coast)	1 ROFF	+ 0.6	0.1
9	Reef Flat Kamenjar	1 ROFF	+ 1.3	0.2
10	Dinariči Islands	1 ROFF	+ 1.9	0.1
11	Gustac Island	1 ROFF	+ 1.5	0.1
12	Reef Flat Galijolica	1 ROFF	+ 3.0	0.2
13	Ošljak Island	2 FF	+ 4.1	0.2
14	R. Kotula Island	2 FF	+ 4.5	0.3
15	Špinata Island***	2 FF	+ 5.5	0.1
16	Rakita Island***	2 FF	+ 5.7	0.1
17	Gira Island	2 FF	+ 4.1	0.2
18	Murvenjak Island	1 ROFF	+ 2.2	0.1
19	Vrtlič Island	1 ROFF	+ 2.4	0.1
20	Žavinac Island	3 PB	+ 3.6	0.2
21	Sestrice Islands	3 PB	+ 3.0	0.1
22	Arta V. Island	3 PB	+ 3.4	0.2
23	Prišnjak V. Island	3 PB	+ 3.5	0.1
24	Prišnjak M. Island	3 PB	+ 3.9	0.2
25	Arta M. Island	3 PB	+ 4.0	0.3
26	Radelj Island	3 PB	+ 4.5	0.2
27	Vinik Island	3 PB	+ 5.0	0.1
28	Cap of Gradina	3 PB	+ 5.1	0.1

reference site **, fish farm***

Table 2. Basic descriptive statistics of nitrogen isotopic composition ($\delta^{15}\text{N}$ values) of *Aplysina aerophoba* collected in the Murter Sea and Pirovac Bay - Central Adriatic in August 2005

Tabela 2. Osnovna statistika za izotopsko sestavo dušika ($\delta^{15}\text{N}$ vrednosti) v *Aplysini aerophobi* na območju Murterskega morja in Pirovaškega zaliva - srednji Jadran (avgust 2005)

Sample group	$\delta^{15}\text{N}$						
	N	Min	Max	Median	Means	S.D.	Variance
1 ROFF	12.00	-0.70	3.00	1.50	1.38	1.04	1.08
2 FF	5.00	4.10	5.70	4.50	4.78	0.77	0.59
3 PB	10.00	3.00	5.10	3.75	3.95	0.70	0.50
All Loc.	27.00	-0.70	5.70	3.40	2.96	1.70	2.89

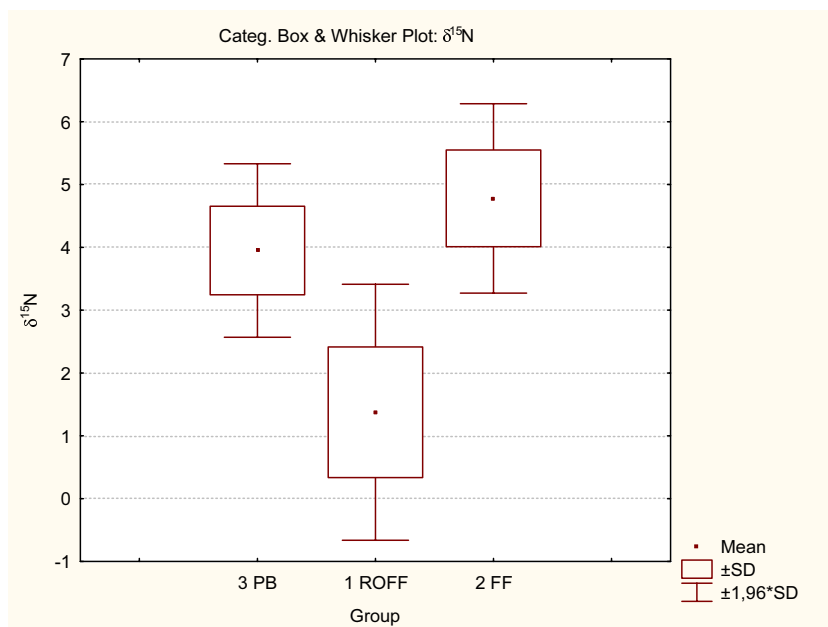


Figure 2. Whisker plots of $\delta^{15}\text{N}$ values of *Aplysina aerophoba* (ROFF - reference and offshore locations; FF - fish-farm sampling sites; PB - Murter Sea and Pirovac Bay sampling sites)

Slika 2. Whiskerjevi diagrami $\delta^{15}\text{N}$ vrednosti v *Aplysini aerophobi* (ROFF – referenčna in oddaljene (od obale) lokacije; FF – vzorčne točke pri ribjih farmah; PB – vzorčne točke v Murterskem morju in Pirovaškem zalivu)

Table 3. Tuckey HSD test; Marked differences (***) of nitrogen isotopic composition ($\delta^{15}\text{N}$ values) of *Aplysina aerophoba* of ROFF, FF and PB group are significant at $p < 0.05$

Tabela 3. Tuckey-jev HSD test; označene razlike (***) izotopske sestave dušika ($\delta^{15}\text{N}$ vrednosti) v *Aplysini aerophobi* za skupine ROFF, FF and PB so značilne pri $p < 0.05$

	1 ROFF	2 FF	3 PB
1 ROFF	-	***	***
2 FF	***	-	-
3 PB	***	-	-

DISCUSSION

Sponges are primitive metazoans. Instead of organs or tissues they possess amoeboid, omnipotent and phagocytotically active cells that move freely through the sponge matrix, termed the mesohyl. Various micro-organisms have evolved to reside in the sponges, including cyanobacteria, diverse heterotrophic bacteria, unicellular algae and zoochlorellae (FREDERICH et al., 2001 and references therein). Three types of associations of micro-organisms with *Aplysina aerophoba* have been described: 1) cosmopolitan bacteria, which most likely serve as a food source, 2) extracellular bacteria, which are probably specific to the sponge mesohyl, and 3) intracellular bacteria, which permanently reside in the nuclei of specific host cells (VACELET, 1975). The presence of the hosted bacteria can amount as much as to 40 % of the total animal biomass (YOUNG-BEON et al., 2003). *Aplysina aerophoba* sponges also contain high concentrations of brominated metabolites (up to 13 % of the dry weight) with antimicrobial activity (SHARMA AND BURKHOLDER, 1967; FAULKNER, 1978), repellent properties

against predators (WEISS et al., 1996), and cytostatic activity in human breast-cancer cell lines (KREUTER et al., 1990). All these compounds, which are probably produced by the sponge itself (EBEL et al., 1997) as well as the hosted bacteria, and the food sources influenced the nitrogen isotope composition of the *Aplysina aerophoba*.

Aplysina aerophoba is a filter feeder, utilizing food particles suspended in the water and captured by the coenocytes. These food particles consist essentially of bacteria, other micro-organisms, and particles of organic debris. The feeding strategies of the suspension filter feeders are assumed to be closely coupled to the seasonal input of POM (IKEN et al., 2001). In marine ecosystems impacted by fish-farm activities or untreated human and animal waste of faecal origin, the effluent related $\delta^{15}\text{N}$ signal is incorporated into the entire food web (MCCLELLAND and VALIELA, 1998; RISK and ERDMAN, 2000; HEIKOOP et al., 2000; BURFORD et al., 2002). Fish-farm loadings and waste-water nutrients derived from septic systems and animal wastes are generally enriched in the heavy nitrogen isotope ^{15}N . This is due to the nitrogen transformation that typically

occurs in such waters before or after discharge (HEIKOOP et al., 2000). Consequently, the POM and biota in marine ecosystems impacted by such anthropogenic nitrogen inputs are also enriched in ^{15}N .

The differences in the $\delta^{15}\text{N}$ values of the *Aplysina aerophoba* among all three groups of sites (FF, PB and ROFF) are in the range of 6.4 ‰, which is quite a lot when compared to the literature data for a single species raised on an identical diet. Kidd et al. (1995) reported that the variation in the $\delta^{15}\text{N}$ values for arctic lake invertebrates was less than 2.0 ‰. Variations in the $\delta^{15}\text{N}$ values in individuals of the same species could be related to size and age effect (MINIWAGA and WADA, 1984; WADA et al., 1991), a depth effect (SAINO and HATORY, 1980; MUSCATINE and KAPLAN, 1994), seasonal effects (MARRIOTTI et al., 1980; COSTANZO et al., 2001), and differences due to varying levels of ^{15}N -enriched fish-farm or human-sewage-derived nitrogen (RISK and ERDMAN, 2000; COSTANZO et al., 2001; MAZZOLA and SARÀ, 2001; VIZZINI and MAZZOLA, 2004; SARÀ et al., 2004). As the size, depth and season of collection were strictly controlled by the sampling design, the observed variations in *Aplysina aerophoba* ^{15}N content appears to be primarily explained by a variation in the extent of the elevated ^{15}N -enriched sewage and/or effluents input into the investigated area.

The isotopic composition of organisms feeding in either clean or polluted environments also depends upon their position in the food chain. The lowest trophic level TL - 1 consists of phytoplankton with $\delta^{15}\text{N}$ values of about +

5 ‰. Sponges, anemones, mussels, small polychaetes and copepods represent the TL - 2 trophic level. Their $\delta^{15}\text{N}$ values range between + 5 and + 7 ‰. The $\delta^{15}\text{N}$ values of the *Verongia aerophoba* tissue analysed during this study were found to be lower than the reported values for trophic level TL - 2. All *Aplysina aerophoba* individuals analyzed during this study also exhibited $\delta^{15}\text{N}$ values that are generally lower relative to the nitrogen isotopic composition of POM (a mixture of phytoplankton, detritus, bacteria and small micro-zooplankton) at the base of the food web (DOLENEC et al., 2006; 2007). This is not consistent with previous studies, which assumed a diet-tissue fractionation factor of between 2.8 and 3.8 ‰, with an average of 3.20 ± 0.14 ‰ (PERSIC et al., 2004) and an enrichment of consumers in terms of ^{15}N with increasing food-web position. Such depletion was already reported for some other species of sponge in oligotrophic environments (*Mycale fistulifera* around the Ardag fish farm in Eilat, Red Sea, LOJEN et al., 2005). The depleted signature in *Aplysina aerophoba*, lower than that of POM, most probably indicated the fractionation of nitrogen isotopes during uptake and assimilation by hosted bacteria (DOLENEC et al., 2007). The symbiotic association between *Aplysina aerophoba* and bacteria, which plays an important role in the nutrition of some shallow-water sponges (REISWIG, 1975; ARILLO et al., 1993), thus leads to lower $\delta^{15}\text{N}$ values. Those bacteria may be able to metabolize highly refractory material, which can then be assimilated by the sponge, leading to a depletion in terms of the ^{15}N of its tissue.

Although the ^{15}N depletion due to bacterial metabolism considerably lowered the

original $\delta^{15}\text{N}$ food signal in *Aplysina aerophoba*, the observed variations in $\delta^{15}\text{N}$ values could be primarily explained in terms of elevated ^{15}N -enriched sewage inputs into the investigated area. This is also supported by the data relating to nitrogen isotope composition in *Anemonia sulcata* and *Balanus perforatus* tissue, which exhibited similar differences between (ROFF), (PB) and (FF) group samples (DOLENEC et al., 2006).

The $\delta^{15}\text{N}$ values of *Aplysina aerophoba* were significantly higher in the coastal part of the Murter Sea and Pirovac Bay (PB group) and around fish farms (FF group) than they were in the less-affected offshore or pristine sites (ROFF group). Similar ^{15}N enrichment was also found in reef molluscs, stomapods, fishes and corals in SE Asia settings exposed to anthropogenic nutrient pollution (RISK and HEIKOOP, 1997; MENDES et al., 1997; HEIKOOP et al., 2000; RISK and ERDMAN, 2000; WEISS et al., 2002). Elevated $\delta^{15}\text{N}$ values from other world sites have also been measured in marine plants exposed to ground-water contaminated by septic systems (MCCLELLAND et al., 1997) and sewage effluents (GRICE et al., 1996; UDY and DENNISON, 1997; CONSTANZO et al., 2001). Nutrients derived from septic systems are generally enriched in ^{15}N and exhibit $\delta^{15}\text{N}$ values of + 10 to + 22 ‰ (HEATON, 1986). Most of the sewage-derived heavy nitrogen ^{15}N in the semi-enclosed Pirovac Bay and in the coastal part of the Murter Sea tend to be related to the inadequate septic systems and wastewater treatment in the surrounding villages, tourist centres (hotel facilities) in Pirovac Bay (Murter, Betina, Tisno, Jezera and Pirovac), marinas (Hramina, Betina and Jezera), and seasonally open auto

camp. The increase in the human population during the touristic season represents an additional impact of human sewage on the marine coastal ecosystems of Murter Island.

Furthermore, the fish-farm biodeposition products also affect the water column and sediment chemistry, the seagrass, the meiofauna and the benthic bacteria (FINDLAY and WATLING, 1997; HARGRAVE et al., 1997; PERGENT et al., 1999; PEARSON and BLACK, 2000; LA ROSA et al., 2001; MIRTO et al., 2002; ALONGI et al., 2003, SARÀ et al., 2004, DOLENEC et al., 2004, 2005). Faecal waste material, several organic pollutants, algicides and herbicides, disinfectants, antibiotics, inducing agents, probiotics, etc. are enriched in ^{15}N and thus contribute to the elevated $\delta^{15}\text{N}$ signal in different organisms close to the fish farms (TACON et al., 1995; DOLENEC et al., 2007). The wastage of feed, which is estimated to be of about 20% (ENELL, 1995), also contributed to the increased $\delta^{15}\text{N}$ signal in the POM and biota in the impacted area. The effects of fish-farm loading depend on the culture method, the feed type, the farm size, the hydrography, the hydrodynamic regime and other environmental features of the area (PILLAY, 1991).

The strongest $\delta^{15}\text{N}$ signal found in *Aplysina aerophoba* from the coastal part of Murter Island and Pirovac Bay (PB group) suggested the input of untreated domestic and industrial effluents and wastewaters, which were discharged into the coastal ecosystems of the investigated area. The elevated $\delta^{15}\text{N}$ signal in *Aplysina aerophoba* from the SW coastal part of Murter Island could be related to the current-derived sewage from the cities of

Split and Šibenik as well as from the tourist centres of Vodice and Tribunj. The dispersion of ^{15}N loading generated by aquaculture at Vrgada Island, however, affected the adjacent offshore ecosystems and the $\delta^{15}\text{N}$ signal in *Aplysina aerophoba* (FF group) and in other biota (DOLENEC et al., 2006; 2007). A pattern of influence caused by farm waste ^{15}N is a function of the local current speed, the water depth, and the total output from the farms. The last factor is important in determining the real impact on the adjacent environment (IWAMA, 1991).

Aplysina aerophoba from ecosystems located further away from cities, harbours and tourist centres with no appreciable sewage is depleted in ^{15}N . However, the lowest $\delta^{15}\text{N}$ values were measured in the more or less pristine offshore reef flats of the Kornati, Žut and Žirje ecosystems with minimal anthropogenic impact (ROFF group). Offshore ecosystems are usually

characteristic of highly oligotrophic conditions, where the algal fixation of atmospheric nitrogen is the major source of nitrogen. As a result, the $\delta^{15}\text{N}$ signal at the base of the food webs is low and the ^{15}N enrichment of various organisms is also relatively low.

The results of this study further indicated that the enrichment in *Aplysina aerophoba* ^{15}N content decreased with the distance from the coast towards the open-sea ecosystems as well as away from the fish cages. Such onshore-to-offshore $\delta^{15}\text{N}$ variations most probably indicate that the sewage-induced ^{15}N -enrichment signal is rapidly attenuated with the distance from the pollution sources. Similar inshore-offshore $\delta^{15}\text{N}$ variations were also observed in stomapods from Sulawesi (RISK and ERDMAN, 2000) and corals from Indonesia, Zanzibar and the Maldives (HEIKOOP et al., 2000; RISK and ERDMAN, 2000).

CONCLUSIONS

The results presented here indicate that an inadequate municipal infrastructure and aquaculture activities are the principal sources of ^{15}N loading in the investigated area. The ^{15}N -enriched nitrogen in effluents from the septic systems of Murter Island and the coastal part of Pirovac Bay, which discharge into the adjacent coastal ecosystems, were found to be incorporated into the *Aplysina aerophoba* living in the shallow water of the Murter Sea and Pirovac Bay. Similarly, the fish-farm-derived ^{15}N -enriched waste could also be

traced in *Aplysina aerophoba* sampled around the fish farms of the Vrgada and adjacent islands. By using the $\delta^{15}\text{N}$ signature of *Aplysina aerophoba* biologically available and therefore ecologically significant, nitrogen can be detected and used to support the monitoring of the human-sewage impact and/or the influence of fish-farm activities in different marine environments. The $\delta^{15}\text{N}$ signature of *Aplysina aerophoba* and of other biota as well as in POM could also be useful in planning the wastewater management in the region.

POVZETKI

¹⁵N v *Aplysini aerophobi* kot sledilo antropogenega dušika v Murterskem morju in Pirovaškem zalivu (srednji Jadran)

Neprimerna komunalna infrastruktura in aktivnosti v ribjih farmah veljata na podlagi predstavljenih rezultatov za glavna vira obremenitve preiskovanega območja z ¹⁵N. Odplake iz septičnih sistemov otoka Murter in priobalnih delov Pirovaškega zaliva se izlivajo v bližnje obalne ekosisteme in vsebujejo povišane vrednosti ¹⁵N, kateri se posledično vgrajuje v spužvo *Aplysina aerophoba*, ki živi v plitkih vodah Murterskega morja in Pirovaškega zaliva. Odpadki ribjih farm so obogateni s povišanimi vrednostmi ¹⁵N, katere prav tako sledimo v *Aplysini aerophobi*, ki je bila povzročena okoli ribjih farm v bližini otoka Vrgade in sosednjih otokov. Meritve izotopske sestave dušika v *Aplysini*

aerophobi so se izkazale kot dober indikator onesnaženosti različnih morskih ekosistemov s komunalnimi in drugimi organskimi odplakami ter kot odličen pokazatelj obremenitve okolja zaradi marikulture dejavnosti. Vrednosti parametra, $\delta^{15}\text{N}$ v *Aplysini aerophobi*, drugi bioti in partikulatni organski snovi (POM) (geokemične karte) lahko uporabimo za pomoč pri novih okoljskih načrtih in konstrukcijah odpadnih sistemov v regiji.

Acknowledgements

This research was financially supported by the Ministry of Higher Education, Science and Technology, Republic of Slovenia (Bilateral Project between Republic of Croatia and Slovenia for the years 2005-2006, research programme P1-0143), and Geoexp, d. o. o., Tržič, Slovenia. Thanks to Dr. Paul McGuinness for the linguistic corrections.

REFERENCES

- BACHTIAR, T., COAKLEY, J. P. & RISK, M. J. (1996): Tracing sewage-contaminated sediments in Hamilton Harbour using selected geochemical indicators. *The Science of the Total Environment*; Vol. 179, pp. 3-16.
- COSTANZO, S. D., DONOHUE, M. J., DENNISON, W. C., LONERAGAN, N. R. & THOMAS, M. (2001): A New Approach for Detecting and Mapping Sewage Impacts. *Marine Pollution Bulletin*; Vol. 42, pp. 149-156.
- DOLENEC, T., LOJEN, S., KNIEWALD, G., DOLENEC, M. & ROGAN, N. (2007): Nitrogen stable isotope composition as a tracer of fish farming in invertebrates *Aplysina aerophoba*, *Balanus perforatus* and *Anemonia sulcata* in central Adriatic. *Aquaculture*; Vol. 262, pp. 237-249.
- DOLENEC, T., LOJEN, S., LAMBAŠA, Ž. & DOLENEC, M. (2006): Effects of fish farm loading on sea grass *Posidonia oceanica* at Vrgada Island (Central Adriatic): a nitrogen stable isotope study. *Isotopes in Environmental and Health Studies*; Vol. 42, pp. 77-85.
- HOLMER, M. (1991): Impacts of aquaculture on surrounding sediments: generation of organic-rich sediments, V: DEPAUW, N. and JOYCE, J. (Eds.). *Aquaculture and the Environment*. Aquaculture Society Special Publication, pp. 155-175.
- LA ROSA, T., MIRTO, S., MAZZOLA, A. & DANOVARO, R. (2001): Differential responses of benthic microbes and meiofauna to fish-farm disturbance in

- coastal sediments. *Environmental Pollution*.; Vol. 112, pp. 427-434.
- LEE, V. & OLSEN, S. (1985): Eutrophication and management initiatives for the control of nutrients input to Rhode Island coastal lagoons. *Estuaries*.; Vol. 8, pp. 191-202.
- MIRTO, S., LA ROSA, T., GAMBI, C., DANOVARO, R. & MAZZOLA, A. (2002): Nematode community response to fish-farm impact in the western Mediterranean. *Environmental Pollution*.; Vol. 116, pp. 203-214.
- NIXON, S. W., OVIATT, C. A., FRITHSEN, J. & SULLIVAN, B. (1986): Nutrients and the productivity of estuarine and coastal marine ecosystems. *Journal of the Limnology Society of South Africa*.; Vol. 12, pp. 43-71.
- PERGENT, G., MENDEZ, S., PERGENT-MARTINI, C. & PASQUALINI, V. (1999): Preliminary data on the impact of fish farming facilities on *Posidonia oceanica* meadows in the Mediterranean. *Oceanologica Acta*.; Vol. 22, pp. 95-107.
- RUIZ, J. M., PEREZ, M. & ROMERO, J. (2001): Effects of Fish Farm Loadings on Seagrass (*Posidonia oceanica*) Distribution, Growth and Photosynthesis. *Marine Pollution Bulletin*.; Vol. 42, pp. 749-760.
- SARA, G., SCILIPOTI, D., MAZZOLA, A. & MODICA, A. (2004): Effects of fish farming waste to sedimentary and particulate organic matter in a southern Mediterranean area (Gulf of Castellammare, Sicily): a multiple stable isotope study ($\delta^{13}\text{C}$ and $\delta^{15}\text{N}$). *Aquaculture*.; Vol. 234, pp. 199-213.

Rock failures in tunnels

Zruški v predorih

MAGDA ČARMAN¹

¹Geological Survey of Slovenia, Dimičeva ulica 14, SI-1000 Ljubljana, Slovenia;
E-mail: magda.carman@geo-zs.si

Received: June 21, 2007 **Accepted:** July 10, 2007

Abstract: Rock failures of various extents are common in tunnel construction. The source and form of a rock failure depend on actual geological conditions at the time of excavation. Regarding the type of rock there are gradual failures in ductile rocks and sudden failures in stiff rocks. For the purpose of my study I chose rock failures the V Zideh Tunnel and Trojane Tunnel as examples of failures in ductile rocks, and rock failures in the Pletovarje Tunnel, Golo rebro Tunnel and Tabor Tunnel as examples of failures in stiff rock. The results of analysis of some extensive failures in different (stiff and soft) rocks show that rock failures appear mostly in geologically unfavourable areas, such as fault zones and zones with unfavourable distribution of bedding, fissility and joints with additional presence of water. Rock failures often appear in parts of tunnels with thin overburden. Markland's test helps us determine whether a rock failure is due to sliding or is it a gravitational failure. In stiff rocks sliding and falls (gravitational failures) of blocks of rock are characteristic. Failure of tectonically disturbed soft rocks appears in a form characteristic for soils.

Izvleček: Pri gradnji predorov prihaja do različno velikih zruškov. Nastanek zruškov in način porušitve sta povezana z dejanskimi geološkimi razmerami v času izkopa. Glede na vrsto kamnine ločimo postopno porušitev v duktilnih kamninah in trenutno porušitev togih kamnin. Za primer zruškov v duktilnih kamninah sem izbrala predora V Zideh in Trojane, za primer zruškov v togih kamninah pa zruške iz predorov Pletovarje, Golo rebro in Tabor. Pri analizi nekaterih večjih zruškov v različnih (togih in mehkih) kamninah se je izkazalo, da do zruškov prihaja večinoma na območjih z neugodnimi geološkimi razmerami kot so prelomna cona, neugodna medsebojna lega plastnatosti, skrilavosti in razpok ob prisotnosti vode. Zruški so pogosti tudi na območjih z nizkim nadkritjem nad predorsko cevjo. S pomočjo Marklandovega testa ugotavljamo, ali je prišlo do zdrsa ali gravitacijskega zruška. Za toge kamnine so značilni zdrsi ali padci (gravitacijski zruški) kamninskih blokov. Močno tektonsko poškodovane mehke kamnine imajo obliko porušitve, ki je značilna za zemljine.

Key words: rock failure, tunnel, Markland test, slide, gravitational failure

Ključne besede: zrušek, predor, Marklandov test, zdrs, gravitacijski zrušek

INTRODUCTION

Rock failures are common in the construction of underground openings. They often appear during the excavation works. Causes of rock failures during tunnel construction with NATM are unexpected geological circumstances, errors in design, construction faults and poor excavation management^[1].

The subject of my study was rock failures caused by unfavourable geological circumstances. Regarding the type of rock there are gradual failures in ductile rocks (compression, swelling, loosening) and sudden failures in stiff rocks (fall, burst and stroke). For the purpose of my study I chose rock failures in the V Zideh Tunnel and Trojane Tunnel as failures in ductile

rock and rock failures in the Pletovarje Tunnel, Golo rebro Tunnel and Tabor Tunnel as failures in stiff rock.

All tunnels that were subject to my study were constructed within the frame of a programme of motorway construction in Slovenia in the last ten years. Excavation and construction works were carried out according to the New Austrian Tunnelling Method (NATM). The Pletovarje Tunnel and Golo rebro Tunnel are located on the Celje – Maribor motorway, the Trojane Tunnel and V Zideh Tunnel on the Ljubljana – Celje motorway, and the Tabor Tunnel on the Razdrto – Fernetiči motorway. They all have one or two tubes with a diameter of 10 m and run through different types of rocks.

GEOLOGY AROUND THE CHOSEN TUNNELS

The northern part of the Pletovarje Tunnel runs through the Donačka fault zone within which tectonic lenses of various lithology (sandstone, dolomite, marl, keratophyre, limestone) and age (Carboniferous, Permian, Lower Triassic, Tertiary) are caught. The second part of the tunnel runs through tectonically disturbed dolomite of the Lower Triassic age and sandstone, marl and tuff of the Oligocene age^[2]. The Golo rebro Tunnel runs through carbonate rocks of the Middle Triassic age and clastic rocks of, probably, the Tertiary age^[2]. The Tabor Tunnel runs through carbonate rocks of the Cretaceous age^[2].

The V Zideh Tunnel and Trojane Tunnel run through Permo-Carboniferous clastic rocks, which show characteristic interchange of shales, siltstones and sandstones. Those rocks are tectonically disturbed, crushed into tectonic clay or millonite^{[2],[3]}. From engineering geological and geomechanical point of view, the rocks in the area around the Trojane Tunnel belong to a special group of rocks representing a passage between soils and rocks. They are called soft rocks and hard soils, respectively. In an undisturbed state they behave as rocks and show a structure of rock. As a consequence of construction works or water intrusion, however, they start behaving as soils. They are very susceptible to physical and chemical

changes. Soft rocks often cause engineering geological problems. The behaviour of soft rocks can be generally

characterized as anisotropic, elastoplastic, dilatational and time dependent^[4].

INVESTIGATIONS OF ROCK FAILURES

Different causes, such as exceeding of shear strength of rock, sliding along discontinuities, unfavourable distribution of joints, fault zones, presence of water, or a combination of some or all of these factors, can lead to a rock failure. Even though rock itself is strong enough, rock failure may start in those parts of rock mass where tensions are high, and are further transmitted to planes of weakness. When local shear strength is exceeded, a rock failure appears.

For the purposes of my study I chose those rock failures that exceeded the volume of 10 m³. They appeared in the Pletovarje Tunnel, Golo rebro Tunnel, V Zideh Tunnel and Trojane Tunnel.

Due to the crushed state of rock, the rock failures in the Tabor Tunnel were not very extensive, only some smaller pieces fell off locally. The majority of the Tabor Tunnel runs through fissured, partly crushed, zones of limestone. The major problem in

this tunnel was the appearance of large karstic caverns.

All rock failures, with the exception of the failure in the V Zideh Tunnel between chainages 0+713 and 0+722, were sudden and appeared at the time when the tunnel face was being opened. The rock failure in the V Zideh Tunnel could have been predicted by means of geotechnical measurements, as the easily observable deformations of the lining on the tunnel appeared a few days before the rock failure appeared. At that time, unfortunately, there weren't any measurement profiles built in. In the Trojane Tunnel surface measurements had also indicated progressive rock failure, which later spread up to the surface.

Data on location and extension of a rock failure, system discontinuities and geological circumstances are shown in Table 1. The data in the table were compiled from inventories of the faces of tunnels. The last column shows the type of a failure determined by Markland's test.

Table 1. Characteristics of the investigated rock failures**Tabela 1.** Značilnosti obravnavanih zruškov

Tunnel	Chainage	Estimated size of rock failure (m ³)	Systems of discontinuities	Rock	Geological circumstances	Type of rock failure
Pletovarje	30+ 329	18	5/85, 30/85, 200/75	fine sandstone, tuff sandstone	fault zone, water seepage	gravitational
Pletovarje	30 +407	12	270/90, 340/80, 210/50	fine sandstone, tuff	fault zone	slide
Golo rebro	27 +599	12	10/60, 80/85, 290/60	crushed dolomite	fault zone, moisture	slide
Golo rebro	27 + 909	10	115/60, 285/60, 250/80, 85/80	dolomite breccia	fault zone	gravitational
Golo rebro	27 + 974	20	145/85, 270/70, 110/40	dolomite	thin overburden	slide
V Zideh	0 + 572	17	250/90, 170/80, 170/30	siltstone, shale	fault zone, moisture	slide
V Zideh	0 +713 to 0 +722	25	45/65, 350/30, 230/55, 15/35	crushed siltstone and finely laminated shale	fault zone, moisture	slide
Trojane	79 +720 left tube	75	340/30, 160/40, 40/30	crushed finely grained sandstone, siltstone, shale	tectonic zone, thin overburden, thick soils, moisture	slide

ANALYSIS USING MARKLAND'S TEST

Hemispherical projection techniques or stereographic projection offer a graphical method for analyzing three-dimensional problems (involving planes, lines and points) in a convenient and easily interpreted two-dimensional form. The Markland test on Schmidt diagram is very valuable tool for identifying those discontinuities that (could) lead to

failure^[5]. A wedge slide is triggered when the intersecting line of at least two systems of joints appears in a critical area. It depends on the position of the systems of joints if rock wedge sliding or gravitational failure appears. The test also considers the shear angle φ of the rock. Figures 1a and 1b show the conditions leading to sliding and the conditions leading to gravitational failure.

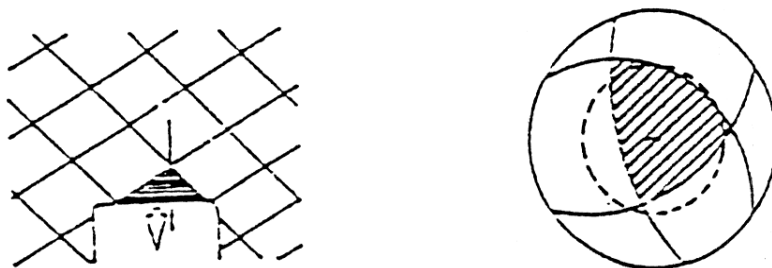


Figure 1a. Conditions leading to gravitational rock failure^[5]
Slika 1a. Pogoji pri gravitacijskem zrušku^[5]



Figure 1b. Conditions leading to rock wedge sliding^[5]
Slika 1b. Pogoji pri drsenju klina^[5]

The mentioned failures were analysed using Markland's test. Figures 2 and 3 show Schmidt diagrams for systems of discontinuity along which failures

appeared in the Golo rebro Tunnel, chainage 27+909, and in the V Zideh Tunnel, chainage 0+713.

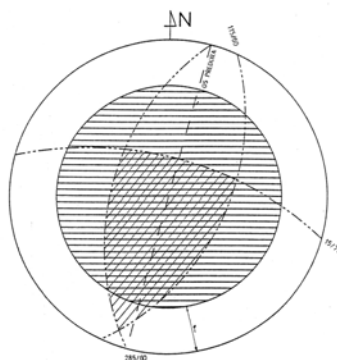


Figure 2. Schmidt diagram for the Golo rebro Tunnel, chainage 27+909
Slika 2. Schmidov diagram za predor Golo rebro na stacionaži 27+909

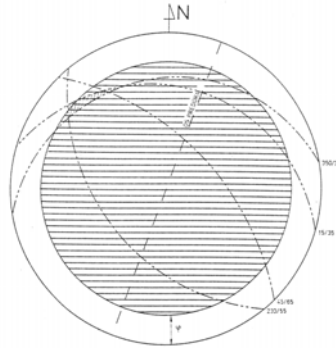


Figure 3. Schmidt diagram for the V Zideh Tunnel, chainage 0+713
Slika 3. Schmidtov diagram za predor V Zideh na stacionaži 0+713

The results show that the majority of the investigated rock failures started with sliding of a rock wedge along a smooth surface. It is especially difficult to discern between sliding and gravitational failure in tectonically disturbed rocks. The test doesn't consider the characteristics of joints, such as roughness, smoothness, fill (millonite and clay have different impact on the shear strength along discontinuities), presence of water and a degree to which the rock has been crushed.

The rock failure in the Trojane Tunnel, shown in Figure 4, had spread to the surface. The form of the sink that can be seen on the surface indicates the presence of pipe flow of crushed and wet sandy silty rock^[3]. This form of failure is characteristic of silty soils. The observed type of failure confirms the classification of Permo-Carboniferous clastic rocks into the group of soft rocks – hard soils.



Figure 4. A rock failure in the Trojane Tunnel, chainage 79+720^[3]. A sink on the surface can be seen in the upper left corner and centre of the picture, while the rock failure in tunnel is indicated in the lower right corner.

Slika 4. Zrušek v predoru Trojane na stacionaži 79+720^[3]. Zgoraj levo in v sredini je viden lijak na površini, spodaj desno pa zrušek v kaloti.

In contrast to the failures in ductile rocks, the rock failure indicated in Figure 5 is characteristic of stiff rocks. The rock failure in the Golo rebro Tunnel appeared

during the breakthrough of a tube of the tunnel. A dolomite block slid along joints oriented in directions 145/85, 270/70, 110/40.



Figure 5. Slide of a dolomite block in the Golo rebro Tunnel at chainage 27+974^[2]
Slika 5. Zdrs dolomitnega bloka v predoru Golo rebro na stacionaži 27+974^[2]

CONCLUSIONS

Regarding the results of the analysis of some extensive rock failures that appeared during tunnel construction we can conclude that a rock failure usually appear in areas characterised by unfavourable geological conditions, such as fault zones, unfavourable distribution of bedding, fissility and joints with the additional presence of water. Failures are especially frequent in the parts of tunnels with thin overburden and thick layer of soils above the tube of a tunnel.

Tectonically disturbed soft rocks have a tendency to fail in a way that is typical for soils. Failures in soft rocks can be detected by measuring devices (if already installed). Slow and progressive rock failure can be predicted on the basis of speedy subsidence of the high point.

Failures in stiff rocks are sudden and usually appear when the face of a tunnel is being opened. Analysis of failures using Markland's test is more suitable for stiff rocks.

POVZETKI

Zruški v predorih

Pri podzemnih gradnjah pogosto prihaja do zruškov. Pojav zruškov je pogosto vezan na geološke razmere v času izkopa. Vzroki porušitev pri gradnji predorov z NATM so nepričakovane geološke razmere, napake pri projektiranju, konstrukcijske napake ali slabo vodenje izkopa^[1]. V članku obravnavam geološko pogojene zruške. Glede na vrsto kamnine ločimo postopno porušitev v duktilnih kamninah (stiskanje, nabrekanje, rahljanje) in trenutno porušitev togih kamnin (padec, izbruh, udar). Za primer zruškov v duktilnih kamninah sem izbrala predora V Zideh in Trojane, za primer zruškov v togih kamninah pa zruške iz predorov Pletovarje, Golo rebro in Tabor.

Vsi naštetih predori so bili zgrajeni v zadnjem desetletju v sklopu gradnje avtocest v Sloveniji. Izkop in gradnja sta potekala po novi avstrijski metodi gradnje predorov (NATM). Predora Pletovarje in Golo Rebro sta zgrajena na AC Celje – Maribor, Trojane in V Zideh na AC Ljubljana – Celje ter predor Tabor na AC Razdrto – Fernetiči. To so eno ali dvocevni predori s premerom 10 m, ki potekajo skozi različne kamnine. Predora V Zideh in Trojane potekata skozi permokarbonske klastične kamnine^{[2],[3]}, ki s stališča inženirske geologije spadajo v posebno skupino mehkih kamnin, ostali predori pa skozi karbonatne in klastične kamnine

različnih starosti, ki jih uvrščamo med toge kamnine.

S pomočjo stereografske projekcije analiziramo prostorske probleme v ravnini. S pomočjo Marklandovega testa na Schmidtovem diagramu ugotavljamo možnost kamninskega zdrsa^[5]. Od položaja sistemov razpok je odvisno ali pride do zdrsa kamninskega klina ali do gravitacijskega zruška. Do porušitve pride, kadar sečnica vsaj dveh sistemov razpok pade v kritično območje. V testu upoštevamo tudi strižni kot kamnine. Pri analizi nekaterih večjih zruškov, ki so nastali v času gradnje predorov, se je izkazalo, da je do zruškov prihajalo večinoma na območjih z neugodnimi geološkimi razmerami kot so prelomna cona, neugodna medsebojna lega plastnatosti, skrilavosti in razpok ob prisotnosti vode. Zruški so pogosti tudi na območjih z nizkim nadkritjem in debelejšo preperino nad predorsko cevjo.

Močno tektonsko poškodovane mehke kamnine imajo obliko porušitve, ki je značilna za zemljine. Za zruške v mehkih kamninah je značilno, da jih z meritvami zaznamo (če meritve na tistem območju že potekajo). Na počasno, toda progresivno rušenje kamnine opozarja hitrost posedanja temenske točke.

Zruški v togih kamninah so trenutni in so se zgodili v času odpiranja kalote. Ugotavljanje in analiziranje zruškov z Marklandovim testom je primernejše za toge kamnine.

REFERENCES

- [1] ROMERO, V., (2002): NATM in soft-grounds: a contradiction of terms? *World tunnelling*. pp. 338-343. Dostopno na svetovnem spletu: www.jacobssf.com/NATMInSoftGround.html.
- [2] ČARMAN, M. (1998): *Metodologija inženirskogeoloških raziskav in spremljave za gradnjo predorov: magistrsko delo*. Ljubljana, GeoZs, 127 str.
- [3] AJDIČ, I., ŠTIMULAK, A. (2004): Geološka spremljava in klasificiranje hribinske mase pri gradnji predora Trojane. *Razprave 4. posvetovanja slovenskih geotehnikov*. Rogaška Slatina, pp. 35-44.
- [4] JOHNSON, I.W., NOVELLO, E.A. (1993): Soft rocks in the geotechnical spectrum. *Geotechnical Engineering of Hard Soils - Soft Rocks.*; Vol. 1, pp. 177-183, Balkema, Rotterdam.
- [5] HOEK, E. & BROWN, E.T. (1994): *Underground Excavations in Rock*. Chapman&Hall, 527 p., London.

The solution of differential equations of fluid flow by numerical program

LEVENT YILMAZ¹

¹Civil Engineering Department, Technical University of Istanbul, Maslak, 80626 Istanbul, Turkey;
e-mail: lyilmaz@itu.edu.tr

Received: June 21, 2007 **Accepted:** July 10, 2007

Abstract: The finite difference methods are used in the solution of engineering problems and in fundamental studies of the behavior of fluids. Considering the basic equations of energy, momentum, and mass conservation in a form in which the fluid properties are constant. In the differential equations the limiting assumptions of linear behavior, incompressibility, continuum properties, and simplifications of boundary properties are given for the solution.

Keywords: fluid flow, finite difference method, incompressibility

INTRODUCTION

The basic equations of energy, momentum, and mass conservation are given in the form in which the fluid properties are constant. These may be written as follows:

Energy:

$$\rho \left(\frac{\partial}{\partial t} + u \cdot \nabla \right) I = k \nabla^2 T - P \nabla \cdot u + \lambda (\nabla \cdot u)^2 + \mu \Phi \quad (1)$$

Momentum:

$$\rho \left(\frac{\partial}{\partial t} + u \cdot \nabla \right) u = \rho g - \nabla P + (\lambda + \mu) \nabla (\nabla \cdot u) + \mu \nabla^2 u \quad (2)$$

Mass:

$$\left(\frac{\partial}{\partial t} + u \cdot \nabla \right) \rho = -\rho (\nabla \cdot u) \quad (3)$$

where I is the internal energy per unit mass, T is the temperature, P is the pressure, u is the velocity, ρ the density, and Φ the frictional heating. k , μ , and λ are the thermal conductivity and the coefficients of dynamic and kinematic viscosity and in the Equation of (2) g is given as the body force. The equations considered here are of flows in which the density variations are small and can be neglected in the sense of the Boussinesq approximation.

The basis of this approximation is that there are flows in which the temperature varies little, and therefore the density varies little, yet in which the buoyancy drives the motion. Thus the variation in density is neglected everywhere except in the buoyancy term. Let ρ_b denotes the density at the bottom where temperature is T_b . For small temperature difference between the top and bottom layer we can write

$$\rho = \rho_b [1 - \alpha(T - T_b)]$$

where α is a coefficient of volume expansion. For liquid α is in the range 10^{-3} to 10^{-4} . For a temperature variation of moderate amount we have

$$\frac{|\delta\rho|}{\rho_b} = \frac{|\rho - \rho_b|}{\rho_b} = \alpha|T - T_b| \ll 1$$

but the buoyancy term $g(\rho - \rho_b)$ is the same order of magnitude as the inertia, acceleration or the viscous stress so is not negligible.

The differential in density in the continuity equation are of the order α and hence neglected to give

$$\frac{\partial u_j}{\partial x_j} = 0 \tag{4}$$

as for an incompressible fluid. Then the stress tensor becomes

$$T_{ij} = -p\delta_{ij} + \mu \left(\frac{\partial u_i}{\partial x_j} + \frac{\partial u_j}{\partial x_i} \right)$$

Again the momentum equation becomes

$$\rho \left(\frac{\partial u_i}{\partial t} + u_j \frac{\partial u_i}{\partial x_j} \right) = -g\rho_b [1 - \alpha(T - T_b)]\delta_{i3} - \frac{\partial p}{\partial x_i} + \mu\Delta u_i$$

which after using the Boussinesq approximation becomes (after a little manipulation)

$$\frac{\partial u_i}{\partial t} + u_j \frac{\partial u_i}{\partial x_j} = -\frac{\partial}{\partial x_i} \left(\frac{p}{\rho_b} + gz \right) - \alpha g (T_b - T) \delta_{i3} + \nu \Delta u_i \quad (5)$$

where $\Delta = \partial^2 / \partial x_j^2$ is the Laplacian operator.

Now we consider the energy equation. The velocity is of the order $[\alpha |\delta T| g d]^{1/2}$ and thus the ratio of Φ term to the term due to conduction of heat is of the order of

$$\frac{\mu \alpha g d}{k}$$

and this is in the range from 10^{-7} to 10^{-8} for gases and liquids and the viscous dissipation is neglected.

The term

$$-p \frac{\partial u_k}{\partial x_k} = \frac{p}{\rho} \frac{D\rho}{Dt} \approx \frac{p}{\rho} \left(\frac{\partial \rho}{\partial T} \right)_p \frac{DT}{Dt} = -\alpha p \frac{DT}{Dt}$$

Using perfect gas relations $p = \rho R T$, $R = (c_p - c_v)$ and $\alpha = 1/T$ we get

$$-p \frac{\partial u_k}{\partial x_k} = -\alpha \rho R T \frac{DT}{Dt} = -\rho (c_p - c_v) \frac{DT}{Dt}$$

Thus though $\partial u_k / \partial x_k = 0$ holds in the equation of continuity, we should not use this relation in the heating due to compression term for gases. For liquids however, this heating is negligible. Thus the final form of the energy equation is

$$\frac{\partial T}{\partial t} + u_j \frac{\partial T}{\partial x_j} = \kappa \Delta T, \quad (6)$$

where $\kappa = k / \rho_b c_p$ for a perfect gas and $k / \rho_b c$ for liquids. Equations (4), (5) and (6) are called Boussinesq equations and describe the motion of a Boussinesq fluid.

The density variation is neglected in all terms except that involving the body force g (3). In this case we take

$$\rho = \rho_o + \delta\rho = \rho_o - \rho_o \alpha (T - T_o) \quad (7)$$

where α is the volume expansion coefficient of the fluid. Neglecting viscous heating Φ we shall take $I = c_v T$, where c_v is the heat capacity at constant volume. Grouping the constant fluid properties in the form

$$\chi = \frac{k}{\rho c_v} \quad \text{and} \quad \nu = \frac{\mu}{\rho} \quad (8)$$

we may rewrite (1) through (3) as

$$\left(\frac{\partial}{\partial t} + u \cdot \nabla \right) T = -\chi (\nabla^2) T \quad (9)$$

$$\left(\frac{\partial}{\partial t} + u \cdot \nabla \right) u = g - \alpha (T - T_o) g - \frac{\nabla P}{\rho} + \nu \nabla^2 u \quad (10)$$

$$\nabla \cdot u = 0 \quad (11)$$

The vorticity is defined by

$$\omega \equiv \nabla \times u \quad (12)$$

Equation (10) may be expressed in terms of vorticity in the form

$$\left(\frac{\partial}{\partial t} + u \cdot \nabla \right) \omega = -\alpha \nabla(T) \times g + \nu \nabla^2 \omega \quad (13)$$

Equations (9), (11), (12) and (13) can be used to establish a set of two-dimensional equations that then can be expressed in finite difference form. In two dimensions the zero divergence of velocity (11) permits us to make use of a stream function defined by the equations

$$u \equiv \frac{\partial \Psi}{\partial y} \quad \text{and} \quad v \equiv -\frac{\partial \Psi}{\partial x} \quad (14)$$

in a rectangular coordinate system. Through (12) the mass conservation equation leads to the relation

$$\frac{\partial^2 \Psi}{\partial x^2} + \frac{\partial^2 \Psi}{\partial y^2} = -\omega \quad (15)$$

The vorticity has only one component in the two-dimensional case and is hence treated as a scalar. If g is taken as a constant body force (gravity) directed in the negative y direction, the momentum equation (13) becomes

$$\frac{\partial \omega}{\partial t} + \frac{\partial u \omega}{\partial x} + \frac{\partial v \omega}{\partial y} = \alpha g \frac{\partial T}{\partial x} + \nu \left(\frac{\partial^2 \omega}{\partial x^2} + \frac{\partial^2 \omega}{\partial y^2} \right) \quad (16)$$

Finally, the energy equation (9) in two dimensional form becomes

$$\frac{\partial T}{\partial t} + \frac{\partial u T}{\partial x} + \frac{\partial v T}{\partial y} = \chi \left(\frac{\partial^2 T}{\partial x^2} + \frac{\partial^2 T}{\partial y^2} \right) \quad (17)$$

THE DIFFERENCE EQUATIONS

To derive a set of finite difference equations, corresponding to differential equations (14) through (17), we prescribe a mesh of cells through which the fluid flows. In Figure 1 it is given one such prescription showing where the variables may be defined for convenient differencing. A square mesh with side length a is given in Figure 1, but a rectangular mesh where Δx is not equal to Δy can be used. The designation of velocities at half points along elements of the cells is important for satisfying conservation properties.

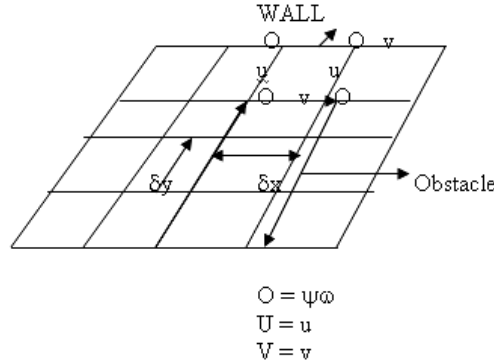


Figure 1. A representative section of the lattice of points used in the finite calculation (ABRAHAM AND TILLER, 1972)

We consider the cell as a volume element of fluid and prescribe mass conservation by

$$\frac{u_{i+1,j+1/2} - u_{i,j+1/2}}{\Delta x} + \frac{v_{i+1/2,j+1} - v_{i+1/2,j}}{\Delta y} = 0 \quad (18)$$

When the velocities are given by

$$u_{i,j+1/2} = \frac{\psi_{i,j+1} - \psi_{i,j}}{\Delta y} \quad \text{and} \quad v_{i+1/2,j} = \frac{\psi_{i,j} - \psi_{i+1,j}}{\Delta x} \quad (19)$$

the continuity equation is automatically satisfied in difference form. Further, the continuity condition is satisfied for groups of four cells in the form

$$\frac{u_{i+1,j} - u_{i-1,j}}{2\Delta x} + \frac{v_{i,j+1} - v_{i,j-1}}{2\Delta y} = 0 \quad (20)$$

if we prescribe the last equation

$$u_{i+1,j} = \frac{\psi_{i+1,j+1} - \psi_{i+1,j-1}}{2\Delta y} = \frac{u_{i+1,j+1/2} + u_{i+1,j-1/2}}{2} \quad (21)$$

Also, if the convection of energy is given in the form

$$\frac{(uT)_{i+1,j} - (uT)_{i-1,j}}{2\Delta x} + \frac{(vT)_{i,j+1} - (vT)_{i,j-1}}{2\Delta y} \quad (22)$$

no extraneous source of sinks of heat will result (ABRAHAM AND TILLER, 1972). This is true both because of the manner of centering the velocities and because of the use of differences of products of the variables. An analogous form to Equation (22) above also may be used for the transport of vorticity. The vorticity at the point i, j may be defined in terms of nearest neighbor velocities as

$$\omega_{i,j} = \frac{u_{i,j-1/2} - u_{i,j+1/2}}{\Delta y} + \frac{v_{i+1/2,j+1} - v_{i-1/2,j}}{\Delta x} \quad (23)$$

Using Equation (19) above,

$$\omega_{i,j} = \frac{(\psi_{i,j} - \psi_{i,j-1}) - (\psi_{i,j+1} - \psi_{i,j})}{\Delta y^2} + \frac{(\psi_{i,j} - \psi_{i+1,j}) - (\psi_{-i,j} - \psi_{i,j})}{\Delta x^2} \quad (24)$$

An explicit differencing scheme with centered time differences is used in this formulation (ABRAHAM AND TILLER, 1972). A variable value at the current time is designated by a superscript n . Backward and forward time values are labeled with superscripts $n-1$ and $n+1$, respectively.

$$\frac{T_{i,j}^{n+1} - T_{i,j}^{n-1}}{2\Delta t} = f(u^n, v^n, T^n) \quad (25)$$

For numerical stability it is necessary to use a special form for the conduction terms, also involving backward and forward time values (RICHTMYER, 1957). In these terms the Dufort-Frankel method is used as, (DUFORT AND FRANKEL, 1953),

$$\ddot{T}_{i,j}^n = \frac{T_{i,j}^{n+1} - T_{i,j}^{n-1}}{2} \quad (26)$$

The two-dimensional conduction terms are

$$\frac{(T_{i,j+1}^n - \ddot{T}_{i,j}^n) - (\bar{T}_{i,j}^n - \ddot{T}_{i,j-1}^n)}{\Delta y^2} + \frac{(T_{i+1,j}^n - \ddot{T}_{i,j}^n) - (\bar{T}_{i,j}^n - \ddot{T}_{i-1,j}^n)}{\Delta x^2} \quad (27)$$

It is convenient for variable mesh specification to introduce a factor $f = \Delta x / \Delta y$. Then if $\Delta y = a$, $\Delta x = fa$, the complete set of difference equations becomes (ABRAHAM AND TILLER, 1972)

(a) Energy conservation (ABRAHAM AND TILLER, 1972)

$$T_{i,j}^{n+1} = \left[1 / \left(1 + \frac{2\chi\delta t}{a^2} \frac{f^2 + 1}{f^2} \right) \right] \left\{ T_{i,j}^{n-1} - \frac{\delta t}{a} \left[\frac{(uT)_{i+1,j}^n - (uT)_{i-1,j}^n}{f} + (vT)_{i,j+1}^n - (vT)_{i,j-1}^n \right] + \frac{2\chi\delta t}{a^2} \left(\frac{T_{i+1,j}^n + T_{i-1,j}^n}{f^2} \right) + (T_{i,j+1}^n + T_{i,j-1}^n - \frac{f^2 + 1}{f^2} T_{i,j}^{n-1}) \right\} \quad (28)$$

(b) Vorticity (ABRAHAM AND TILLER, 1972)

$$\omega_{i,j}^{n+1} = \left[1 / \left(1 + \frac{2\nu\delta t}{a^2} \frac{f^2 + 1}{f^2} \right) \right] \left\{ \omega_{i,j}^{n-1} - \frac{\delta t}{a} \left[\frac{(u\omega)_{i+1,j}^n - (u\omega)_{i-1,j}^n}{f} + (v\omega)_{i,j+1}^n - (v\omega)_{i,j-1}^n \right] + \frac{\alpha g \delta t}{fa} (T_{i+1,j}^{n+1} - T_{i-1,j}^{n+1}) + \frac{2\nu\delta t}{a^2} \left(\frac{\omega_{i+1,j}^n + \omega_{i-1,j}^n}{f^2} + \omega_{i,j+1}^n - \omega_{i,j-1}^n - \frac{f^2 + 1}{f^2} \omega_{i,j}^{n-1} \right) \right\} \quad (29)$$

(c) Stream function (ABRAHAM AND TILLER, 1972)

$$\psi_{i,j} = \frac{1}{2(f^2 + 1)} (\psi_{i+1,j} + \psi_{i-1,j}) + \frac{f^2}{2(f^2 + 1)} (\psi_{i,j+1} + \psi_{i,j-1} + a^2 \omega_{i,j}) \quad (30)$$

(d) In Equation (29) it is chosen to give the temperature gradient term using advanced times since these are available if the temperature is computed first. The order of calculation, assuming known values throughout the mesh at times n and $n-1$, is that of advancing the time to t^{n+1} for the temperature field, then the vorticity field, following this with a simultaneous solution of the stream function field with the new vorticities as source terms in Poisson's equation. The time step size Δt must in general be restricted in size both for stability and accuracy (FROMM, 1963). In Equation (30) we do not indicate an iteration procedure but latest values are always used. These latest values of course depend upon the direction in which one sweeps

the field of values. A simple criterion to determine adequate convergence of Equation (30) is given from the experimental set-up (ABRAHAM AND TILLER, 1972).

$$\psi^{h+1} - \psi^h \leq 0.0002 \quad (31)$$

The Block Diagram for incompressible flows computation:

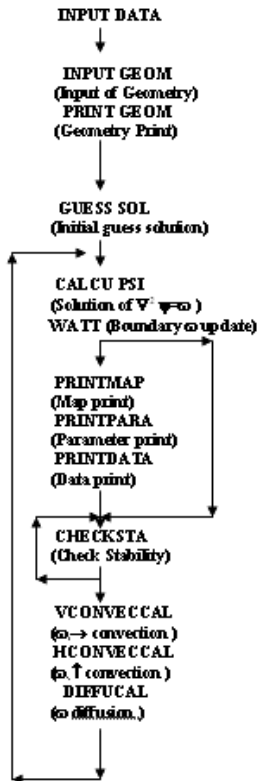


Figure 2. Block Diagram of the numerical program

For understanding of the numerical methods, it is included a skeleton program for computing incompressible flows. Only the main equation of the incompressible flows are used, giving just the basic flow dynamics in the absence of all but the convective or inertial and viscous forces. There is a certain completeness in the given program in that additions may be

made as insertions without involving major reprogramming.

We begin the block program by entering INPUT DATA which reads input data. The input data include a minimum of input parameters such as grid size, grid aspect ratio, print interval, and Reynolds number. The INPUT DATA program also is used to

consolidate parameters to provide for simplified constants that will later speed the computation. It also determines the size of the initial time step. The program INPUT GEOM, like INPUT DATA, reads input data but is specialized to give a flexibility of geometry with a minimum number of data words. The boundary must consist of straight line segments passing through mesh points, but this is the only restriction on the geometry. INPUT GEOM also establishes the initial values for boundary points. The program PRINT GEOM gives a symbolic printout of input geometry for checkout purposes. The symbols used characterize the type of boundary condition that is to be imposed.

Before starting the computation it is convenient to introduce an additional program GUESS SOL to establish initial guess values based on already prescribed boundary values. An intelligent guess enables us to speed up the convergence of our initial ψ solution. This initial guess varies from a crude layout of values given by a linear interpolation between boundary values all the way to known exact solutions. If some initially specified distribution is to be perturbed, this is also programmed in the subroutine (GUESS SOL). The program enters the subroutine CALCU PSI for actual solution of Poisson's equation. Here, through an iteration averaging process, it is obtained the stream function distribution. Most often the stream function is the potential flow solution for the given geometry.

After obtaining convergence to some specified accuracy it is established boundary values of vorticity at no-slip surfaces. This is done in the subroutine WATT. At this point in the calculation we

have a complete solution with a consistent set of numbers for ψ and ω . It also may be desirable to include input parameters or functions evaluated from the data for identification relative to the printouts. The program PRINTMAP is used to print a sheet of normalized and highly rounded values to give a picture that bears some resemblance to a contour map. A good printer map in some cases may provide a substitute for a contour map (ABRAHAM AND TILLER, 1972). The PRINTDATA program simply prints out the data values at all grid points in a layout that is geometrically similar to the given maps but usually requires several sheets to contain the information. Finally PRINTPARA serves as a labelling program, providing orientation information for the given printouts. This is a logical point to terminate the program.

However, we have not yet advanced the solutions in time, but we have only obtained a consistent initial solution. From this initial solution we now may reevaluate the size of time step required to maintain stability. This is done in the program CHECKSTA which tells us to reduce the time step that was initially furnished, we can use CHECKSTA to reevaluate any constants that are affected by this change. The arrow in the block diagram symbolizes a repeated reentry into the program until stability conditions are appropriate for proceeding with the computation. The next set of subroutines allows for the advancement of the vorticity distribution to correspond to a new time, one time increment as Δt established by CHECKSTA beyond the previous solution. VCONVECCAL computes the convection of the vorticity distribution in the coordinate direction of the u velocity in the

x -coordinate. Similarly, HCONVECCAL gives the convection associated with the v velocity in the y -direction. Finally, DIFFUCAL incorporates the diffusion of vorticity that will occur over the time interval. The time-advanced distribution of vorticity will induce a change in the flow so we now must evaluate a new stream function distribution by reentering CALCUL PSI. Each passage through this loop of subroutines amounts to the advancement in time of the solution by a small discrete time interval. We may or may not record data at each time step, but the stability is tested every time step.

One important point about the program listing is that there are no details missing so far as the physics of the calculation is concerned. Because the program has been

extracted from a more extensive set of programs, there are more parameters defined in the data lists than are here applicable. The subroutine calls sometimes contain redundant arguments. Generally, the best procedure for correction a program from listings is to draw flow charts, including all detail, for each subroutine.

INPUT data involves array size information and data as read by INPUT DATA and INPUT GEOM. The array size data is given in the first six lines of the mainline program, while the remaining data is included at the end of the program deck. Logical arrays are used to establish boundary condition for both ψ and ω fields.

REFERENCES

- ABRAHAM, F. F., and TILLER, W. A. (1972): *An introduction to computer simulation in applied science*. Plenum Press, New York – London.
- DUFORT, E. and FRANKEL, S. (1953): Stability conditions in the numerical treatment of parabolic differential equations. *Math. Tables and Other Aids to Computation*.; Vol. 7, pp. 135-152.
- FROMM, J., (1963): A method for computing nonsteady, incompressible, viscous fluid flows. *Los Alamos Scientific Laboratory Report*.; LA 2910, Los Alamos.
- RICHTMYER, R., (1957): *Difference Methods for Initial Value Problems*. Interscience Publishers, Inc., New York.
- RUSHTON, K. R., and REDSHAW, S. C. (1979): *Seepage and Groundwater Flow: Numerical Analysis Description*. Chichester John Wiley & Sons, pp. 339.

Optimization of geo-mechanical-structural drilling with diamond crowns

Optimizacija geomehansko strukturnega vrtnja z diamantnimi kronami

JURIJ ŠPORIN¹, ŽELJKO VUKELIĆ²

¹IRGO, Slovenčeva ulica 93, SI-1000 Ljubljana, Slovenia;

E-mail: jurij.sporin@irgo.si

²University of Ljubljana, Faculty of Natural Sciences and Engineering, Department of Geotechnology and Mining, Aškerčeva cesta 12, SI-1000 Ljubljana, Slovenia;

E-mail: zeljko.vukelic@ntf.uni-lj.si

Received: June 21, 2007 **Accepted:** July 10, 2007

Abstract: For successful projecting and performance in all segments of mining, geo-technological and construction projects relating or depending on rock conditions where work is going on, quality geo-mechanical-structural drilling is of extreme importance. In article special attention will be focused on performing research drilling using diamond crowns because this is the way how most quality samples of rock which are later on fully examined in laboratory, can be obtained. Significance of optimal drilling for geo-mechanic-structural wells will be presented.

Izvleček: Za uspešno projektiranje in izvajanje del pri vseh segmentih rudarskih, geotehnoških in gradbenih projektov, ki se nanašajo oz. so odvisni od pogojev hribine v kateri se izvajajo, je izjemnega pomena izvajanje kvalitetnega geomehansko-strukturnega vrtnja. V članku se bomo predvsem osredotočili na izvajanje raziskovalnega vrtnja z uporabo diamantnih kron, saj na ta način pridobimo najkvalitetnejše vzorce hribin, ki jih nato lahko detajlno preiščemo v laboratoriju. Prikazali bomo pomen optimalnega načina vrtnja pri izvedbi geomehansko-strukturnih vrtin.

Key words: research drilling, crown loading, crown, core

Ključne besede: raziskovalno vrtnje, obremenitev na krono, krona, jedro

INTRODUCTION

For successful projecting and performance in all segments of mining, geo-technological and construction projects

relating or depending on rock conditions where they are carried out, quality geo-mechanical-structural drilling is of extreme importance. In article special attention will be focused on performing research drilling

using diamond crowns since in this way most quality samples of rock which will be fully examined in laboratory, can be

obtained. Significance of optimal drilling for geo-mechanical-structural wells will be presented.

CORE SAMPLING

Core sampling is a process of drilling using drilling devices with advancing tool construction shaped in a way which enables them to take rock and soil samples. Sample – core is accumulated in a special tube, called core tube, which enables to bring the sample to surface. The aim of core sampling is gaining quality, intact core suitable for further research in laboratory. Drilling method and used equipment have major influence on core quality. Less influence to the core quality is later produced by manipulating with core in course of investigation.

In Slovenia in general a so called core tubes made according to Swedish (Craelius) metric standard are used. Core tube diameters move from 36 mm to 146 mm.

The following core barrels are in use:

- single tube core barrel;
- double tube core barrel;
 - rigid double tube core barrel
 - double tube core barrel with bearing
- three wall core tube;
- core sampling according to "wire line".

CORE SAMPLING WITH CORE CROWNS AND CORE TUBES

At core sampling an optimum among the following parameters is striven for:

- rotation speed of drilling accessories and tool;
- force magnitude on crown;
- ways of well flushing out (quantity, pressure, quality and flushing type).

Regarding soil and rock properties we can state the following:

1. Because of great diversity in soil and rock quality the probability of proper advancing speed determination is low irrespective of small number of drilling parameters. Rock materials are complex and heterogeneous. Although micro-structure and composition (minerals, grain size, bonds between grains etc.) are

the same, macrostructure (cracks, frequency etc.) varies because of different factors such as surface loadings which affect advancing speed.

2. Crown activity on rock material influenced by various drilling parameters is mutually dependent and complex. Independent variables while drilling are the following:

- characteristics of drilling tools – crown (number, shape and size, used matrix and geometry of the crown) rock type (hardness, solidness, abrasion, mineralogical composition, cracks etc.);
 - drilling method (moments, axis force, rotation speed etc.).
- Dependent variables that affect drilling advancement are:
- wear out of teeth;

- rock fracture;
- detritus size and shape;
- input specific energy during drilling.

3.Characteristic wear-out of teeth is defined by the drilling mode:

- Drilling advancement (m/h) unsuitable;
- Loading on single tooth is too low so teeth have not adequate contact with rock. Teeth penetration obstructed dew to increased surface arising from polishing teeth and getting blunt. Friction between teeth and rock is low.

- Drilling by too high loading on crowns resulting in teeth breaking, high friction, unsuitable well washing out, unsuitable crown cooling and well bottom cleaning. Penetration speed does not grow up resulting in so called burning drilling crown.

Optimal drilling advancement (m/h):

- Rock fracturing and borehole particles formation uniform and constant.
- Teeth and crown matrix wear out evenly, adv ancement, number of revolutions and loading on crown are also even.

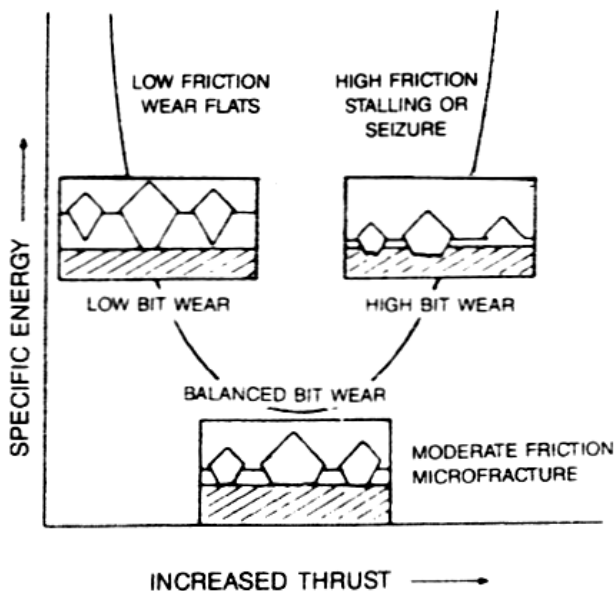


Figure 1. Presentation of drilling crown tooth wear out in dependence of loading

Slika 1. Prikaz obrabe zob vrtalne krone v odvisnosti od obtežbe

Regarding above stated facts we can conclude:

- Loading of the crown is at optimal drilling dependent on strength and

hardness of the rock and on teeth and crown conditions.

- Equilibrium between wear out of teeth and crown begins at maximal

advancement at optimal loading which is a little over minimal needed specific energy by individual drilling mode and rock type.

- Wear out of teeth is the best indicator on drilling mode.
- Teeth of smaller dimensions require higher loadings for effective drilling, achieve better advancements and produce finer particles detritus.
- Tests and investigations showed that major part of input energy is not used for rock fracturing but for secondary crushing and grinding of bore particles. Therefore quality washing out of well bottom and bore quantity are very important.
- Work done for crown loading is much smaller than the work input to overcome the torque.

For better understanding of entire drilling mode operation it is necessary to show the principle of tooth crown cutting. Drilling mode is described in following phases:

- **Ploughing**

In very soft formations teeth can penetrate into rock and cause local overcoming of shear strength as shown in Figure 2. During crown rotation around axis and loading action on it teeth scratch bottom surface of the well like plough while

ploughing field. Axial loadings are higher than shear ones so major part of work is done by axial loading. Provided that teeth are set in matrix in way that one furrow overlaps the other one the next tooth pushes some particles of the former tooth and the depth of furrow is equal as at former - in this case crown advances into rock. It is very important to wash out relatively big particles of the borehole.

- **Stress relaxation**

Stress relaxation occurs when pressure strength of the rock is high and static loading on single tooth is too low for immediate penetration into rock. Fracturing is triggered by tension discharge in the tooth furrow when the furrow traversed and caused a series of characteristic cracks and their widening as shown in Figure 2. In general a tooth during cutting never penetrates into rock if the latter had not been damaged before.

- **Grinding, abrasion**

In final phase grinding and abrasion are present and used at drilling into very hard rocks and at very high rotary speed. In principle that mechanism is very similar to mechanism of tension relaxation, the only difference are much more shallow cracks present here.

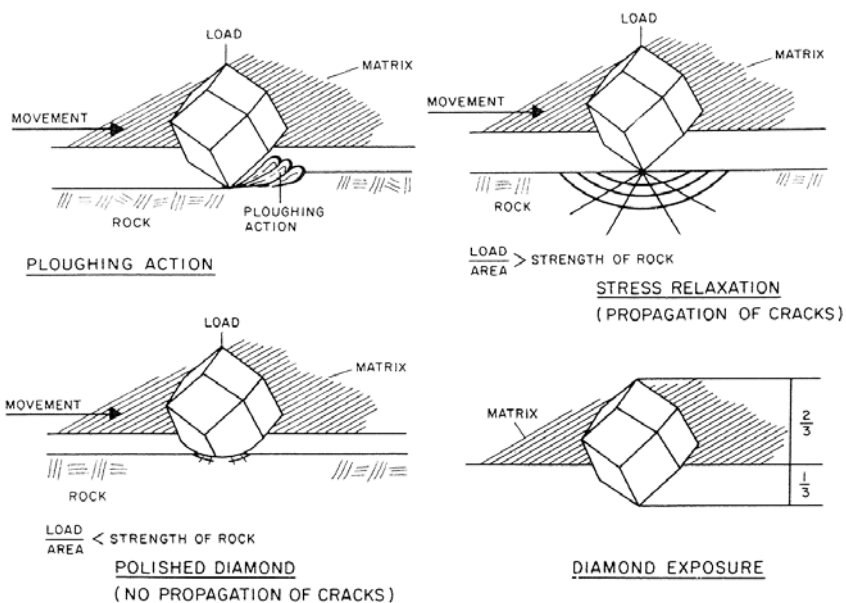


Figure 2. Operation of crown tooth depending on loading
Slika 2. Delovanje zob vrtalne krone v odvisnosti od obtežbe

For rock demolition crown tooth has to operate in accordance to the following principle:

1. Under influence of axial loading single crown tooth impresses into rock
2. Crown's turning torque generates shear force which fracturing the rock

Axial loading on single tooth is given by the equation:

$$F_0 = \frac{F}{m} \tag{1}$$

Where is:

F_0 - axial loading on single tooth [N]

F - axial loading on whole crown created by drilling device [N]

m - number of crown teeth [/]

Advancement into rock is possible only under condition:

$$F_0 > S \cdot \sigma_p \tag{2}$$

Where is:

F_0 - axial loading on single tooth [N]

S - touching surface of tooth [m²]

σ_p - one axis pressure strength of rock [N/m²]

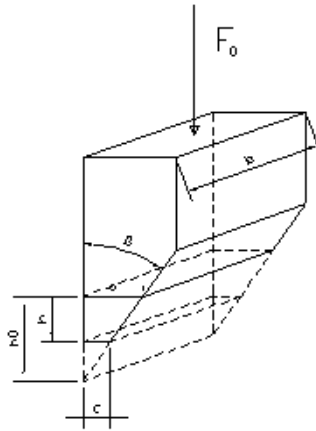


Figure 3. Crown tooth with technical elements

Slika 3. Zob krone s tehničnimi elementi

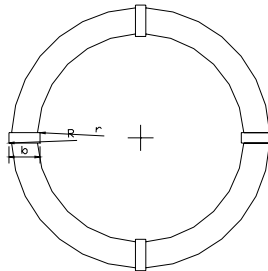


Figure 4. Scheme of the crown with teeth

Slika 4. Shema krone z zobmi

$$S = b \cdot c \quad (3)$$

Where is:

b - tooth width [m]

c - tooth thickness [m]

Tooth width is therefore given by expression:

$$b = R - r \quad (4)$$

Where is:

R - external crown radius [m]

r - internal crown radius [m]

In case of a new and unused tooth its surface is given by expression:

$$S = a \cdot b = h_0 \cdot \operatorname{tg}\beta \cdot (R - r) \quad (5)$$

Where is:

β - sharp edge angle of tooth [$^\circ$]

h_0 - penetration depth of tooth into rock [m]

Axial loading on single tooth is equal to expression:

$$F_0 = S \cdot \sigma_p = h_0 \cdot \operatorname{tg}\beta \cdot (R - r) \cdot \sigma_p \Rightarrow h_0 = \frac{F_0}{\operatorname{tg}\beta \cdot (R - r) \cdot \sigma_p} \quad (6)$$

In this case at m number of teeth in crown and n number of crown revolutions, advancement in a unit of time is:

$$L_{0-t} = h_0 \cdot m \cdot n \cdot t = \frac{F_0 \cdot m \cdot n \cdot t}{\operatorname{tg}\beta \cdot (R - r) \cdot \sigma_p} = \frac{F \cdot n \cdot t}{\operatorname{tg}\beta \cdot (R - r) \cdot \sigma_p} \quad (7)$$

Where is:

b - tooth width [m]

c - tooth thickness [m]

β - sharp edge angle of tooth [$^\circ$]

h_0 - penetration depth of tooth into rock [m]

R - external crown radius [m]

r - internal crown radius [m]

t - time of crown operation until teeth wear out [s]

n - number of tool revolutions [rev/s]

It seems that during drilling when tooth traverses very cracked regions cutting depth is very small compared to crack size. This shows a more complex relaxation system of rock and removing borehole than foreseen from the above stated drilling modes.

It is very likely that in praxis the turning and tension relaxation mechanism is used in every softer rock formation. Every time when tooth travels across a furrow it causes changes according to the same principle of drilling mode under surface.

Operational effect of every drilling mode depends on hardness and rock tension and relations among tooth hardness, rock grain size and rock non-homogeneity.

Drilling modes mentioned above do not consider washing out of detritus from the crown operation area. Nevertheless experiences show how great influence washing out, tool cooling, flushing medium leading mode, quantity of washed medium etc. have on gained core quality, advancing speed and wear out of drilling tools and accessories.

INFLUENCING FACTORS ON CORE SAMPLING QUALITY

From the drilling theory we know that the following factors have major influence on advancement speed:

- rotational speed;
- single tooth penetration depth into rock;
- physical mechanical properties of rock;
- drilling tool loading;
- teeth shape and conditions in tool;
- rinsing medium quality, flow and type.

Cutting speed

Drilling tool rotational speed has great influence on cutting speed. For quicker and more convenient calculation of cutting speed we can assume that it is equal to:

$$v = \pi \cdot D \cdot n \quad (8)$$

Where it is:

v - cutting speed [m/min]

D - drilling tool diameter [m]

n - number of tool revolutions [rev/min]

Figure 5 shows a graph for quick determination of cutting speed regarding rotational speed and tool diameter.

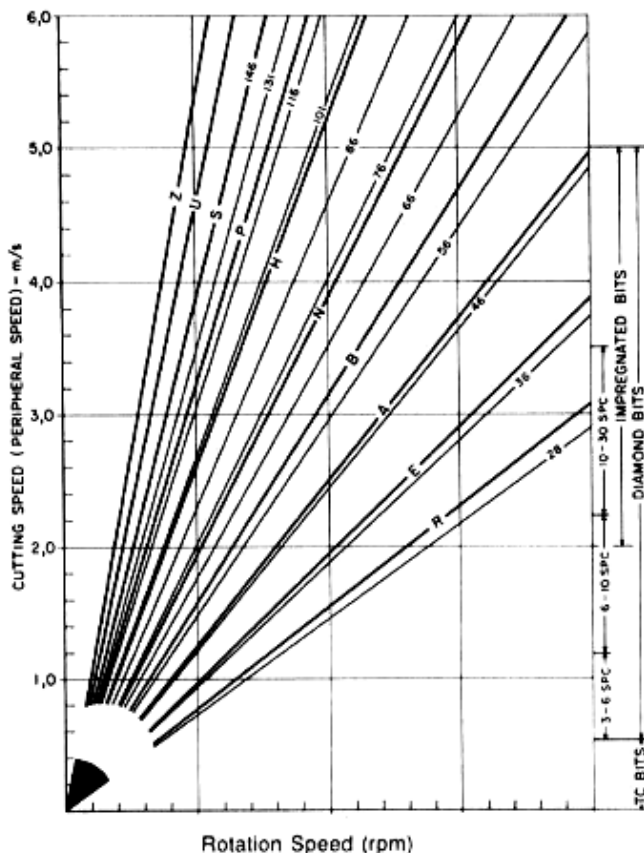


Figure 5. Graph for cutting speed determination
Slika 5. Graf za določitev hitrosti rezanja

Lower or higher speed has influence on advancement speed but it depends on rock formation properties. Final rotational speed is determined during drilling and mainly depends on rock properties and drilling techniques used.

Crown loading

Proper loading of tool – crown, is as important as proper rotational speed. During drilling crown loading is most easily determined by multiplying teeth number and the force that single tooth can withstand. This force is dependent on single tooth material quality.

As shown above axial loading on single tooth is equal to the expression:

$$F_0 = S \cdot \sigma_p = h_0 \cdot \operatorname{tg} \beta \cdot (R - r) \cdot \sigma_p \Rightarrow h_0 = \frac{F_0}{\operatorname{tg} \beta \cdot (R - r) \cdot \sigma_p} \quad (9)$$

In this case at the number of crown teeth m and crown number of revolutions n time advancement is equal to:

$$L_{0-t} = h_0 \cdot m \cdot n \cdot t = \frac{F_0 \cdot m \cdot n \cdot t}{\operatorname{tg} \beta \cdot (R - r) \cdot \sigma_p} = \frac{F \cdot n \cdot t}{\operatorname{tg} \beta \cdot (R - r) \cdot \sigma_p} \quad (10)$$

In a definite time t crown teeth wear out for an amount y . Therefore tooth height effected by axial force F_0 equals to:

$$h = h_0 - y \quad (11)$$

Where it is:

h_0 - height of a new and unused tooth [m]

y - tooth wear out [m]

Tooth wear out extent in time t can be expressed by equation:

$$v = \frac{y^2 \cdot \operatorname{tg} \beta \cdot (R - r)}{2} \quad (12)$$

Tooth alloy material wear out can be expressed by:

$$v = \omega \cdot A \quad (13)$$

Where it is:

ω - coefficient of volume tooth friction wear out on every Nm [m^3/Nm]

Friction work for thin wall crown in time t can be expressed by equation:

$$A = F_0 \cdot f \cdot \pi \cdot (R + r) \cdot n \cdot t \quad (14)$$

Where it is:

f - coefficient of friction between rock and tooth

The last expression can be put into equation for tooth material wear out so we get the following:

$$v = \omega \cdot F_0 \cdot f \cdot \pi \cdot (R + r) \cdot n \cdot t$$

$$v = \frac{y^2 \cdot \operatorname{tg} \beta \cdot (R - r)}{2} \quad (15)$$

Equalizing both equations we get:

$$\frac{y^2 \cdot \operatorname{tg} \beta \cdot (R-r)}{2} = \omega \cdot F_0 \cdot f \cdot \pi \cdot (R+r) \cdot n \cdot t \quad (16)$$

Arranging the equations can express tooth wear out extent by:

$$y = \sqrt{\frac{2 \cdot \omega \cdot F_0 \cdot f \cdot \pi \cdot (R+r) \cdot n \cdot t}{\operatorname{tg} \beta \cdot (R-r)}} \quad (17)$$

If we know values of ω and f we can determine tooth sharpness loss (bluntness) in time t and tooth penetration depth into rock material under influence of axial force F_0 in the same time t .

Actually it is $h = h_0 - y$ as shown in the Figure 6.

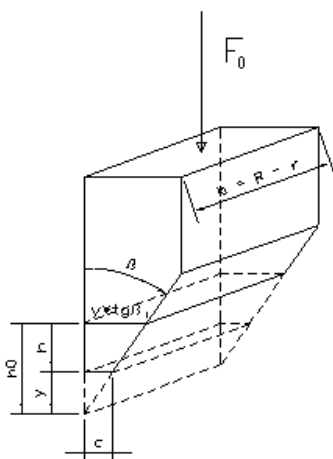


Figure 6. Crown tooth with technical elements with geometrical laws taken in account

Slika 6. Zob krone s tehničnimi elementi ob upoštevanju geometrijskih zakonitosti

Considering tooth wear out it follows:

$$h = \frac{F_0}{\sigma_p \cdot (R-r) \operatorname{tg} \beta} - \sqrt{\frac{2 \cdot \omega \cdot F_0 \cdot f \cdot \pi \cdot (R+r) \cdot n \cdot t}{\operatorname{tg} \beta \cdot (R-r)}} \quad (18)$$

Productive crown work will cease when $h = h_0 - y$. In this case penetration will go just by grinding where advancements are very low.

In this case $h_0 = y$

So:

$$\frac{F_0}{\sigma_p \cdot (R-r) \operatorname{tg} \beta} = \sqrt{\frac{2 \cdot \omega \cdot F_0 \cdot f \cdot \pi \cdot (R+r) \cdot n \cdot t}{\operatorname{tg} \beta \cdot (R-r)}} \quad (19)$$

Solving equation after time t and using relation $F \cdot m$ for axial force F_0 we get crown working time until teeth bluntness.

$$\begin{aligned} t_{\max} &= \frac{F_0^2 \cdot \operatorname{tg} \beta \cdot (R-r)}{\sigma_p^2 \cdot (R-r)^2 \cdot \operatorname{tg}^2 \beta \cdot \omega \cdot 2 \cdot F_0 \cdot f \cdot \pi \cdot (R+r) \cdot n} = \\ &= \frac{F}{2 \cdot \sigma_p^2 \cdot \operatorname{tg} \beta \cdot \omega \cdot f \cdot \pi \cdot (R+r)(R-r) \cdot n \cdot m} \end{aligned} \quad (20)$$

From the above expression it follows that we can increase crown working time t_{\max} by increasing axial force F proportionally with crown teeth bluntness.

With regard to above stated expression we can conclude:

- crown working time until teeth bluntness t_{\max} quickly falls by increasing one axial pressure rock strength σ_p ;
- increasing number of teeth in crown m shortens crown working time to bluntness t_{\max} .

Data about single tooth loading capability can be obtained from crown manufacturer. In practice it applies that loading on single tooth should be 2/3 of maximal allowed loading.

Advancement speed

The most important parameter in drilling practice is exactly advancement speed provided that the other costs (e.g. tool and equipment) of achieving fastest progress are acceptable or as low as possible.

During drilling we must find optimal rotational speed, tool loadings and rinsing for every rock formation separately.

Crown advancement time until full teeth wear out can be expressed, provided we add meaning of t_{\max} for time t , from above expression. We get following:

$$L_{0-t} = n \cdot t_{\max} \cdot \left(\frac{F}{\sigma_p \cdot (R-r) \cdot \operatorname{tg} \beta} - \frac{2}{3} \sqrt{\frac{2 \cdot \omega \cdot F \cdot f \cdot \pi \cdot (R+r) \cdot n \cdot m \cdot t_{\max}}{(R-r) \cdot \operatorname{tg} \beta}} \right) =$$

$$\begin{aligned}
&= \frac{F \cdot n \cdot F}{\sigma_p \cdot (R-r) \cdot \text{tg}\beta \cdot 2 \cdot \sigma_p^2 \cdot \text{tg}\beta \cdot \omega \cdot f \cdot \pi \cdot (R+r)(R-r) \cdot m \cdot n} \\
&= \frac{2 \cdot \sqrt{\frac{2 \cdot \omega \cdot F \cdot f \cdot \pi \cdot (R+r) \cdot n^3 \cdot m \cdot F^3}{(R-r) \cdot \text{tg}\beta \cdot 8 \cdot \sigma_p^6 \cdot \text{tg}^3\beta \cdot \omega^3 \cdot f^3 \cdot \pi^3 \cdot (R+r)^3 \cdot (R-r)^3 \cdot m^3 \cdot n^3}}}{F^2} = \\
&= \frac{6 \cdot \sigma_p^3 \cdot \text{tg}^2\beta \cdot m \cdot \omega \cdot f \cdot \pi \cdot (R-r)^2 (R+r)}{F^2} \quad (21)
\end{aligned}$$

Mean drilling speed in time t_{max} can be calculated by dividing equation for advancement L_{0-t} with the equation for crown advancement time to the point of absolute teeth wear out t_{max} .

$$v_{sr} = \frac{L_{0-t_{max}}}{t_{max}} = \frac{1}{3} \frac{F \cdot n}{\sigma_p \cdot \text{tg}\beta \cdot (R-r)} \quad (22)$$

From the equation for mean drilling speed we can conclude that the advancement speed is proportional to axial force of the crown on the rock.

Investigations have shown that advancement speed does not change proportionally to axial force increase but even more intensively and that the connection of above stated factors is much more complex.

Rinsing type and characteristics

All previous derivations about advancement speed and tool loading were based on the presumption that removing borehole particles, rinsing and tool cooling is always good.

In practice we know that flushing effect is rarely ideal. It depends on:

- crown shape and diameter;
- pole diameter;
- well conditions;
- used rinsing medium type;
- core tube and drilling pole diameter ratio.

- removal of drilling particles from the well;
- cleaning of well bottom and removing particles from crown teeth activity area;
- crown cooling;
- greasing and improving cutting process;
- protection of well walls where needed;
- friction reduction during drilling pole rotation;
- decreasing vibrations.

In any case the most important drilling fluid functions are cooling drilling tool and removing drilled particles. On basis of these functions we calculate the necessary quantity of drilling fluid.

Drilling fluid in phase of core sampling the following important functions:

The drilling fluid is pumped through drilling poles and the space between outer

and inner tube of the core tube to the crown where it proceeds to the bottom of the well and, together with drilled material in annular between core tube and well walls, to the surface.

We have to make sure that the flow velocity of lifting drilling fluid and drilled material in annular is higher than sinking speed of largest particles of detritus.

CHOICE OF A DRILLING TOOL - CROWN

Primary aim of core sampling is getting quality cores from any depth in any rock formation. Quality of gained core is a function of used drilling techniques (conventional core sampling, wire line), choice of proper drilling tool for formations we are drilling through and choice and equipment of core tube.

The choice of proper crown for core sampling in individual rocks is a matter of experienced operator. This is especially important when using diamond crowns. In general same principles of drilling crown choice apply for both prevailing crown types i.e. crowns made of carbide materials and diamond crowns.

Crowns from carbide materials

In general these crown types are used only in incoherent and soft materials since carbide inserted pieces wear out rapidly. Their use is slowly giving up in the world. Particular crown selection is limited to size and teeth distribution and crown wall thickness.

Quantity of the drilling fluid must ensure suitable tool cooling - in the hard rock, the more fluid is necessary for cooling the tool.

Usually flow rate in annular move from 0.3 to 0.5 m/s. Flow rate in annular is dependent mainly on rock density and drilled grain size and on rinsing density and viscosity.

Diamond crowns

Selecting a diamond crown which will be used in particular rock formation requires an experienced operator. Besides the fact that diamond crowns are expensive consumer goods, proper choice enables faster advancement and gaining more quality cores. Diamond crowns are characterized by following:

- geometrical and cutting profile;
- number, distribution and size of diamonds in crown;
- matrix characteristics into which diamonds are built-in.

Geometrical and cutting crown profile

Crown must be shaped in the way to ensure even and effective rock cut. Crown teeth must be well cooled and drilled material needs to be removed immediately.

Ideal crown cutting width is as narrow as possible. Because of their characteristics some rocks to a certain degree dictate the width and height of cutting profile. Cutting profiles are shown in Figure 7.



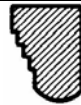









Crown with on-surface inserted teeth	
<p>Flat, rounded profile Standard profile with good efficiency</p>	
<p>Semicircular profile Profile resistant to use in cracked formations</p>	
<p>Graded profile High advancements in fragile and cracked formations</p>	
<p>Pointed profile Good advancements, more resistant than graded profile</p>	
<p>Pilot profile Good well stabilization, usable in medium hard formations</p>	
<p>Bi-conical profile For thin wall crowns, usable in soft and uncracked formations</p>	
Impregnated crowns	
<p>Flat profile Standard profile for thin wall crowns, usable in very hard and cracking formations</p>	
<p>Semicircular profile Standard profile for thick wall crowns, usable in hard and cracking formations</p>	
<p>Graded profile Profile for thick wall crowns, usable in very hard formations</p>	
<p>Pointed profile Good advancements</p>	
<p>Double graded profile Profile usable only for thick wall crowns</p>	
<p>Saw shaped profile Usable in very hard uncracked formations</p>	

Figure 7. Typical cutting profiles of diamond crowns
Slika 7. Tipični rezalni profili diamantnih kron

Supplying drilling fluid on the crown is performed through so called flushing channels or ways situated in the crown. Number of those channels depends on the rock we are drilling. Crowns for softer materials have more flushing channels than crowns for harder materials. Number and shape of flushing channels have great influence on crown geometry.

Number, distribution and teeth size in a crown

Size, number and distribution of teeth is dependent mostly on rock formations we shall drill through.

Tooth size in crown is directly dependent on rock material hardness. The harder material is, the smaller grains and the larger number of diamonds are in the crown.

Teeth are inserted into crown in patterns. Where the teeth are on-surface inserted furrow (made by teeth) overlapping must be assured. Therefore particular pattern of inserted teeth depends on their size.

REVIEW OF DRILLING PARAMETERS AT RESEARCH DRILLING FOR A BIG UNDERGROUND ROOM MAKING PROJECT

For determination of rock composition in the area where we plan to make large cavern a geo-mechanical – structural drilling was performed. In the area of investigations of limestones, dolomites and breccias with thin insertions of marl have been altering. According to mapping and geophysical measurements various layers quickly alter between themselves, from geo-mechanical viewpoint they do not

Characteristics of matrix in which teeth are inserted

Purpose of matrix in which teeth are inserted is to keep them as long as they effectively cut stoneware and to ensure stable connection with crown body.

Crowns with on-surface inserted teeth must have matrix resistant to abrasion arising from particles of drilled rock. These matrixes are made of tungsten carbide connected by copper alloy.

Matrix composition must be adapted to rock material and tooth size in crown. In general problems arise from matrix wear out in softer material where abrasion generated by drilled particles very high. In this case teeth begin to fall out before they are worn out. Improper matrix wear out is one of indicators of well rinsing quality.

By impregnated matrixes teeth must be evenly distributed in matrix body. Matrix material must be evenly wear out together with teeth enabling that new surfaces are opening by unused teeth.

differ significantly. RMR values range this part in the medium class of rock quality. Drillings are performed using diamond crowns and double tube core barrels. The well was made to 246 m depth. For our analysis on suitability and determination of optimal drilling parameters with diamond crowns it was important that we had besides exact presentation of drilling by means of drilling reports, available many data from laboratory investigations of core samples. In the Table 1 there is a list of samples investigated in laboratory.

Table 1. List of core samples for laboratory investigations and results of one axis pressure strength
Tabela 1. Popis vzorcev jedra za laboratorijske preiskave in rezultati enoosne tlačne trdnosti

Depth [m]	Description	One axis pressure strength cylinder σ_c [MPa]
30.5 - 30.8	limestone	35.2
64.2 - 64.6	marl breccia	17.2
71.4 - 71.6	breccia with marl	24.6
98.0 - 98.6	marl dolomite	31.6
118.2 - 118.5	limestone breccia	37.7
124.3 - 124.6	dolomite marl breccia	31.9
130.1 - 130.5	dolomite breccia	30.4
134.0 - 134.3	dolomite breccia	40.1
142.0 - 142.4	dolomite	16.1
152.4 - 152.6	dolomite breccia	32.7
153.5 - 153.7	dolomite breccia	61.7
155.7 - 156.0	dolomite breccia	27.1
171.0 - 171.2	dolomite breccia	73.7
177.7 - 178.0	dolomite limestone	65.3
179.7 - 180.0	breccia dolomite	89.5
183.8 - 184.0	breccia dolomite	94.3
184.0 - 184.3	dolomite limestone	56.4
187.7 - 188.0	dolomite breccia	96.0
192.4 - 192.6	dolomite breccia	102.9
193.5 - 193.7	breccia dolomite limestone	29.9
203.0 - 203.2	limestone with clay	27.8
214.0 - 214.2	limestone	59.4
236.7 - 236.9	limestone	91.7
246.0 - 246.2	limestone	65.8

While drilling the following drilling parameters were observed:

- torque;
- crown loading;
- advancement speed.

Number of revolutions of drilling accessories was between 300 and 400 rev/min.

After calculating and optimizing drilling parameters we performed laboratory investigations by crown loadings cited in Table 2.

Table 2. Loading on drilling crown

Tabela 2. Obremenitve na vrtno krono

Depth [m]	Rock type -	Used loading on crown	
		[kN]	[t]
30.5 - 30.8	limestone	14	1.4
64.2 - 64.6	marl breccia	7	0.7
71.4 - 71.6	breccia with marl	10	1.0
98.0 - 98.6	marl dolomite	13	1.3
118.2 - 118.5	limestone breccia	15	1.5
124.3 - 124.6	dolomite marl breccia	13	1.3
130.1 - 130.5	dolomite breccia	12	1.2
134.0 - 134.3	dolomite breccia	16	1.6
142.0 - 142.4	dolomite	6	0.6
152.4 - 152.6	dolomite breccia	13	1.3
153.5 - 153.7	dolomite breccia	25	2.5
155.7 - 156.0	dolomite breccia	11	1.1
171.0 - 171.2	dolomite breccia	30	3.0
177.7 - 178.0	dolomite limestone	26	2.6
179.7 - 180.0	breccia dolomite	36	3.6
183.8 - 184.0	breccia dolomite	38	3.8
184.0 - 184.3	dolomite limestone	22	2.2
187.7 - 188.0	dolomite breccia	38	3.8
192.4 - 192.6	dolomite breccia	41	4.1
193.5 - 193.7	breccia dolomite limestone	12	1.2
203.0 - 203.2	limestone clay	11	1.1
214.0 - 214.2	limestone	24	2.4
236.7 - 236.9	limestone	37	3.7
246.0 - 246.2	limestone	26	2.6

In tests diamond crown Ø 96/63.5 mm was used, double tube core barrel Ø 93 mm, drilling rods Ø 2 3/8" and drilling machine Fraste ML.

adaptations of crown loading were needed. The reason was the non-homogeneity of rock masses or non-homogeneity in particular rock as for instance cracks etc.

In spite the fact that geological list of core in particular segments shows same rocks for obtaining optimal advancement

From determined loadings investigations for particular rock massifs we can give recommended optimal loadings as follows:

Table 3. Recommended optimal loading
Tabela 3. Priporočene optimalne obremenitve

Rock type	Loading	
	[kN]	[t]
dolomite	6	0.6
marl breccia	7	0.7
breccia with marl	10	1
limestone with clay	11	1.1
breccia dolomite limestone	12	1.2
dolomite breccia	12 – 41	1.2 – 4.1
marl dolomite	13	1.3
dolomite marl breccia	14	1.4
limestone	14.0 – 24.0	1.4 – 2.4
limestone breccia	15	1.5
dolomite limestone	23 - 26	2.3 – 2.6
breccia dolomite	36 – 38	3.6 – 3.8

CONCLUSION

Optimization methods of geo-mechanical – structural drilling is a complex procedure with no universal solution. Because of geo-mechanical and structural characteristics of rock massifs it is hard to forecast or predict drilling parameters needed to gain quality core. Great role in optimization plays experience and operator's knowledge of the

device. Undoubtedly it is possible to give a report for optimal drilling method where we know expected geological rock structure that we shall investigate. Non-quality drilling works and savings at this point in practice means unsuitable projecting of pretentious surface and underground objects and many times increased investment costs.

POVZETKI

Optimizacija geomehansko strukturnega vrtanja z diamantnimi kronami

Metoda optimiranja geomehansko – strukturnega vrtanja je kompleksen postopek, ki nima univerzalne uniformne rešitve. Zaradi geomehanskih in strukturnih značilnosti hribinskih masivov, je težko natančno napovedati oziroma predpisati parametre vrtanja, ki so potrebni za pridobitev kvalitetnega jedra. Veliko

vlogo pri optimiranju vrtalnih parametrov ima izkušnost in znanje operaterja vrtalne naprave. Nedvomno pa je mogoče podati priporočila za optimalen način vrtanja, kjer dobro poznamo predvideno geološko strukturo hribin, ki jih bomo raziskovali. Nekvalitetno opravljena vrtalna dela in varčevanje pri le-teh, pa v praksi pomeni neustrezno projektiranje zahtevnih površinskih in podzemnih objektov in mnogokrat veliko povečanje stroškov investicije.

REFERENCES

BOART LONGYEAR (1997): Diamond products field manual. USA.
 INA NAFTAPLIN (1976): Priručnik za duboko bušenje i pridobivanje nafte i plina. Zagreb.
 OHNO, T., KARASAWA, H. AND KOBAYASHI, H. (2000): Durability improvement and manufacturing cost reduction of polycrystalline diamond compact bits for geothermal well drilling, National

Institute for Resources and Environment. Proceedings World Geothermal Congress 2000, Kyushu - Tohoku, Japan, May 28 - June 10, 2000.
 HEINZ W.F. (1994): Diamond drilling handbook -Third edition. Republic of South Africa.
 ZAG LJUBLJANA (2000): Poročilo o presiometričnih meritvah za skladišče plinov Senovo-Zakov. Ljubljana, junij 2006.

Filling-up mine spaces of »Block 1« and »Block 2« in the Uranium mine Žirovski vrh from the surface and remediation of a damaged cementation of well for filling-up mine spaces

Zapolnjevanje jamskih prostorov bloka 1 in 2 rudnika urana Žirovski vrh iz površine in sanacija poškodovane cementacije vrtine za zapolnjevanje jamskih prostorov

JURIJ ŠPORIN¹, ŽELJKO STERNAD¹, ŽELJKO VUKELIČ², BORIS LIKAR³, IVAN GANTAR³

¹IRGO, Slovenčeva ulica 93, SI-1000 Ljubljana, Slovenia;

E-mail: jurij.sporin@irgo.si; zeljko.sternad@irgo.si

²University of Ljubljana, Faculty of Natural Sciences and Engineering, Department of Geotechnology and Mining, Aškerčeva cesta 12, SI-1000 Ljubljana, Slovenia;

E-mail: zeljko.vukelic@ntf.uni-lj.si

³Rudnik urana Žirovski vrh v zapiranju, d.o.o., Todraž 1, 4224 Gorenja vas, Slovenia;

E-mail: boris.likar@rudnik-zv.si; ivan.gantar@rudnik-zv.si

Received: June 21, 2007 **Accepted:** July 10, 2007

Abstract: Due to the closure of uranium mine Žirovski vrh maintenance of mining spaces have been abandoned. Abandoning of maintenance consequently brought to abatement of supporting measures which resulted in widening of the destruction processes around excavated areas. In the case of uranium mine Žirovski vrh radiological contamination of the area above excavated spaces of blocks 1 and 2 could appear through cracks. Idea about filling up isolated places with the filling concrete which could be poured into the mine through drills, made from the surface, has emerged. For filling up excavated spaces in blocks 1 and 2 of uranium mine Žirovski vrh 11 wells have been made for integrating filling concrete in open mine spaces. During the fill-up of mine spaces with the filling concrete in block 2 an increased inflow of water from upper layers into the mine was discovered. The article presents realization of wells for filling up excavated areas, the process of filling up itself and the procedure of remediation of a damaged part of the well's cementation.

Izvleček: Zaradi zapiranja rudnika urana Žirovski vrh je bilo opuščeno vzdrževanje jamskih prostorov. Opustitev vzdrževanja ima za posledico popuščanje podpornih ukrepov, kar posledično vodi do širjenja rušnih procesov okoli odkopanih prostorov. S časom se zlasti v primeru nizkega nadkritja pojavijo deformacije površine nad odkopanimi prostori. V primeru rudnika urana Žirovski vrh bi preko razpok, ki se tvorijo v toku napredovanja rušnih procesov, prišlo do radiološke kontaminacije območja nad

odkopanimi prostori blokov 1 in 2 rudnika urana Žirovski vrh. Kot ideja se je ponudilo izvajanje zapolnjevanja izoliranih prostorov s polnilnim betonom, ki bi se ga v jamo zapolnjevalo preko vrtin izdelanih iz površine. Za zapolnjevanje odkopanih prostorov blokov 1 in 2 rudnika urana Žirovski vrh je bilo izdelanih 11 vrtin, skozi katere se je vgrajevalo polnilni beton v odprte jamske prostore. Tekom zapolnjevanja jamskih prostorov s polnilnim betonom je bil na eni izmed vrtin v bloku 2 ugotovljen povečan dotok vode iz zgornjih plasti v jamo. V članku bo predstavljena izvedba vrtin za zapolnjevanje odkopanih prostorov, zasipavanje samo in postopek sanacije poškodovanega dela cementacije vrtine.

Key words: injecting, well, remediation, drilling, cement suspension

Ključne besede: injektiranje, vrtina, sanacija, vrtanje, cementna suspenzija

INTRODUCTION

Due to the way how the excavated mine spaces were closed-out in the end of 1980s of the previous century, blocks 1 and 2 remained isolated. Long-term isolation of the area and top to bottom winning method triggered a destructive process which has advanced towards the surface. Due to demolished excavations and partially removed ore and consequent radiation, the usual way of closing down mining sites by filling them up from the inside was not possible.

We came up with an idea of performing the filling of isolated sites by the usage of filling concrete which could be brought into mine openings through wells made from the surface. For the purpose of filling-up excavated parts of blocks 1 and 2 in the uranium mine Žirovski vrh 11 wells have been drilled and used for integrating filling concrete into open mine spaces. At first 8 wells were made and filling of the block 1 was realized, so it was possible to check efficiency of the projected method. It was ascertained that the method is usable since the level of the fill-up of the mine

space was sufficiently high comparing to the filling-up done inside the mine. Due to positive experiences another three wells were made in the area of block 2.

Creation of wells for filling up openings in block 1 and 2

Creation of wells took place with a percussion rotational method using DTH hammers and compressed air. For the case of troubles which were expected in »Jazbeška luska« area another option of drilling with rolling bits and drilling mud with addition of bentonite had been anticipated.

Before starting with works a geodetic situation of the area had been well investigated using mining maps. Wells were positioned above areas which enabled as high level of filling-up openings as possible. In order to cut drilling costs all of the wells were projected with the same drilling parameters. Wells construction was as follows:

Column	Well	Tubing
Introduction column	Ø 584.2 mm (23")	Ø 508 × 6.3 mm (St37, weight = 77.9 kg/m)
Technical column	Ø 311.1 mm (12 ¼")	Ø 244 × 6.3 mm (St37, weight = 77.9 kg/m)
Reserve profile	Ø 431.8 mm (17")	Ø 355.6 × 6.3 mm (St37, weight = 54.3 kg/m)

Due to our presumption that »Jazbeška luska« will cause problems in the course of drilling, extra »reserve profile«, which could be used in case of a need, was added to the construction of the drill.

Cementation of the column

For additional stabilization of the well the columns were cemented. Cementation took place in accordance to Perkins – i.e. cementation through the tubes into the inter-space using separation fluids or caps. For cementing a cap in the inter-space a cementation basket was used.

PREPARATION OF FILLING CONCRETE, TRANSPORTATION AND TECHNOLOGY OF FILLING EXCAVATION SPACES THROUGH WELLS

Preparation of mine spaces for filling

Before the filling and stabilization of open mine spaces in blocks 1 and 2 started, it had been necessary to create ferroconcrete barricades around those two blocks in order to prevent the possibility of uncontrolled pouring of the filling concrete out of the area of former openings of the block 1 and 2.

Filling concrete preparation

Filling concrete was mixed in an existent concrete plant which was situated in the area of Jazbec, i.e. P-11. According to the data about the size of the openings it was estimated that it would take around 40.000 m³ of the filling concrete in order to fill-up all open spaces in the area of block 1 and 2. For filling concrete preparation the following ingredients were used:

- Sifted mining tailings, fraction 0/10 mm (gray flint sandstone)
- Electrofilter ashes from the steam power station Šoštanj
- Cement CEM II 42,5 N
- Chemical additives – retarder and aerant
- Water

For 1 m³ of the filling concrete 180 kg of cement, and 240 kg of ashes was used, the rest was composed of sifted mining tailings 0/10 mm and water. This recipe was tested in October 2003 in the ZJ 10/11 shaft. Aggregate 0/10 mm showed acceptable properties in prepared filling concrete.

Transportation of the filling concrete

Transportation of the filling concrete was carried out with concrete-mixing trucks. Influx of the well was equipped with a pouring funnel through which the concrete was poured-in. Special care was taken because of the danger of cap creation. Owing to advanced technology this did not happen. For just in case a drilling set of machinery was prepared so it would have been possible to pierce an eventual cap.

Filling-up with filling concrete through wells commenced on wells, located on the edges of excavated fields of the block 1 and 2. After completing outermost edges of the fields further filling through wells, located in the central part of former excavating fields continued. Filling of each well was finished when it was completely stuffed with filling concrete right to the top.

CONCLUSION OF FILL-UPS OF BLOCK 1 AND 2 EXCAVATED PLACES

During the fill-up of mine spaces the quality and quantity of the filling were constantly examined. It was concluded that places were filled with quality because the quantity of the filling was regularly

PROBLEMS WITH THE V-2/3 WELL

Few weeks after the well V-2/3 was accomplished the water inflow of the barrage near Laz dried up. This spring is provided with water from »Jazbeška luska«. And at the same an increased inflow of mine water on the purifying plant was detected. It was established that the

Inspection of filling concretes

At fresh filling concretes it was necessary to control quality of its making. This procedure included the following:

- Inspection of ingredients of the filling concrete (aggregate, cement, water and additives to the filling concrete (retarder and aerant));
- Inspection of fresh mixture of the filling concrete (temperature, water-cement factor W/C, consistency, containment of cement and containment of micro-pores);
- Examination of pressure solidity.

Remediation of well places

When the works were finished, drilling and filling places, including working plateau and access road, were restored into their original states.

controlled by observations made through the wells (using a camera) and from controlling points inside mine.

Quality of the material actually used and predicted before was within 5 % deviation. Less concrete was used than planned.

inflow of water in the area of the V-2/3 well increased. The well was inspected by the camera. Established and confirmed was an increased inflow of the water at the outside wall of the protecting column of the well.

Due to the technology used in drilling (percussion rotational method) which

resulted in creation of vertical and horizontal cracks around the well, water from the »Jazbeška luska« area changed its course and started to pour into the mine.

Increased flow of water from »Jazbeška luska« into the mine resulted in additional leaching of the uranium from open mine corpuses in blocks 1 and 2 which brought to increased contamination on the exit of the mine. Increased inflow of suspended particles could mean additional burden for the purifying plant which should assure cleaning of the water, flown from the mine. In eventual raining period the inflow of the water could reach a level at which it could not get cleaned enough. Our additional desire was to re-establish levels of clean water in the barrage of Laz which provides nearby farm with drinking water. Due to this fact it was necessary to find a technical solution which would divert water flow away from the V-2/3 area.

Geological situation in the V-2/3 well area

In the area of the drilling filling wells above demolished parts of the ramparts in block 1 and 2 we found ourselves in inverted wing of the upper fault in double-faulted structure of Žirovski vrh which is typical for this part of the mining zone. Under the surface there is a layer of decayed material (clayed lateral rubble) and highly decayed rockery. According to the data from surface wells thickness of this layer above block 2 is between 7 and 10 m.

Under the decayed layer there are sandy and silt aggregates of different thicknesses, subordinately conglomerates can occur as well. All listed rockeries, particularly sandstones and conglomerates contain high percentage of flint which makes incline very abrasive. Layers lie in inversed positions and their angle of incidence is from 30 to 70 ° facing north-east i.e. they slope down-hill. Slate nature of the rockery which is most obvious in finely grained rockery inclines in the same direction.

Most important among tectonic characteristics is presence of pile zone of »Jazbeška luska« which occurs mostly in the area of the longitudinal profile 1000, 34 to 58 m deep. Its depth on the spot of V-2/3 well is 35 to 38 m. Aside the pile zone the rockery is crushed, inside the tectonic clay occurs which makes pile zone an impermeable layer. Above the pile zone hanging underground water occurs which makes water inflows more likely.

Determination of crack closings around V-2/3 well

In IRGO Ljubljana we decided to carry out crack closings around V-2/3 by injection of the surrounding. Injection had to be performed in the entire area of »Jazbeška luska« with special attention on the spot where loss of the drilling mud was noticed when the V-2/3 well was drilled.

After exact study of diaries and notes, written during the drill of the V-2/3 well the composition of the well was determined and can be found in Table 1.

Table 1. Diameters of drilling and well tubing of the V-2/3 well by separate sections**Tabela 1.** Premeri vrtnanja in cevovte vrtnine V-2/3 po posameznih odsekih

Depth	Type and diameter of the drilling tool	Diameter of tubes
0 – 17.8 m	Rolling chisel D = 660.4 mm (26")	Steel tube D = 508 × 6.3 mm
17.8 m – 57 m	Rolling chisel D = 444.5 mm (17 1/2")	Steel tube D = 355 × 6.3 mm
57 m – 110.5 m	Rolling chisel D = 311.1 mm (12 1/4")	Steel tube D = 244 × 6.3 mm

Ascertained losses of the rinsing media are given in Table 2.

Table 2. Losses of the rinsing media**Tabela 2.** Izgube izplačnega medija

Section	Lost quantity of the rinse
35 m	30 m ³
36 – 38 m	30 m ³
49 – 50 m	20 m ³
58 m	20 m ³
72 – 78 m	60 m ³
Total:	160 m ³

According to the data about geology, direction of the underground water stream and factors of the drilling it was determined that injecting of the well V-2/3 area with two 58 m deep injecting wells will be carried out. The injecting will be performed in phases with a cement suspension MB25 and WC=0,4.

Implementation of drilling and injection

Drilling injecting wells

Drilling of injection wells was implemented in striking-rotational manner using depth hammers and compressed air. The performer of the drilling and injecting works was ROVS d.o.o. from Ljubljana. Arrangement of injecting wells is shown in Figure 1.

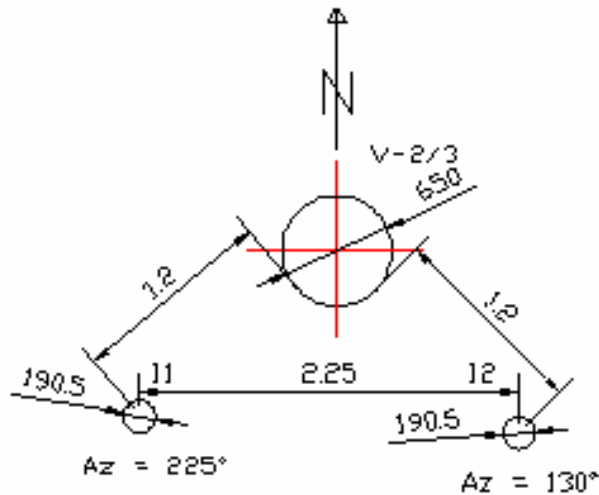


Figure 1. Arrangement of injecting wells
Slika 1. Razporeditev injekcijskih vrtin

Construction of an injection well

• **Introduction column**

Up to 20 m an introduction column was implemented in order to prevent losses of the cement suspension and consequently pressure drop in upper decayed zone. Drilling of the introduction column was carried out with the drilling tool \varnothing 190.5 mm (7 1/2").

In the well a steel tube \varnothing 168.3 \times 4 mm (6 5/8") was built-in. Junctions among tubes were welded using electro-welding. The tube of the introduction column had to be quality cemented. Cementation was done according to Perkinson method. Influx of the introduction column was equipped with a flange, a manometer for controlling pressure and a valve.

• **Technical column**

From the depth of 20 m to the anticipated final depth of 58 m, the well was drilled using a drilling tool \varnothing 114.3 mm (4 1/2"). During the drilling of the first injection well presence of a geologist, who defined the final depth of the wells was assured. Tubing of the technical column was not necessary.

During the drilling process it was necessary to follow losses and interruptions of the circulation of the rinsing media. In particular it was necessary to be careful about sections where losses of the rinsing media occurred during the drilling of the V-2/3 well. Construction of the injection well is shown on Figure 2.

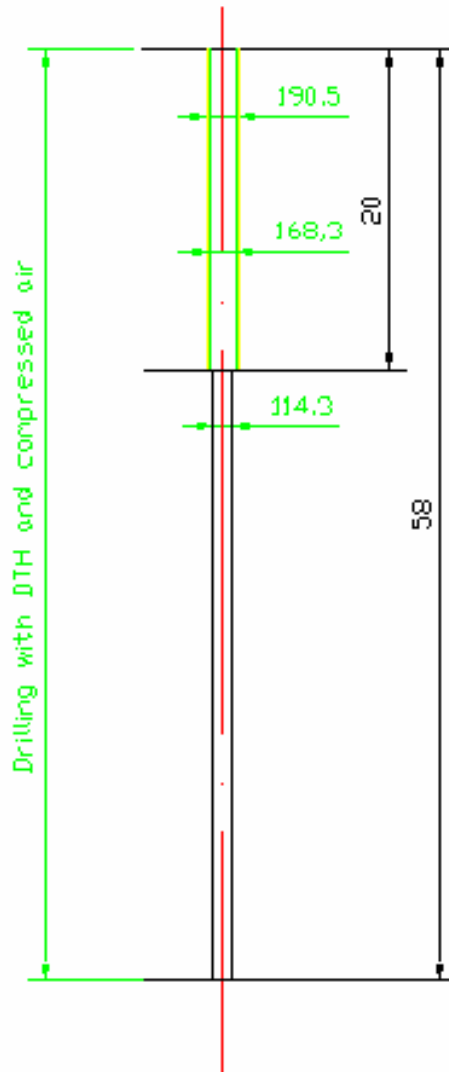


Figure 2. Construction of the injection well
Slika 2. Konstrukcija injekcijske vrtine

Injection

Before the injection begun it was necessary to carry out a pouring test in order to determine permeability of the layer. This test showed the speed of injection mass sinking and thus determined times needed for preparation and supplying of the mass

into the well as well as confirmed and disclosed required changes in the recipe for cement suspension. Injecting with cement suspension MB25 and WC=0,4 was anticipated.

Pouring tests showed that the permeability of the layer is very low so we had to adapt the recipe for cement suspension. WC factor was increased to 1.3. Because of this the final solidness of the cement suspension was decreased which turned not to be very important in the end, but we gained better dispersion in the layer and penetration into micro-cracks.

Inflow of the suspension was assured through temporary tubing on the bottom of the well. Owing to the over-pressure the cement suspension poured gravitationally on the bottom of the well with no extra help of a pump. Injection of the surrounding of the well was performed through both injecting wells simultaneously in two phases, first phase on the

depth of around 38 m and the other on 58 m. In both wells around 75 m³ of the cement suspension was built-in.

Injection efficiency

After the end of phase one of the injection on depths of about 38 m, the V-2/3 well was inspected with a camera. Reduction of the water income from the outside of the well was discovered. At the end of the second phase of the injecting the V-2/3 well was re-inspected with a camera. The water income was discovered to be ceased. After some time water in »V Lazu« barrage reemerged which brought us to conclusion that the V-2/3 remediation was successfully carried out.

CONCLUSIONS

At the reconstruction of the V-2/3 well it can be concluded that all conditions, needed for a quality realization of works was met. Conditions, needed for quality realization of works are:

- good knowing of the problems;
- very good familiarity of geological circumstances in the area of the well;

- quality metrical data of the mine with a connection to the surface;
- good knowledge of used technologies;
- good workmanship;
- good cooperation between the projecting engineer and executants of the works.

Remediation was well implemented and carried out with minimal expenses.

POVZETKI

Zapolnjevanje jamskih prostorov bloka 1 in 2 rudnika urana Žirovski vrh iz površine in sanacija poškodovane cementacije vrtine za zapolnjevanje jamskih prostorov

Ob izvedeni sanaciji vrtine V-2/3 lahko ugotovimo, da so bili izpolnjeni vsi pogoji, ki so potrebni za kvalitetno izvedbo del.

Pogoji potrebni za kvalitetno izvajanje del so:

- dobro poznavanje problematike;
- zelo dobro poznavanje geoloških razmer na območju vrtine;
- kvalitetni jamomerski podatki s površinsko navezavo;
- dobro poznavanje tehnologije po kateri se dela izvajajo;
- kvaliteten projekt za izvajanje del;
- kvaliteten izvajalec del;

- dobra sodelovanje med projektantom in izvajalcem. Sanacija je bila izvedena kvalitetno z minimalnimi stroški.

REFERENCES

- IRGO Ljubljana: *RPZI "Technology of filling-up and stabilization of open mine spaces in blocks 1 and 2"*. March 2004.
- IRGO Ljubljana: *RPZI "Injection of the V-2/3 well surroundings in the area of block 2 of Žirovski vrh uranium mine"*.

Geotechnical conditions for construction of sanitary disposal site »Lukavačka rijeka«, B&H

NIJAZ ŠKRIPIC¹, MIRZA BAŠAGIĆ¹, ZLATKO LANGOF¹, FERID SKOPLJAK¹

¹Civil Engineering Faculty of the University of Sarajevo, Geology Institute, Stjepana Tomića st. 3, 71000 Sarajevo; E-mail: mbasagic@lol.ba

Received: July 17, 2007 **Accepted:** July 20, 2007

Abstract: Construction of regional sanitary waste disposal site "Lukavačka rijeka" is planned on the place of internal overburden disposal site of surface coalmine, 3 km in the north of Lukavac city. In the area of 56 ha, disposed are coherent materials that were created during removal of overburden in surface mine in quantity of $V \approx 5.5 \cdot 10^6 \text{ m}^3$. Geological structure of terrain is composed of remains of coal seams and sand of upper Pontian (PI_1^2), thick 150 m. In the roof, disposed are pre-consolidated clay and clayey-dusty sand. In the aim of reduction of settlement effects, that realistically cannot be absolutely removed, it is proposed to remove upper part in thickness of 5.0 m, in order to provide acceptable total settlement. Analyses of stability for the most unsatisfactory case when the water content is the highest, they resulted with stability factor $F = 1.56$. In case of water level at depth of 4.0 m, stability factor is $F = 3.16$, what proves that base of the disposal site is stable. Researches proved that this location could be accepted for construction of sanitary disposal site.

Key words: sanitary waste disposal site, research works, classes of material, construction conditions, drainage system

INTRODUCTION

Waste material is disposed at wild disposal sites in Tuzla Canton. One of significant steps of this acute problem and rehabilitation of wild disposal sites is proposed construction of regional sanitary disposal site. During selection of location, care was primarily taken about parameters of production of waste at present condition and also for further 20 years. Tuzla Canton is placed in the area of 2649 km². It includes 13 municipalities with population

of 500,504 citizens. In future 20 years prognoses are that population will increase to 625,630 (increase of 1.25 % annually), specific production of waste 380 kg/citizen/year, in total quantity of $V = 4.8$ million tons. Noted quantity of waste should be placed at sanitary disposal site in approximate surface of $F = 17 - 20$ ha and height $h = 35$ m.

Multidisciplinary analyses of numerous natural, economic, social-politic, administrative and other factors, out of nominated

6 potential locations, for construction of regional disposal site, selected location Lukavačka rijeka. Construction of regional sanitary disposal site Lukavačka rijeka is planned on the place of internal disposal site of overburden of surface coal mine, 3 km in the north of city of Lukavac.

In the area of overburden disposal site in surface of 56 ha, disposed are loose materials that are created in process of removal of overburden of surface mine in quantity of $V = 5.5 \cdot 10^6 \text{ m}^3$. Materials are disposed without any special requirements in aspect of regularity of surface of disposal site and without compaction. Over those materials of the fill pack, planned is construction of regional sanitary disposal site.

Task and goal of researches was provision of necessary geological-geotechnical basis for preparation of the main project design for construction of Regional sanitary disposal site. In the aim of determination of geotechnical conditions of construction, research works are done together with geological-geotechnical researches. In this paper, results of performed researches are represented.

RESULTS AND DISCUSSION

Geological structure

Locality of Lukavačka rijeka in its geographic placement belongs to northwest part of Kreka north synclinal area. In terrain, determined are sediments of the upper Miocene (Pontian) and recent Quaternary materials of the fill.

Regarding detailed research of this area (for requirements of exploitation of coal) the following research works were conducted on purpose:

Site and laboratory works:

- Geodetic survey of terrain;
- 9 research boreholes with core sampling and conduction of SPT tests, in total length of 140 m;
- 24 research boreholes without core sampling and with conduction of SPT tests, in total length of 357 m;
- 220 SPT tests;
- Laboratory tests of 33 samples of core (standard geomechanical parameters, oedometric tests and Proctor's), and
- Geological mapping.

Office works:

- Collection and analyses of the existing data;
- Preparation of geological, engineering-geological and hydrogeological maps and profiles;
- Analyses of stability of the slope of mine disposal site, and
- Calculation of settlement.

Lower Pontian (Pl₁^l) – Novorossian pack

The floor coal seam with belonging sediments in its roof belongs to this part of Pontian (clays in close and sand in further roof). Thickness of the floor coal seam varies in wide range from 0.6 to 9.9 m. In this locality, this coal seam was not subject of exploitation.

Upper Pontian (Pl₁^u)

Zone of the main coal seam with belonging sediments (clays and sand in its floor and

roof) belongs to this part of Pontian, and I and II roof coal seams that are not developed in the area of Lukavačka rijeka but they outcrop in the distant southern parts.

Thickness of the main coal seam before exploitation varied in the range from 1.3 – 8.8 m. In conducted researches in 22 boreholes, thickness of “unexploited cloths” of the coal seam was confirmed to 0.2 – 1.3 m. Thickness of sand in the floor of the main coal seam is 150 m.

Quaternary sediments (Q) – recent anthropogenic creations of fills, are mainly of clayey, sandy, and detritus composition. Thickness of those sediments is variable and it varies in the range from 8.0 – 24.7 m, what is confirmed in conducted researches in boreholes B-9/5 and B-1.5/4.

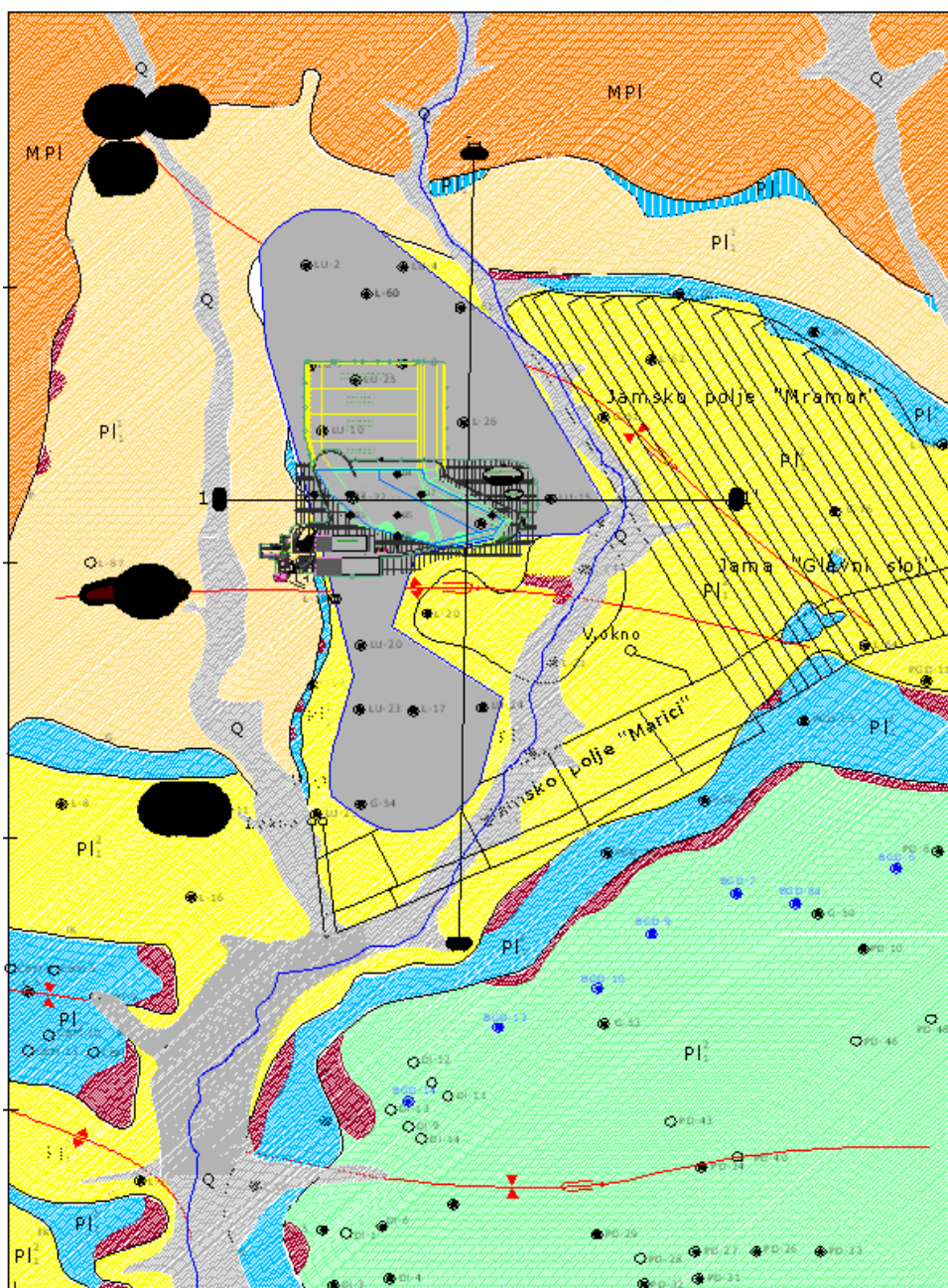
Representation of geological structure is given in geological map Figure 1.

Structural – tectonic characteristics and morphology









Kreka basin, to which area disposal site also belongs, is formed as depression most probably in the first stage of alpine organogenesis. Occurrences in this basin are in causal connection with general occurrences in the inner parts of Dinarides.

In the basin, several plication structures are formed, among which the most significant is anticline Ravna trešnja, Krekanska and Lukavačka syncline. In Lukavačka syncline, more exactly in its northwest part (area of disposal site), seams are formed in syncline, with mild centripetal inclination of 10 °. In this part of basin, faults tectonics are not expressed just folding tectonics.

Geological structure and structural-tectonic structure of the area of Lukavačka rijeka are represented in Figure 1.



LEGENDA/LEGEND:

	Holocen i Pleistocen <i>Holocene and Pleistocene</i>	KVARTAR <i>QUATERNARY</i>
	Glina, glina pjeskovita i pijesak <i>Clay, sandy clay and sand</i>	GORNJI PONT <i>UPPER PONTIAN</i>
	Pijesak <i>Sand</i>	
	Glina i laporovita glina <i>Clay and marly clay</i>	DONJI PONT <i>LOWER PONTIAN</i>
	Pijesak <i>Sand</i>	
	Glina i laporovita glina <i>Clay and marly clay</i>	
	Pijesak, šljunak i laporovita glina <i>Sand, gravel and marly clay</i>	
	Goretina <i>Burned are (coal ash)</i>	

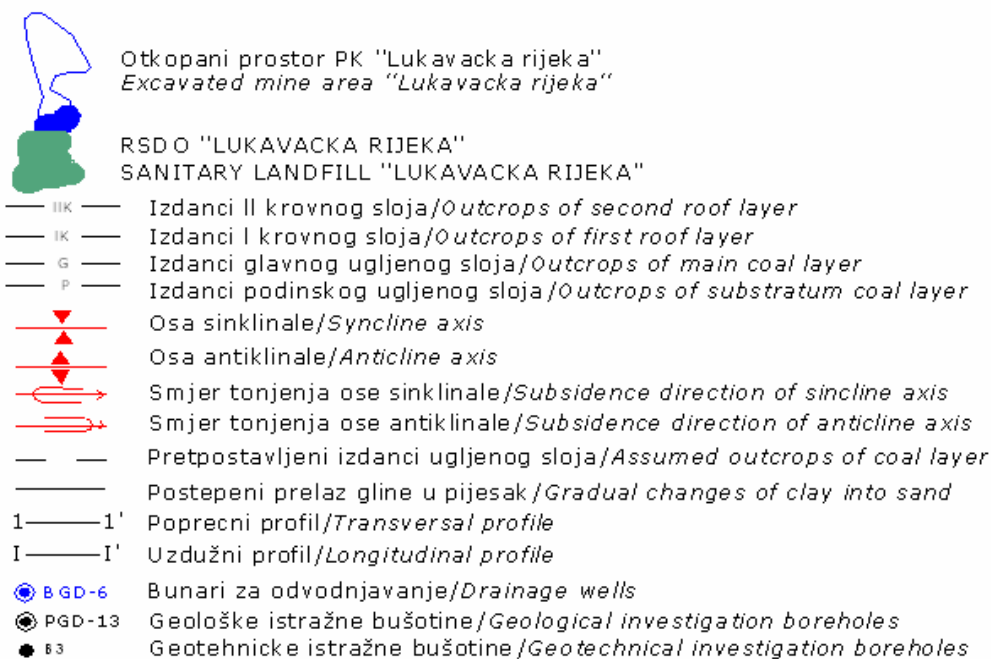


Figure 1. Geological map of wider area of RSDO "Lukavačka rijeka"

In morphological aspect, present appearance of terrain is in the shape of amphitheatre. That is a result of tectonic activities, more exactly formation of internal disposal site of surface coal mine. Inclination of terrain is relatively mild, most often $6^\circ - 10^\circ$.

Additional processes of pre-consolidation, erosion and denudation, and sliding of disposed material on technically unprepared slopes, have caused irregular forms, unsatisfactory for sanitary disposal of waste, and prior to construction of sanitary disposal site, it will be necessary to perform satisfactory preparation and shaping of the surface base.

Seismic characteristics

From the aspect of macro seismic belonging (Seismic map of BH for returning period of 500 years, Association for seismology SFRY, Belgrade 1987), area of disposal site belongs to zone of 7° MCS. On the basis of determined geological structures, rocks in the basis and determined levels of underground water, regarding the fact that purposeful researches were not conducted, for determination of seismic hazard and risk, it should be considered with increase of seismicity of $+2.3-2.6^\circ$ MCS.

Hydrogeological relations

Geological structure and structural terrain structure have caused specific hydrogeological relations. Cyclic change of sand in function of aquifer with clay and coal seams, as aquiclude, resulted in formation of artesian and sub-artesian water bearing horizons, in each of sand layers. Sand layers in locality of Lukavačka rijeka are separated from each other in two water-bearing horizons:

- I water bearing layer – sand in the floor of floor coal seam, and
- II water bearing layer – sand in the floor of the main coal seam.

Recharge of those water bearing layers in natural conditions is from outcropping surfaces of sand members that, depending on inclination of the layer and terrain configuration, create significant surfaces for infiltration of water into undergrounds. Due to mutual relations of water bearing layers and hydrogeological barriers, aquifers are mutually separated and under pressure. Both aquifers are characterised with intergranular porosity and good water permeability. An outcrop in the floor sand layer of the main coal seam is drained with battery of wells for drainage of the mine. Drainage reduces level of underground water to depth of 80 - 100 m under terrain surface. On the basis of data of pumping, calculations for those sand layers provided values of coefficients of filtration $K = 2.98 \cdot 10^{-7}$ m/s, transmission $T = 1.54 \cdot 10^{-2}$ m²/s and piezo-permeability $a = 8.58 \cdot 10^{-2}$ m²/s and specific capacity $k = 2.5 \cdot 10^{-2}$ in average. Anthropogenic material from mining operations – fills is disposed directly over sand of II water bearing layer. Materials of fill, according to results of conducted researches, represent hydro-geological complex of poorly water permeable rock masses of intergranular porosity. Average coefficient of filtration for those materials is determined in the value of $K = 2 \cdot 10^{-7}$ m/s. Even though poorly water permeable materials of fill do not fulfil basic criteria of water tightness towards basis (water bearing sand) with $K_{min} = 1 \cdot 10^{-8}$ m/s, what about should be taken special consideration during construction of sanitary waste disposal site.

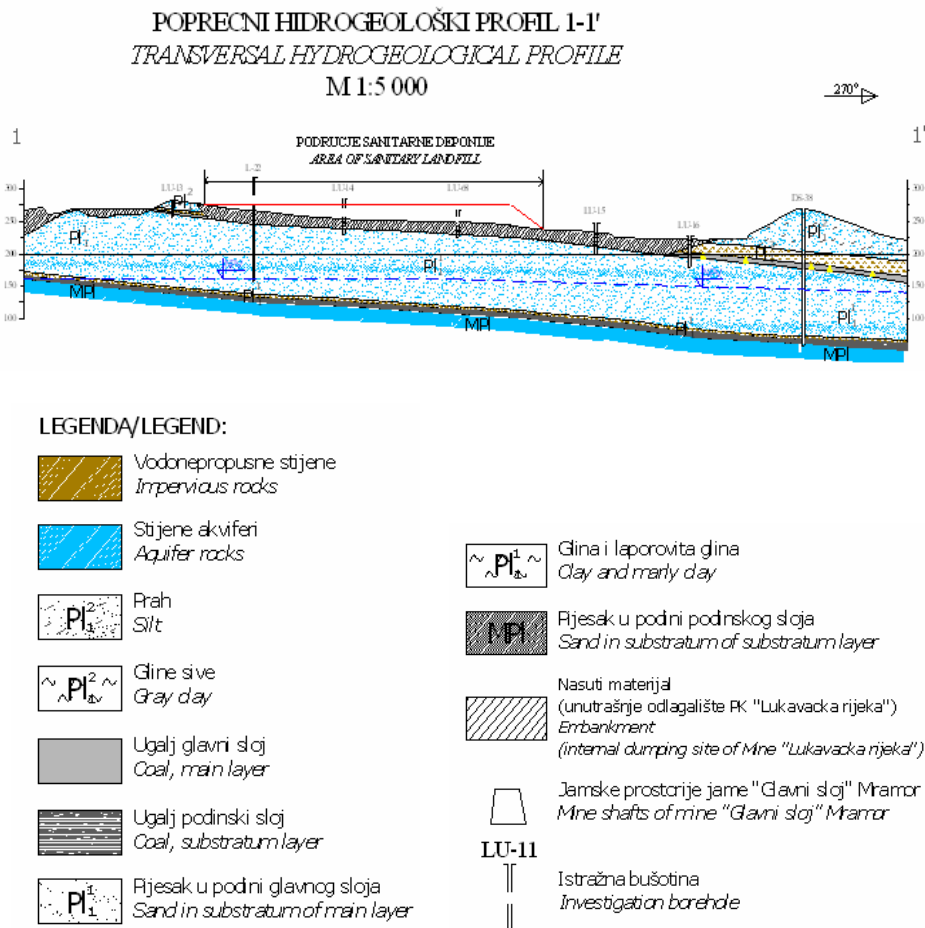


Figure 2. Hydrogeological cross section 1-1' of the area of RSDO “Lukavačka rijeka”

Engineering geological characteristics

According to engineering geological classification, rock masses are selected as basic mapped units and selected into basic taxonomic units: lithological types (LT) and complexes (LC). According to grade of diagenesis and hardness of the bonds of mineral aggregates, separated units are selected into two basic groups:

- Solid and soft rocks, in other words coal of the main and floor seam;
- Incoherent and coherent soils, in other words clays and sand of geological substrata and anthropogenic creations of the fill of mainly clayey, dusty, sandy and detritus composition.

On the basis of engineering geological characteristics, prepared is classification

and determination of rock masses as real environments where sanitary waste disposal site would be constructed. In terrain three basic material classes are selected:

Class I – deposits with poor geomechanical characteristics;

Class II – deposits with satisfactory geomechanical characteristics;

Class III – geological substrata and parts of deposit with satisfactory geomechanical characteristics.

Selected classes of material are in the following authoritative geotechnical characteristics:

CLASS I – disposed material of lower values

Standard penetration $N = 1$ to 10 hits (very compressible material)

Consistency index $I_c = 0.55$ (soft materials)

Natural moisture $W = 36\%$ (very wet soils)

Cohesion $c = 8 \text{ kN/m}^2$ (low value of cohesion)

Angle of inner friction $\varphi = 7^\circ$ (very low value)

Compressibility modulus $M_s = 3,500 \text{ kN/m}^2$ (very compressible soil)

CLASS II - disposed materials with satisfactory values

Standard penetration $N = 11$ to 30 hits (moderately compressible material)

Consistency index $I_c = 0.8$ (moderately plastic materials)

Natural moisture $W = 33\%$ (very wet soils)

Cohesion $c = 12 \text{ kN/m}^2$ (low value of cohesion)

Angle of inner friction $\varphi = 13^\circ$ (very low value)

Compressibility modulus $M_s = 6,000 \text{ kN/m}^2$ (erately compressible soil)

CLASS III – substrata and parts of disposed materials

Standard penetration $N > 30$ hits (very hard material)

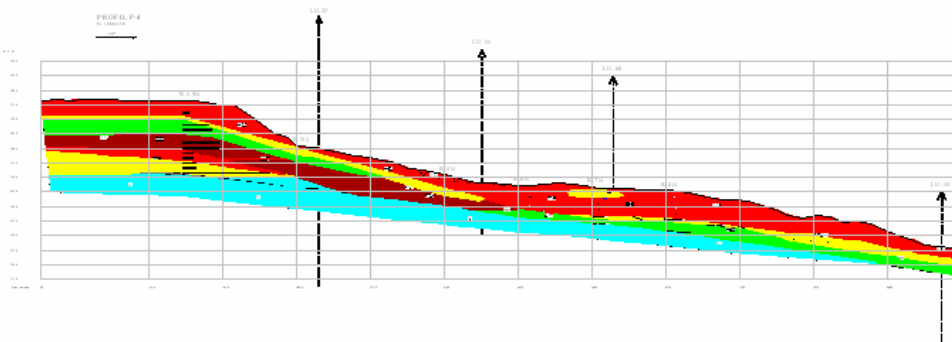
Consistency index $I_c = 1.2$ (hard consistency)

Natural moisture $W = 9.3\%$ (low soil moisture)

Cohesion $c = 0.0 \text{ kN/m}^2$ (without cohesion)

Angle of inner friction $\varphi = 35^\circ$ (high value)

Compressibility modulus $M_s > 40,000 \text{ kN/m}^2$ (low compressible soil)



Legenda
Legend

Geotehnička klasifikacija materijala
Geotechnical material classification

Klasa materijala Material class	Zapremina (P3 - P4) Volume (P3 - P4)	SPT (H 30) SPT (H 30)	Indeks konzistencije Consistency index
I	456 357.0	1-10	0.55
II	399 112.5	11-30	0.80
III <small>nebankoviti supstratum</small>	102 657.0	>30	0.88-0.94
		>50	>1.2

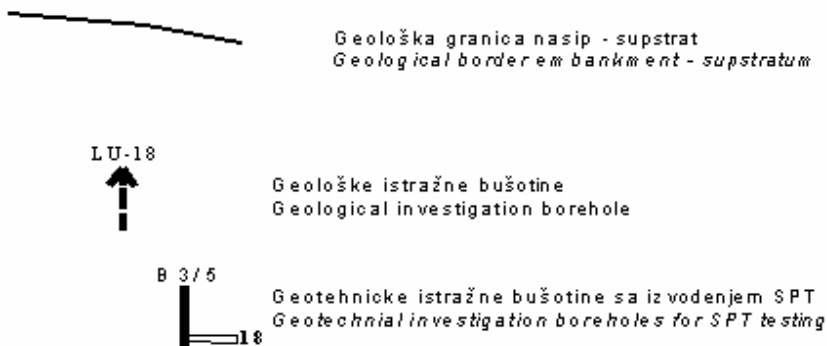


Figure 3. Vertical engineering geological profile of the area of RSDO "Lukavačka rijeka"

Analysis of stability and value of settlement

It is known that in case of disposal site that not only values of load bearing capacity of the base are authoritative but also settlement and resistance to sliding and especially unequal settling. For tension of weight goes $\sigma = 250 \text{ kN/m}^2$ and condition of removal of the upper layer of class I to 5.0 m thickness, calculated was total value of settlement $S_u = 0.25 \text{ m}$ and differences in settlement in different layers in value of $S_r = 0.126 \text{ m}$. Evaluation of influence of permitted values of unequal settlements depends on rigidity of water permeable system and final evaluation will be provided only after detailed analyses.

According to acknowledgements of conducted researches, those values of total settlements and differences in settlement due to different thickness of layers should not be critical for system. Analyses of stability proved that base of sanitary disposal site is stabile:

$F = 1.56$ – stability factor for case of complete wateriness;

$F = 3.16$ – stability factor for measured level of water at the depth of 4.0 m.

Geotechnical conditions for construction

Regarding geotechnical aspects of construction, the following can be summarised:

- In the aspect of satisfaction for construction, terrain belongs to category of conditionally stabile terrain.
- Irregular morphological forms of disposed material are unsatisfactory for

sanitary disposal of waste, and before construction of sanitary disposal site appropriate preparation and shaping of the surface shall be done.

- In the aspect of seismic hazard and risk, terrain belongs to category of unsatisfactory terrain with possibility of increase of seismicity, what should be considered during designing and shaping of construction of sanitary disposal site.
- Disposed material is characterised with heterogeneous lithological composition and variable physical-mechanical characteristics that makes complex geotechnical conditions of construction.
- Main problem that has to be solved in disposed material is related to reduction of scope of settlement, especially unequal settlement.
- In the aim of reduction of the settlement effects, that cannot realistically be absolutely removed, proposed is removal of the upper part (class I) in thickness of 5.0 m, as well as construction of drainage system, what will provide consolidation of the surface and acceptable total settlement could be provided.
- Floor sand represent water permeable layers ($K = 2.98 \cdot 10^{-6} \text{ m/s}$), and materials of the fill represent poorly water permeable rock masses ($K = 2 \cdot 10^{-7} \text{ m/s}$), that does not fulfil the basic criteria for initiation of the water towards the base (water bearing sand) of $K_{min} = 1 \cdot 10^{-8} \text{ m/s}$. In the aim of protection of pollution of aquifer, it is necessary to construct anti filtration structures.

CONCLUSIONS

It has been proved with research works that this location with complex geotechnical conditions can be accepted for construction of sanitary waste disposal site with application of appropriate technical measures:

- In the aim of reduction of the effect of settlement it is necessary to remove upper part (class I) in thickness of 5.0 m,

what can provide acceptable total settlement;

- In the aim of increase of consolidation of the base it is necessary to construct drainage system;
- In the aim of protection of aquifer it is necessary to construct anti filtration structure in the base.

REFERENCES

- BAŠAGIĆ, M., LANGOF, Z., ŠKRIPIC, N., SKOPLJAK, F. (2006.): *Elaborate about conducted research works at locality of sanitary disposal site "Lukavačka rijeka"*. Civil Engineering Faculty of University of Sarajevo, Institute for Geology, Sarajevo.
- ORUČ, E., JAHIC, I., ŽIGIĆ, I. (2004): *Analysis of influence of regional sanitary disposal site "Lukavačka rijeka" to development of mining operations in Coal mine company "Kreka"*. Mining Institute, Tuzla.
- ORUČ, E., JAHIC, I. (2002.): *Main mining project design for opening and exploitation of mining fields "Dobrinja", "Mramor" and "Marići" in underground mine "The main seam", Technical project of drainage of floor and roof layers of the underground mine "The main seam" in Mramor, Book 1-Text and Book 2-Attachments*. D.D. Mining Institute Tuzla, Tuzla.
- ŽUNIĆ, M. (1987.): *Elaborate about reserves of coal in the area of exploitation field "North syncline" Kreka*. OOUR Institute for mining researches, Tuzla.

Author's Index

BAŠAGIĆ MIRZA	mbasagic@lol.ba	127
ČARMAN MAGDA	magda.carman@geo-zs.si	77
DOLENEC MATEJ	matej.dolenec@s5.net	63
DOLENEC TADEJ	tadej.dolenec@ntfgeo.uni-lj.si	63
FAJFAR PETER	peter.fajfar@ntf.uni-lj.si	1
FAZARINC MATEVŽ	matevz.fazarinc@guest.arnes.si	1, 33
GANTAR IVAN	ivan.gantar@rudnik-zv.si	117
KEJŽAR RAJKO	rajko.kejzar@fs.uni-lj.si	49
KEJŽAR UROŠ	uroš.kejzar@iskra-varjenje.si	49
KUGLER GORAN	goran.kugler@ntf.uni-lj.si	1, 15, 33
LAMBAŠA ŽIVANA		63
LANGOF ZLATKO		127
LIKAR BORIS	boris.likar@rudnik-zv.si	117
LOJEN SONJA	sonja.lojen@ijs.si	63
MRVAR PRIMOŽ	primoz.mrvar@ntf.uni-lj.si	33
PERUŠ IZTOK	iperus@siol.net	1, 15
ROGAN NASTJA	nastja.rogan@ntfgeo.uni-lj.si	63
SKOPLJAK FERID		127
STERNAD ŽELJKO	zeljko.sternad@irgo.si	117
ŠKRIPIC NIJAZ		127
ŠPORIN JURIJ	jurij.sporin@irgo.si	97, 117
TERČELJ MILAN	milan.tercelj@ntf.uni-lj.si	1, 15, 33
TURK RADO	rado.turk@ntf.uni-lj.si	15, 33
VEČKO PIRTOVŠEK TATJANA	tpirtovsek@metalravne.com	1, 15
VUKELIĆ ŽELJKO	zeljko.vukelic@ntf.uni-lj.si	97, 117
YILMAZ LEVENT	lyilmaz@itu.edu.tr	87

INSTRUCTIONS TO AUTHORS

RMZ-MATERIALS & GEOENVIRONMENT (RMZ- Materiali in geokolje) is a periodical publication with four issues per year (established 1952 and renamed to RMZ-M&G in 1998). The main topics of contents are Mining and Geotechnology, Metallurgy and Materials, Geology and Geoenvironment.

RMZ-M&G publishes original Scientific articles, Review papers, Technical and Expert contributions (also as short papers or letters) **in English**. In addition, evaluations of other publications (books, monographs,...), short letters and comments are welcome. A short summary of the contents in Slovene will be included at the end of each paper. It can be included by the author(s) or will be provided by the referee or the Editorial Office.

** Additional information and remarks for Slovenian authors:*

English version with extended "Povzetek", and additional roles (in Template for Slovenian authors) can be written. Only exceptionally the articles in the Slovenian language with summary in English will be published. The contributions in English will be considered with priority over those in the Slovenian language in the review process.

Authorship and originality of the contributions. Authors are responsible for originality of presented data, ideas and conclusions as well as for correct citation of data adopted from other sources. The publication in RMZ-M&G obligate authors that the article will not be published anywhere else in the same form.

Specification of Contributions

Optimal number of pages of full papers is 7 to 15, longer articles should be discussed with Editor, but 20 pages is limit.

Scientific papers represent unpublished results of original research.

Review papers summarize previously published scientific, research and/or expertise articles on the new scientific level and can contain also other cited sources, which are not mainly result of author(s).

Technical and Expert papers are the result of technological research achievements, application research results and information about achievements in practice and industry.

Short papers (Letters) are the contributions that contain mostly very new short reports of advanced investigation. They should be approximately 2 pages long but should not exceed 4 pages.

Evaluations or critics contain author's opinion on new published books, monographs, textbooks, exhibitions...(up to 2 pages, figure of cover page is expected).

In memoriam (up to 2 pages, a photo is expected).

Professional remarks (Comments) cannot exceed 1 page, and only professional disagreements can be discussed. Normally the source author(s) reply the remarks in the same issue.

Supervision and review of manuscripts. All manuscripts will be supervised. The referees evaluate manuscripts and can ask authors to change particular segments, and propose to the Editor the acceptability of submitted articles. Authors can suggest the referee but Editor has a right to choose another. **The name of the referee remains anonymous.** The technical corrections will be done too and authors can be asked to correct missing items. The final decision whether the manuscript will be published is made by the Editor in Chief.

The Form of the Manuscript

The manuscript should be submitted as a complete hard copy including figures and tables. The figures should also be enclosed separately, both charts and photos in the original version. In addition, all material should also be provided in electronic form on a diskette or a CD. The necessary information can conveniently also be delivered by E-mail.

Composition of manuscript is defined in the attached Template

The original file of Template is temporarily available on E-mail addresses:
peter.fajfar@ntf.uni-lj.si,
barbara.bohar@ntfgeo.uni-lj.si

References - can be arranged in two ways:

- first possibility: alphabetic arrangement of first authors - in text: (Borgne, 1955),
or
- second possibility: ^[1] numerated in the same order as cited in the text: example^[1]

Format of papers in journals:

Le Borgne, E. (1955): Susceptibilite magnetic anomale du sol superficiel.
Annales de Geophysique, 11, pp. 399-419.

Format of books:

Roberts, J. L. (1989): Geological structures, *MacMillan, London*, 250 p.

Text on the hard print copy can be prepared with any text-processor. The electronic version on the diskette, CD or E-mail transfer should be in MS Word or ASCII format.

Captions of figures and tables should be enclosed separately. **Figures (graphs and photos)** and tables should be original and sent separately in addition to text. They can be prepared on paper or computer designed (MSExcel, Corel, Acad).

Format. Electronic figures are recommended to be in CDR, AI, EPS, TIF or JPG formats. Resolution of bitmap graphics (TIF, JPG) should be at least 300 dpi. Text in vector graphics (CDR, AI, EPS) must be in MSWord Times typography or converted in curves.

Color prints. Authors will be charged for color prints of figures and photos.

Labeling of the additionally provided material for the manuscript should be very clear and must contain at least the lead author's name, address, the beginning of the title and the date of delivery of the manuscript. In case of an E-mail transfer the exact message with above asked data must accompany the attachment with the file containing the manuscript.

Information about RMZ-M&G:

Editor in Chief prof. dr. Peter Fajfar (tel. ++386 1 4250-316) or
Secretary Barbara Bohar Bobnar, un. dipl. ing. geol. (++386 1 4704-630),
Aškerčeva 12, Ljubljana, Slovenia

or at E-mail addresses:

peter.fajfar@ntf.uni-lj.si,
barbara.bohar@ntfgeo.uni-lj.si

Sending of manuscripts. Manuscripts can be sent by mail to the **Editorial Office** address:

- RMZ-Materials & Geoenvironment
Aškerčeva 12,
1000 Ljubljana, Slovenia

or delivered to:

- **Reception** of the Faculty of Natural Science and Engineering (for RMZ-M&G)
Aškerčeva 12,
1000 Ljubljana, Slovenia
- E-mail - addresses of Editor and Secretary
- You can also contact them on their phone numbers.

TEMPLATE

**The title of the manuscript should be written in bold letters
(Times New Roman, 14, Center)**

NAME SURNAME¹, , & NAME SURNAME^X
(TIMES NEW ROMAN, 12, CENTER)

^XFaculty of ... , University of ... , Address..., Country, e-mail: ...
(Times New Roman, 11, Center)

THE LENGTH OF FULL PAPER SHOULD NOT EXCEED TWENTY (20, INCLUDING FIGURES AND TABLES) PAGES (OPTIMAL 7 TO 15), SHORT PAPER FOUR (4) AND OTHER TWO (2) WITHOUT TEXT FLOWING BY GRAPHICS AND TABLES.

Abstract (Times New Roman, Normal, 11): The text of the abstract is placed here. The abstract should be concise and should present the aim of the work, essential results and conclusion. It should be typed in font size 11, single-spaced. Except for the first line, the text should be indented from the left margin by 10 mm. The length should not exceed fifteen (15) lines (10 are recommended).

Key words: a list of up to 5 key words (3 to 5) that will be useful for indexing or searching. Use the same styling as for abstract.

INTRODUCTION (TIMES NEW ROMAN, BOLD, 12)

Two lines below the keywords begin the introduction. Use Times New Roman, font size 12, Justify alignment.

There are two (2) admissible methods of citing references in text:

1. by stating the first author and the year of publication of the reference in the parenthesis at the appropriate place in the text and arranging the reference list in the alphabetic order of first authors; e.g.:
“Detailed information about geohistorical development of this zone can be found in: Antonijević (1957), Grubić (1962), ...”
“... the method was described previously (Hoefs, 1996)”
2. by consecutive Arabic numerals in square brackets, superscripted at the appropriate place in the text and arranging the reference list at the end of the text in the like manner; e.g.:

“... while the portal was made in Zope^[3] environment.”

MATERIALS AND METHODS (TIMES NEW ROMAN, BOLD, 12)

This section describes the available data and procedure of work and therefore provides enough information to allow the interpretation of the results, obtained by the used methods.

RESULTS AND DISCUSSION (TIMES NEW ROMAN, BOLD, 12)

Tables, figures, pictures, and schemes should be incorporated in the text at the appropriate place and should fit on one page. Break larger schemes and tables into smaller parts to prevent extending over more than one page.

CONCLUSIONS (TIMES NEW ROMAN, BOLD, 12)

This paragraph summarizes the results and draws conclusions.

Acknowledgements (Times New Roman, Bold, 12, Center - optional)

This work was supported by the ****.

REFERENCES (TIMES NEW ROMAN, BOLD, 12)

In regard to the method used in the text, the styling, punctuation and capitalization should conform to the following:

FIRST OPTION - in alphabetical order

Casati, P., Jadoul, F., Nicora, A., Marinelli, M., Fantini-Sestini, N. & Fois, E. (1981): Geologia della Valle del'Anisici e dei gruppi M. Popera - Tre Cime di Lavaredo (Dolomiti Orientali). *Riv. Ital. Paleont.*; Vol. 87, No. 3, pp. 391-400, Milano.

Folk, R. L. (1959): Practical petrographic classification of limestones. *Amer. Ass. Petrol. Geol. Bull.*; Vol. 43, No. 1, pp. 1-38, Tulsa.

SECOND OPTION - in numerical order

- [¹] Trček, B. (2001): *Solute transport monitoring in the unsaturated zone of the karst aquifer by natural tracers*. Ph.D. Thesis. Ljubljana: University of Ljubljana 2001; 125 p.
- [²] Higashitani, K., Iseri, H., Okuhara, K., Hatade, S. (1995): Magnetic Effects on Zeta Potential and Diffusivity of Nonmagnetic Particles. *Journal of Colloid and Interface Science* 172, pp. 383-388.

Citing the Internet site:

CASREACT-Chemical reactions database [online]. Chemical Abstracts Service, 2000, updated 2.2.2000 [cited 3.2.2000]. Accessible on Internet: <http://www.cas.org/CASFILES/casreact.html>.

POVZETEK (TIMES NEW ROMAN, 12)

A short summary of the contents in Slovene (up to 400 characters) can be written by the author(s) or will be provided by the referee or by the Editorial Board.

TEMPLATE for Slovenian Authors

**The title of the manuscript should be written in bold letters
(Times New Roman, 14, Center)**

Naslov članka (Times New Roman, 14, Center)

NAME SURNAME¹,..., & NAME SURNAME^X (TIMES NEW ROMAN, 12, CENTER)
IME PRIIMEK¹, ..., IME PRIIMEK^X (TIMES NEW ROMAN, 12, CENTER)

^XFaculty of ... , University of ... , Address..., Country; e-mail: ...
(Times New Roman, 11, Center)

^XFakulteta..., Univerza..., Naslov..., Država; e-mail: ...
(Times New Roman, 11, Center)

THE LENGTH OF ORIGINAL SCIENTIFIC PAPER SHOULD NOT EXCEED TWENTY (20, INCLUDING FIGURES AND TABLES) PAGES (OPTIMAL 7 TO 15), SHORT PAPER FOUR (4) AND OTHER TWO (2) WITHOUT TEXT FLOWING BY GRAPHICS AND TABLES.

DOLŽINA IZVIRNEGA ZNANSTVENEGA ČLANKA NE SME PRESEGATI DVAJSET (20, VKLJUČNO S SLIKAMI IN TABELAMI), KRATKEGA ČLANKA ŠTIRI (4) IN OSTALIH PRISPEVKOV DVE (2) STRANI.

Abstract (Times New Roman, Normal, 11): The text of the abstract is placed here. The abstract should be concise and should present the aim of the work, essential results and conclusion. It should be typed in font size 11, single-spaced. Except for the first line, the text should be indented from the left margin by 10 mm. The length should not exceed fifteen (15) lines (10 are recommended).

Izvleček (TNR, N, 11): Kratek izvleček namena članka ter ključnih rezultatov in ugotovitev. Razen prve vrstice naj bo tekst zamaknjen z levega roba za 10 mm. Dolžina naj ne presega petnajst (15) vrstic (10 je priporočeno).

Key words: a list of up to 5 key words (3 to 5) that will be useful for indexing or searching. Use the same styling as for abstract.

Ključne besede: seznam največ 5 ključnih besed (3-5) za pomoč pri indeksiranju ali iskanju. Uporabite enako obliko kot za izvleček.

INTRODUCTION – UVOD (TIMES NEW ROMAN, BOLD, 12)

Two lines below the keywords begin the introduction. Use Times New Roman, font size 12, Justify alignment. All captions of text and tables as well as the text in graphics must be prepared in English and Slovenian language.

Dve vrstici pod ključnimi besedami se začne Uvod. Uporabite pisavo TNR, velikost črk 12, z obojestransko poravnavo. Naslovi slik in tabel (vključno z besedilom v slikah) morajo biti pripravljene v slovenskem in angleškem jeziku.

Figure (Table) X. Text belonging to figure (table)

Slika (Tabela) X. Pripadajoče besedilo k sliki (tabeli)

There are two (2) admissible methods of citing references – obstajata dve sprejemljivi metodi navajanja referenc:

1. by stating the first author and the year of publication of the reference in the parenthesis at the appropriate place in the text and arranging the reference list in the alphabetic order of first authors; e.g.:

1. z navedbo prvega avtorja in letnice objave reference v oklepaju na ustreznem mestu v tekstu in z ureditvijo seznama referenc po abecednem zaporedju prvih avtorjev; npr.:

“Detailed information about geohistorical development of this zone can be found in: Antonijević (1957), Grubić (1962), ...”

“... the method was described previously (Hoefs, 1996)”

or/ali

2. by consecutive Arabic numerals in square brackets, superscripted at the appropriate place in the text and arranging the reference list at the end of the text in the like manner; e.g.:

2. z zaporednimi arabskimi številkami v oglatih oklepajih na ustreznem mestu v tekstu in z ureditvijo seznama referenc v številčnem zaporedju navajanja; npr.:

“... while the portal was made in Zope^[3] environment.”

MATERIALS AND METHODS (TIMES NEW ROMAN, BOLD, 12)

This section describes the available data and procedure of work and therefore provides enough information to allow the interpretation of the results, obtained by the used methods.

Ta del opisuje razpoložljive podatke, metode in način dela ter omogoča zadostno količino informacij, da lahko z opisanimi metodami delo ponovimo.

RESULTS AND DISCUSSION – REZULTATI IN RAZPRAVA (TIMES NEW ROMAN, BOLD, 12)

Tables, figures, pictures, and schemes should be incorporated (inserted, not pasted) in the text at the appropriate place and should fit on one page. Break larger schemes and tables into smaller parts to prevent extending over more than one page.

Tabele, sheme in slike je potrebno vnesti (z ukazom Insert, ne Paste) v tekst na ustreznem mestu. Večje sheme in tabele je potrebno ločiti na manjše dele, da ne presegajo ene strani.

CONCLUSIONS – SKLEPI (TIMES NEW ROMAN, BOLD, 12)

This paragraph summarizes the results and draws conclusions.
Povzetek rezultatov in zaključki.

Acknowledgements – Zahvale (Times New Roman, Bold, 12, Center - optional)

This work was supported by the
Izvedbo tega dela je omogočilo

REFERENCES - VIRI (TIMES NEW ROMAN, BOLD, 12)

With regard to the method used in the text, the styling, punctuation and capitalization should conform to the following:

Glede na uporabljeno metodo citiranja referenc v tekstu upoštevajte eno od naslednjih oblik:

FIRST OPTION (recommended) – PRVA MOŽNOST (priporočena) – in alphabetical order (v abecednem zaporedju)

Casati, P., Jadoul, F., Nicora, A., Marinelli, M., Fantini-Sestini, N. & Fois, E. (1981): Geologia della Valle del'Anisici e dei gruppi M. Popera – Tre

Cime di Lavaredo (Dolomiti Orientali). *Riv. Ital. Paleont.*; Vol. 87, No. 3, pp. 391-400, Milano.

Folk, R. L. (1959): Practical petrographic classification of limestones. *Amer. Ass. Petrol. Geol. Bull.*; Vol. 43, No. 1, pp. 1-38, Tulsa.

SECOND OPTION – DRUGA MOŽNOST - in numerical order (v numeričnem zaporedju)

[¹] Trček, B. (2001): *Solute transport monitoring in the unsaturated zone of the karst aquifer by natural tracers*. Ph.D. Thesis. Ljubljana: University of Ljubljana 2001; 125 p.

[²] Higashitani, K., Iseri, H., Okuhara, K., Hatade, S. (1995): Magnetic Effects on Zeta Potential and Diffusivity of Nonmagnetic Particles. *Journal of Colloid and Interface Science* 172, pp. 383-388.

Citing the Internet site:

CASREACT-Chemical reactions database [online]. Chemical Abstracts Service, 2000, updated 2.2.2000 [cited 3.2.2000]. Accessible on Internet: <http://www.cas.org/CASFILES/casreact.html>.

Citiranje Internetne strani:

CASREACT-Chemical reactions database [online]. Chemical Abstracts Service, 2000, obnovljeno 2.2.2000 [citirano 3.2.2000]. Dostopno na svetovnem spletu: <http://www.cas.org/CASFILES/casreact.html>.

POVZETEK – SUMMARY (TIMES NEW ROMAN, 12)

An extended summary of the contents in Slovene (from one page to approximately 1/3 of the original article length).

Razširjeni povzetek vsebine prispevka v Angleščini (od ene strani do približno 1/3 dolžine izvirnega članka).

No. of indexing of RMZ-M&G in singular Databases
(Število indeksiranih člankov iz RMZ-M&G v posameznih bazah)
 (prepared by Fajfar, P. – from search done by Šercelj, M., CTK Ljubljana, 15.2.2007)

DATABASE NAME	HITS
1: Civil Engineering Abstracts	773
2: CA SEARCH® - Chemical Abstracts® (1967- present)	760
3: Inside Conferences	313
4: Materials Business File	253
5: METADEX®	164
6: ANTE: Abstracts in New Technologies and Engineering	158
7: GeoRef	154
8: Aluminium Industry Abstracts	36
9: PASCAL	30
10: Energy Science and Technology	27
11: TEME - Technology and Management	27
12: Ei Compendex®	13
13: CSA Aerospace & High Technology Database	12
14: Computer and Information Systems	10
15: Mechanical & Transportation Engineering Abstracts	8
16: Engineered Materials Abstracts®	3
17: Corrosion Abstracts	3
18: Analytical Abstracts	1
19: FLUIDEX	1
20: Solid State and Superconductivity Abstracts	1
21: Electronics and Communications Abstracts	1
	2748



ŠTOREQSTEEL
155 let

železarska c. 3 3220 štore slovenija
www.store-steel.si

